

Interim  
Report

March 1978

---

# Analysis and Test for Space Shuttle Propellant Dynamics

## (1/60th Scale Model Test Results)

(NASA-CR-151681) ANALYSIS AND TEST FOR	N78-21301
SPACE SHUTTLE PROPELLANT DYNAMICS: 1/60TH	
SCALE MODEL TEST RESULTS (Martin Marietta	
Corp.) 116 p HC A06/MF A01	CSCI 21I
	Unclas
	G3/28 15638

**MARTIN MARIETTA**

ANALYSIS AND TEST  
FOR SPACE SHUTTLE PROPELLANT DYNAMICS  
(1/60TH SCALE MODEL TEST RESULTS)

Authors:

Robert L. Berry  
James R. Tegart

MCR-78-523

Approved by:



---

H. Harcrow  
Program Manager

Prepared for:

National Aeronautics and Space Administration  
Lyndon B. Johnson Space Center  
Houston, Texas 77058

MARTIN MARETTA CORPORATION  
Denver Division  
Denver, Colorado 80201

FOREWORD

This report, prepared by the Martin Marietta Corporation, Denver Division, under contract NAS9-15302, presents the results of an analytical and experimental study of Space Shuttle propellant dynamics during ET/Orbiter separation in the RTLS (return to launch site) mission abort sequence. The study employed a 1/60<sup>th</sup> scale model of the ET LOX tank. The study was performed from April 1977 to February 1978 and was administered by the National Aeronautics and Space Administration, Lyndon B. Johnson Space Center, Houston, Texas, under the direction of Mr. Mark Craig.

In addition to this report, a high speed 16 mm movie has been produced which documents the test results.

ABSTRACT

This report presents the results of a ten month experimental investigation of Space Shuttle propellant dynamics during ET/Orbiter separation in the RTLS (return to launch site) mission abort sequence. During this abort sequence, the ET and orbiter separate under aerodynamic loading, with propellant remaining in the ET. The separation event includes a seven second decelerating coast period during which the residual propellant accelerates relative to the ET/orbiter. At separation, ET clearance is primarily provided by aerodynamics acting on the ET to move it away. The motion of the propellant, primarily LOX, significantly influences the resulting ET motion and could cause the ET to recontact the orbiter. A test program was conducted in the Martin Marietta Drop Tower Test Facility involving thirty-two drops with 1/60th scale models of the ET LOX tank. The objective was to acquire data on the nature of low g propellant reorientation, in the ET LOX tank, and to measure the forces exerted on the tank by the moving propellant. The data will provide a basis for correlation with an analytical model of the slosh phenomenon in Phase II of this contract.

ACKNOWLEDGEMENTS

The authors would like to express their appreciation to several individuals who contributed to the successful completion of this study. Mr. Mark Craig, NASA JSC, assisted in laying out the test program and monitored the entire study. Mr. Leonard Demchak, MMC Analytical Mechanics, provided invaluable assistance in data reduction and computer programming. Mr. E. R. Wilson, MMC, designed the model tanks. Mr. Duane Brown and Mr. Don Hershfield, MMC, fabricated the tanks, assembled the test module and instrumentation and Mr. Brown performed the drop tower tests.

CONTENTS

	<u>Page</u>
List of Symbols . . . . .	viii
I. Introduction . . . . .	I-1
II. Experimental Investigation . . . . .	II-1
A. Scaling Analysis . . . . .	II-1
B. Evaluation of Feedline Draining . . . . .	II-6
C. Test System Description . . . . .	II-9
1. Test Module . . . . .	II-9
2. Drop Test Facility . . . . .	II-17
3. Instrumentation . . . . .	II-17
D. Test Conditions . . . . .	II-21
E. Data Reduction . . . . .	II-24
1. Applied Accelerations . . . . .	II-24
2. Force Data . . . . .	II-27
III. Evaluation of Test Results . . . . .	III-1
A. Test Conditions . . . . .	III-1
B. Observations on Liquid Motion . . . . .	III-1
1. Liquid Motion in the Bare Tank . . . . .	III-19
2. Liquid Motion in the Baffled Tank . . . . .	III-22
3. Effect of Acceleration Magnitude . . . . .	III-25
4. Effect of Liquid Inflow . . . . .	III-26
C. Parameter Effects on Reorientation Forces . . . . .	III-27
1. Comparison of Baffled and Unbaffled Test Data . . . . .	III-27
2. Effects of Liquid Viscosity . . . . .	III-36
3. Effects of Percent Fill Volume . . . . .	III-39
4. LOX Inflow . . . . .	III-39
D. Analytical Correlation . . . . .	III-39
IV. Conclusions and Recommendations . . . . .	IV-1
V. References . . . . .	V-1
 <u>Appendices</u>	
A. Force Time Histories . . . . .	A-1

## CONTENTS (Continued)

	<u>Page</u>
<u>List of Tables</u>	
II-1	Liquid Properties . . . . . II-7
II-2	Dimensionless Parameters . . . . . II-7
II-3	Test Matrix . . . . . II-23
II-4	Test Constants . . . . . II-28
III-1	Test Conditions . . . . . III-2
<u>List of Figures</u>	
II-1	Orientation of Tank Axes . . . . . II-2
II-2	Froude/Bond Number Relationship . . . . . II-4
II-3	Effect of Reynolds Number . . . . . II-4
II-4	Test Module . . . . . II-10
II-5	Force Measurement Module with Calibration Fixture Installed . . . . . II-11
II-6	1/60th Scale Model Design . . . . . II-12
II-7	Unbaffled Tank . . . . . II-14
II-8	Baffled Tank Prior to Assembly . . . . . II-15
II-9	Baffled Tank . . . . . II-16
II-10	Complete Drop Capsule . . . . . II-18
II-11	Complete Drop Test System . . . . . II-19
II-12	Drop Test Facility . . . . . II-20
II-13	Longitudinal Acceleration Calculation . . . . . II-25
II-14	Digital Filter Shape . . . . . II-29
II-15	Adjustment of Longitudinal Test Forces . . . . . II-29
II-16	Tank - Measurement Coordinate System . . . . . II-30
III-1	Test 5, FC-114B2, $\gamma = 13^\circ$ , 10% Fill . . . . . III-3
III-2	Test 6, FC-43, $\gamma = 13^\circ$ , 10% Fill . . . . . III-4
III-3	Test 32, Hexane, $\gamma = 13^\circ$ , 10% Fill . . . . . III-5
III-4	Test 7, FC-114B2, $\gamma = 13^\circ$ , 10% Fill . . . . . III-6
III-5	Test 9, FC-114B2, $\gamma = 13^\circ$ , 2% Fill . . . . . III-7
III-6	Test 11, FC-114B2, $\gamma = 13^\circ$ , 2% Fill . . . . . III-8
III-7	Test 13, FC-114B2, $\gamma = 13^\circ$ , 2% Fill . . . . . III-9

## CONTENTS (continued)

	<u>Page</u>
III-8	Test 16, FC-114B2, $\gamma = 13^{\circ}$ , 10% Fill . . . . . III-10
III-9	Test 18, FC-114B2, $\gamma = 13^{\circ}$ , 10% Fill . . . . . III-11
III-10	Test 22, FC-114B2, $\gamma = 13^{\circ}$ , 15% Fill . . . . . III-12
III-11	Test 20, FC-114B2, $\gamma = 13^{\circ}$ , 15% Fill . . . . . III-13
III-12	Test 25, FC-114B2, $\gamma = 30^{\circ}$ , 10% Fill . . . . . III-14
III-13	Test 26, FC-114B2, $\gamma = 30^{\circ}$ , 10% Fill . . . . . III-15
III-14	Test 30, FC-114B2, $\gamma = 0^{\circ}$ , 10% Fill . . . . . III-16
III-15	Test 29, FC-114B2, $\gamma = 0^{\circ}$ , 10% Fill . . . . . III-17
III-16	Test 31, FC-114B2, $\gamma = 13^{\circ}$ , 2% Fill . . . . . III-18 LOX Line Outflow Into Tank
III-17	Comparison Test 10/Test 12 $\gamma = 13^{\circ}$ , 2% Fill, FC-43 . . . . . III-28
III-18	Comparison Test 6/Test 8 $\gamma = 13^{\circ}$ , 10% Fill, FC-43 . . . . . III-29
III-19	Comparison Test 9/Test 11 $\gamma = 13^{\circ}$ , 2% Fill, FC-114B2 . . . . . III-30
III-20	Comparison Test 19/Test 21 $\gamma = 13^{\circ}$ , 5% Fill, FC-114B2 . . . . . III-31
III-21	Comparison Test 5/Test 7 $\gamma = 13^{\circ}$ , 10% Fill, FC-114B2 . . . . . III-32
III-22	Comparison Test 20/Test 22 $\gamma = 13^{\circ}$ , 15% Fill, FC-114B2 . . . . . III-33
III-23	Comparison Test 25/Test 26 $\gamma = 30^{\circ}$ , 10% Fill, FC-114B2 . . . . . III-34
III-24	Comparison Test 16/Test 18 $\gamma = 13^{\circ}$ , 10% Fill, FC-114B2 . . . . . III-35
III-25	Comparison Test 5/Test 6/Test 32 $\gamma = 13^{\circ}$ , 10% Fill . . . . . III-37
III-26	Comparison Test 7/Test 8 $\gamma = 13^{\circ}$ , 10% Fill . . . . . III-38
III-27	Comparison Test 5/Test 9/Test 21 $\gamma = 13^{\circ}$ , FC-114B2 . . . . . III-40
III-28	Comparison Test 5/Test 21/Test 22 $\gamma = 13^{\circ}$ , FC-114B2 . . . . . III-41
III-29	Analytical Model Concept . . . . . III-42
III-30	Test/Analytical Correlation . . . . . III-44

LIST OF SYMBOLS

$a$	Semi-major axis of ellipse
$A$	Acceleration
$b$	Semi-minor axis of ellipse
$B_0$	Bond number
$D$	Diameter and drag force
$f_m$	Mass factor
$F$	Force
$F_r$	Froude number
$g$	Acceleration of gravity
$K$	Coefficient
$K_{Re}$	Coefficient
$L$	Lateral travel distance
$m$	Mass
$M$	Moment
$NF$	Number of frames
$r$	Tank radius
$R$	Radius of curvature
$Re$	Reynolds number
$S$	Axial travel distance
$t$	Time
$V$	Velocity
$W$	Weight
$X, Y, Z$	Coordinate system
$\gamma$	Angle of inclination
$\rho$	Density
$\sigma$	Surface tension
$\mu$	Viscosity

## I. INTRODUCTION

---

The Space Shuttle has been designated as America's prime launch vehicle for the eighty's and beyond. The Shuttle system is a manned flight system requiring extensive mission planning and contingency operations. One prime mission planning event is the contingency mission abort, prior to orbital insertion. During this intact abort mode, the mated orbiter/external tank (ET) "flies" back to the launch site, at an altitude of 200,000 + feet, using the main orbiter engines. This RTLS (return to launch site) abort sequence requires that the orbiter and external tank separate under aerodynamic loading with a significant amount of propellant remaining in the ET. The typical separation sequence is as follows:

<u>Time</u>	<u>Event</u>
MECO - 10 sec	<ul style="list-style-type: none"> <li>• Begin pitchdown, from angle of attack <math>\geq 40^\circ</math></li> <li>• Using thrust vector control and aft RCS, achieve an angle of attack of <math>-4^\circ</math></li> </ul>
MECO	<ul style="list-style-type: none"> <li>• Main orbiter engine cutoff</li> <li>• Coast <math>\approx 7</math> sec using RCS to maintain attitude</li> </ul>
MECO + 7 sec	<ul style="list-style-type: none"> <li>• Separation of orbiter/ET using all downfiring orbiter RCS thrusters to move the orbiter away from the ET</li> </ul>

During the separation sequence, the ET nominally contains a 2% volume of liquid oxygen (LOX). This is approximately  $11.0 \text{ m}^3$  (12,628 kg). The LOX feedline is also full at this time. The liquid hydrogen tank in the ET also contains a residual volume, but its impact due to propellant motion is small in comparison to the LOX tank.

After MECO, during the 7 sec coast, the combined orbiter/ET decelerates due to aerodynamic drag at approximately 0.005 to 0.015g's. This deceleration results in reorientation of the residual propellant, toward the nose of the ET. At separation, clearance between the orbiter and ET is primarily achieved by aerodynamics acting to move the ET away from the orbiter. The deceleration of the ET increases to approximately 0.03g upon separation. The transient interaction forces between the ET and the moving residual propellant can drastically affect ET motion after separation; possibly resulting in ET/orbiter collision.

Analytical studies at JSC indicate possible orbiter/ET recontact after separation. However, no empirical data has existed to verify JSC's analytical model. This report details Phase I of a study to analytically and experimentally investigate Space Shuttle propellant dynamics during the RTLS separation. The overall objectives of the

ORIGINAL PAGE IS  
OF POOR QUALITY.

study are: 1) to develop an experimental data bank on which to base a mechanical analog which simulates large amplitude propellant reorientation during the RTLS abort separation; and 2) to develop the technique to analytically simulate the interaction forces between the ET and reorienting propellant in full-scale simulations.

Phase I of this study was performed between April 1977 and February 1978. In this phase thirty-two tests were conducted in Martin Marietta's Drop Tower Test Facility utilizing two 1/60<sup>th</sup> scale models of the ET LOX tank: one with internal baffles, and one without. During the tests, small biaxial accelerations were applied to the tanks simulating aerodynamic deceleration of the ET during the RTLS separation sequence. The resulting propellant reorientation was photographed at 200 frames/sec and reorientation forces exerted on the tank were measured by crystal load cells. Appropriate scaling was performed to insure that the test results were representative of the full-scale RTLS abort propellant reorientation. Chapter II details the experimental phase of this study, including scaling, test conditions, and data reduction techniques.

Tests were conducted both with and without LOX tank baffles in order to facilitate analytical model development and to assess the effect of baffles on reorientation. In addition a limited number of tests were performed simulating inflow from the LOX feedline. The test data was reduced to engineering units and analyzed to determine scaling validity, and applicability of JSC's mechanical analog. Three test liquids were employed in the testing: FC114B2, FC43, and Hexane. Chapter III presents the results of the study including observations on the liquid motion and scaling, effects of the baffles, and analytical correlations using a model similar to JSC's SVDS simulation computer code.

Chapter IV presents the conclusions of the study along with recommendations for Phase II.

## II. EXPERIMENTAL INVESTIGATION

---

Propellant motion representative of that which would occur in the LOX tank, as the external tank separates during an RTLS abort, was simulated during the experimental investigation. The full-scale conditions were scaled so that representative propellant motion could be produced in a subscale tank, using Martin Marietta's Drop Tower Test Facility. The primary objective of the test program was to acquire data on the characteristics of propellant reorientation in the LOX tank and the interaction forces applied to the tank by the moving propellant. The tests also demonstrated the influence of various parameters, such as the internal baffles and feedline draining, on the motion of the liquid. This chapter details the experimental investigation.

### A. SCALING ANALYSIS

During the RTLS separation maneuver, the external tank experiences axial and lateral accelerations due to aerodynamic forces. The accelerations are indicated as  $A_x$  and  $A_z$  in Figure II-1, with respect to the X and Z axes of the orbiter. The initial position of the residual liquid oxygen is established by the direction of the main engine thrust vector and is oriented at an angle  $\gamma$  to the X axis. The following values for each of these variables defined the full-scale conditions that were considered in the test program:

$$A_x = 0.015g \text{ and } 0.030g$$

$$A_z = 0.005g, 0.015g \text{ and } 0.030g$$

$$\gamma = 0^\circ, 13^\circ, \text{ and } 30^\circ$$

Propellant volume = 2%, 5%, 10% and 15%.

A dimensional analysis of the variables related to liquid reorientation in a container yields the following dimensionless groups that characterize the motion:

$$Fr = \frac{V}{\sqrt{Ar}} \quad (\text{Froude number}); \text{ ratio of inertia to gravity force}$$

$$Bo = \frac{\rho Ar^2}{\sigma} \quad (\text{Bond number}); \text{ ratio of gravity to surface tension force}$$

$$Re = \frac{\rho Vr}{\mu} \quad (\text{Reynolds number}); \text{ ratio of inertia to viscous force}$$

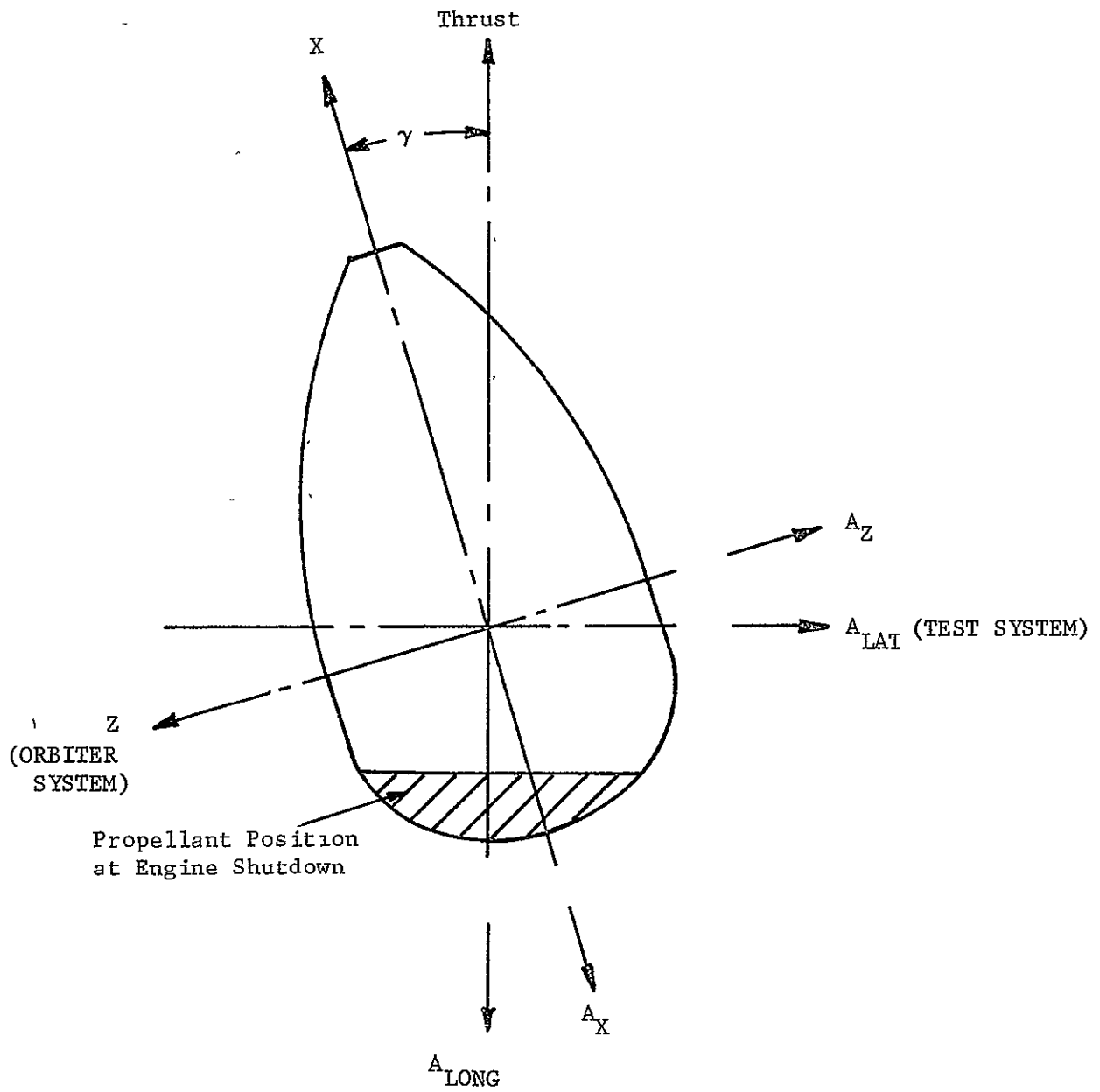


Figure II-1. Orientation of Tank Axes

ORIGINAL PAGE IS  
OF POOR QUALITY

The Froude number can be related to the two other dimensionless groups.

$$Fr = f (Bo, Re)$$

Based on numerous liquid reorientation tests, empirical coefficients have been established so that the above relationship can be expressed as (Reference 1):

$$Fr = K_{Re} \left\{ 0.48 \left[ 1 - \left( \frac{0.84}{Bo} \right)^{\frac{Bo}{4.7}} \right] \right\}$$

Considering only the relationship between the Froude number and Bond number, their variation is shown graphically in Figure II-2. It can be seen that the Froude number is constant if the Bond number is greater than 10. This implies that surface tension forces are negligible, in comparison to the inertia and gravity forces, when Bo is greater than 10. The factor  $K_{Re}$  in the equation accounts for viscous effects as a function of the Reynolds number. The variation of  $K_{Re}$  is shown in Figure II-3. If the Reynolds number is greater than 50, viscous effects are negligible. Therefore, this correlation indicates that for any propellant reorientation which has a Bond number greater than 10 and a Reynolds number greater than 50, scaling can be based on Froude number alone.

As will be shown later, the above requirements for Bo and Re were satisfied for the propellant reorientation conditions in both the full-scale and model tanks. Froude number can be used to scale between the two cases.

$$Fr_p = Fr_m$$

The subscript "p" refers to the prototype or full-scale tank and the subscript "m" refers to the model. Therefore, equating Froude numbers:

$$\frac{V_p}{\sqrt{A_p r_p}} = \frac{V_m}{\sqrt{A_m r_m}}$$

Since velocity is proportional to the product of acceleration and time,

$$\frac{t_p}{t_m} = \sqrt{\frac{A_m r_p}{A_p r_m}}$$

ORIGINAL PAGE IS  
OF POOR QUALITY

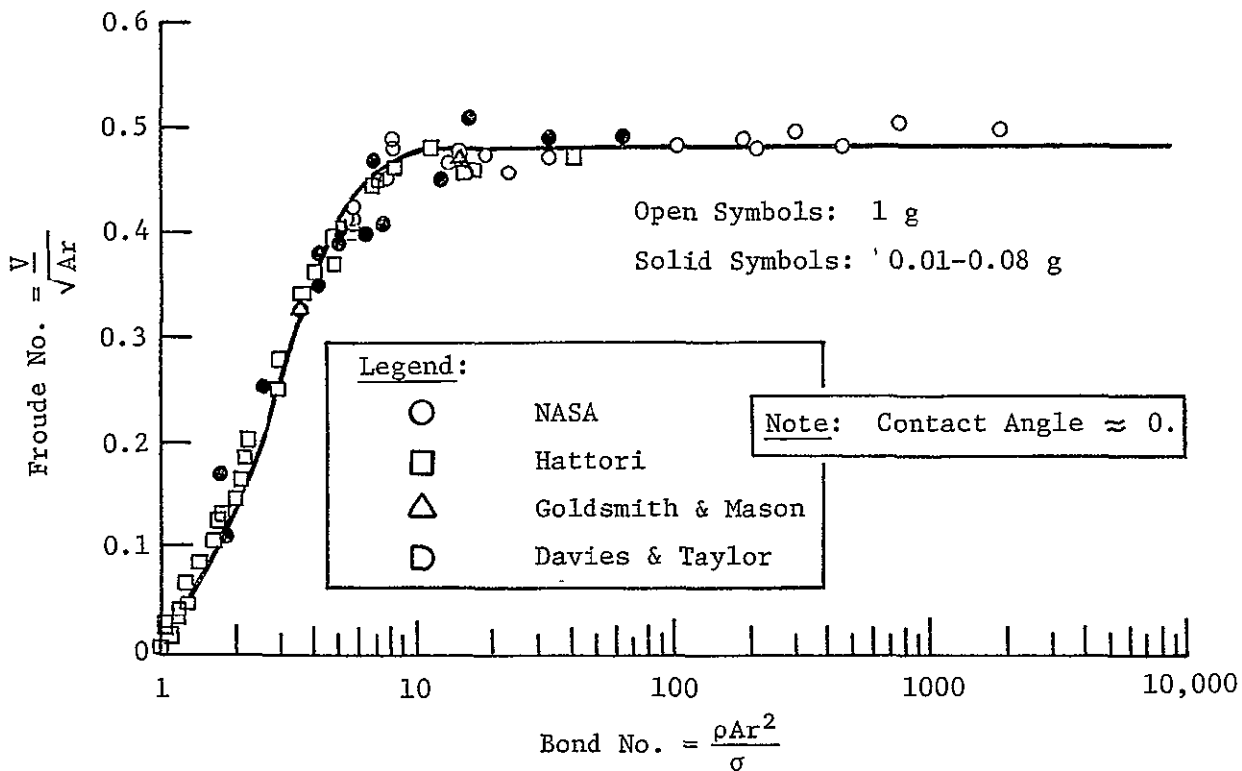


Figure II-2. Froude/Bond Number Relationship (from Reference 1)

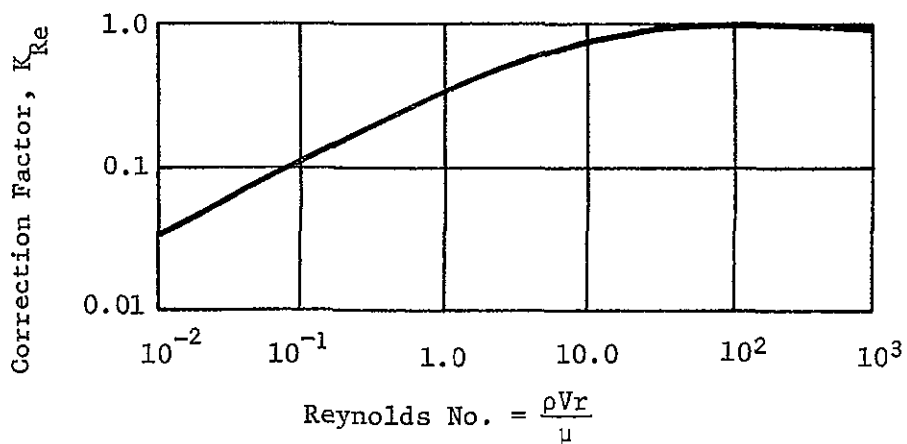


Figure II-3. Effect of Reynolds Number (from Reference 1)

The preceding equation yields the time scaling for a selected dimensional scaling and the ratio of prototype to model accelerations. It is independent of the liquid properties.

The propellant motion was simulated using Martin Marietta's Drop Tower Test Facility. The facility imposes limits on the values of  $t_m$ ,  $A_m$  and  $r_m$ , in establishing the time scaling for the tests. In order to make the time scaling ratio as large as possible ( $t_p$  large),  $A_m$  should be large. A large value of  $A_m$  increases the forces applied to the model, making them easier to measure. However, large values for the model acceleration, limit the test time because the drop capsule is accelerated with respect to a drag shield; the travel distance is fixed. A value of 0.09g is a practical upper limit for  $A_m$  and will still provide approximately 1.6 seconds of model test time.

A number of factors influence the selection of the value of  $r_m$ , which determines the dimensional scaling of the model. A small value of  $r_m$  would help to make the simulated period time ( $t_p$ ) large. On the other hand, a large value of  $r_m$  will improve the force resolution since the liquid volume is increased. The value of  $Re$  is directly proportional to  $r_m$  and  $Bo$  is proportional to  $r_m^2$ , so increasing  $r_m$  helps to make both numbers larger.

Since the LOX tank is so large and force resolution was important, as large a value as possible for  $r_m$  was selected. Only minor modifications to the existing test fixture were permitted, so the maximum value of  $r_m$  that could be obtained was 7.0 cm; the tank barrel section radius. The tank dimensional scaling is therefore, 60:1 ( $r_p/r_m$ ).

More than adequate scaling of time was possible with the selected values of  $A_m$  and  $r_m$ . Considering the axial accelerations, the full-scale time period that was simulated ( $t_p$ ) was 30.4 seconds, when  $A_p$  was 0.15g, and was 21.5 seconds when  $A_p$  was 0.030g. The significance of this time period can be appreciated by considering the amount of time required for the propellant to move from its initial position to the other end of the tank. This period is approximately equal to the time required for an object to free-fall the tank length. The free-fall time is 10.1 seconds in the full-scale tank at 0.030g and 14.3 seconds at 0.015g. For the model tank this period is 0.75 seconds at 0.09g. This comparison indicates that the liquid will be reoriented to the other end of the tank during the test, simulating the period during which the forces of the liquid on the tank are the most significant. Complete, quiescent collection of the liquid at its final equilibrium position was not possible during this test period.

The liquid properties enter into the scaling in assuring that the Bond number and Reynolds number are sufficiently large. A very dense liquid helps to make both  $Re$  and  $Bo$  large, and also assures that the forces due to a given volume of liquid will be large. Low surface tension and viscosity are also desirable.

Three different liquids were used in the testing: fluorocarbon (FC) FC-43, FC-114B2, and hexane. The properties of these liquids, along

with those of the liquid oxygen they simulate, are listed in Table II-1. The two fluorocarbons have very high densities and low surface tensions, which improve the scaling. The FC-43 has a viscosity that is almost nine times that of FC-114B2, so the two liquids offer a good comparison of the influence of viscous effects. The FC-114B2 has a kinematic viscosity that is close to the lower limit for liquids. Hexane has a kinematic viscosity that places it in between FC-43 and FC-114B2, in terms of Reynolds number and the influence of viscous effects. Another important parameter that can influence the liquid motion is the contact angle formed by the liquid and the tank wall. All the test liquids have near zero contact angles, as does oxygen, indicating that the liquid wets the wall.

FC114B2 was selected as the primary test liquid, due to its ideal properties. Several tests were repeated using FC-43, to evaluate viscous effects. One test was conducted using the hexane, also to evaluate viscous effects.

Having selected the test system parameters, the premise that  $Bo$  and  $Re$  be sufficiently large can now be verified. Listed in Table II-2 are the calculated values for these numbers for the full-scale tank and for each of the test liquids in the model tank. In order to specify  $Re$ , the value to be used for the velocity must be defined. A representative velocity is the free-fall velocity based on the tank length, which would approximate the maximum velocity achieved by the liquid as it first moves to the other end of the tank.

As shown by the values in Table II-2, the basic requirements, that  $Bo$  be greater than 10 and  $Re$  greater than 50, have been satisfied. The influence of  $Bo$  is exponential in nature. Small changes in  $Bo$  can produce significant changes in the reorientation when  $Bo$  is less than 10 (Reference 6). At  $Bo$  greater than 10 the influence of surface tension forces is small. When  $Bo$  exceeds 100 they are much less and they should be completely negligible at  $Bo$  greater than  $10^3$ . At a  $Bo$  of 500 (model conditions) the primary influence of surface tension forces is some cohesiveness of the surface. At  $Bo$  of  $10^3$  and greater (full-scale conditions), any remaining cohesiveness of the surface would be lost. More breakup of the surface would occur during reorientation in the full-scale tank in comparison to reorientation in the model. When axisymmetric reorientation occurs at large  $Bo$  ( $>10^3$ ), the liquid motion has the form of rain. However, with off-axis acceleration, as is the case being simulated here, the lateral acceleration component acts to hold the liquid mass together as it moves along the walls of the tank. This type of motion has been demonstrated at  $Bo$  of up to  $6 \times 10^3$  under both axisymmetric and off-axis reorientation conditions (Reference 7).

## B. EVALUATION OF FEEDLINE DRAINING

Following the shutdown of the main engines, the LOX tank feedline is full of propellant. The volume of this line ( $\sim 0.9\%$  of tank volume) is significant in comparison to the small volume of propellant that will

ORIGINAL PAGE IS  
OF POOR QUALITY

TABLE II-1. Liquid Properties

Liquid	Density (grams/cm <sup>3</sup> )	Surface Tension (dynes/cm)	Viscosity (cp)
Oxygen (-163°C) (Refs 2 and 3)	1.14	13.5	0.195
FC-43 (20°C) (Ref 4)	1.91	16.7	6.5
FC-114B2 (20°C) (Ref 5)	2.18	18.8	0.75
Hexane (20°C) (Refs 2 and 3)	0.66	18.4	0.33

TABLE II-2. Dimensionless Parameters

Conditions	Bond Number	Reynolds Number
<u>Full-Size Tank, Oxygen</u>		
$A_p = 0.015g$	$4.39 \times 10^5$	$7.31 \times 10^7$
$A_p = 0.030g$	$2.19 \times 10^5$	$5.17 \times 10^7$
<u>Model Tank, <math>A_m = 0.09g</math></u>		
FC-43	491	$1.36 \times 10^4$
FC-114B2	449	$1.35 \times 10^5$
Hexane	154	$9.30 \times 10^4$

ORIGINAL PAGE IS  
OF POOR QUALITY

remain in the tank at separation. If complete draining of the line could occur as the propellant was reorienting, the mass and, therefore, the forces due to the motion would be increased. An evaluation of the feedline draining was performed to determine if draining will occur and if so, how much propellant will drain from the line.

The line is closed at the engine valve and the axial drag acceleration is acting to make the propellant drain back into the tank. If the acceleration, line diameter and liquid surface tension are such that a stable gas-liquid interface can exist in the feedline, no draining of the line will occur. During RTLS separation, however, the interface is unstable; hence, the residual LOX will "fall" out of the feedline. The filter screen over the tank outlet has pores small enough to allow a stable interface. However, the lateral acceleration that will be acting parallel to this screen will produce hydrostatic pressure differentials that will far exceed the pressure retention capability of this screen. Propellant will drain from the feedline due to the combined action of the lateral and axial acceleration components.

Since the line is closed at the other end, gas must enter the line before liquid can leave. Large gas bubbles will enter the line producing "slug" flow. Empirical correlations for the buoyant rise of such bubbles have been derived (Reference 8) to predict the velocity of the entering gas.

$$V_{\text{gas}} = K (AD)^{\frac{1}{2}}$$

The value used for K is a function of the Reynolds number and Bond number of the liquid in the line. For the conditions being considered here (liquid oxygen, A = 0.015 to 0.030g, D = 43.2 cm) the coefficient has the maximum possible value of 0.345.

As the gas enters along the center of the line, a layer of liquid flows out along the wall. It is conservatively assumed that the layer of liquid is moving at the free fall velocity, that is

$$V_{\text{liquid}} = At$$

The flow resistance of the screen filter has also been neglected. By applying continuity, an expression for the flow rate can be derived,

$$Q = \frac{D^2}{4} \left( \frac{V_{\text{gas}} V_{\text{liquid}}}{V_{\text{gas}} + V_{\text{liquid}}} \right)$$

When this equation is solved as a function of time for the condition that would produce the maximum flow rate ( $A = 0.030g$ ), the flow rate is found to become constant at  $0.017 \text{ m}^3/\text{sec}$  after a period of 5 seconds. Flowing at this rate for 15 seconds, a volume of  $0.26 \text{ m}^3$  of LOX would leave the line. This volume is 0.05% of the tank volume and would drain only 5% of the liquid in the line.

This conservative analysis indicates that draining of liquid from the feedline will have a negligible effect on the propellant reorientation. Regardless, a few tests, in which the inflow of liquid from the feedline was simulated, were added to the test matrix. The approach was to inflow as much liquid as possible to determine what effect on the reorientation there might be. Scaling the feedline volume to the model size gives  $22 \text{ cm}^3$ . Complete emptying of the line during the test ( $\sim 1.6 \text{ sec}$ ) would require a flow rate of about  $14 \text{ cm}^3/\text{sec}$ . Inflow rates close to this magnitude were simulated during 5 of the tests performed.

### C. TEST SYSTEM DESCRIPTION

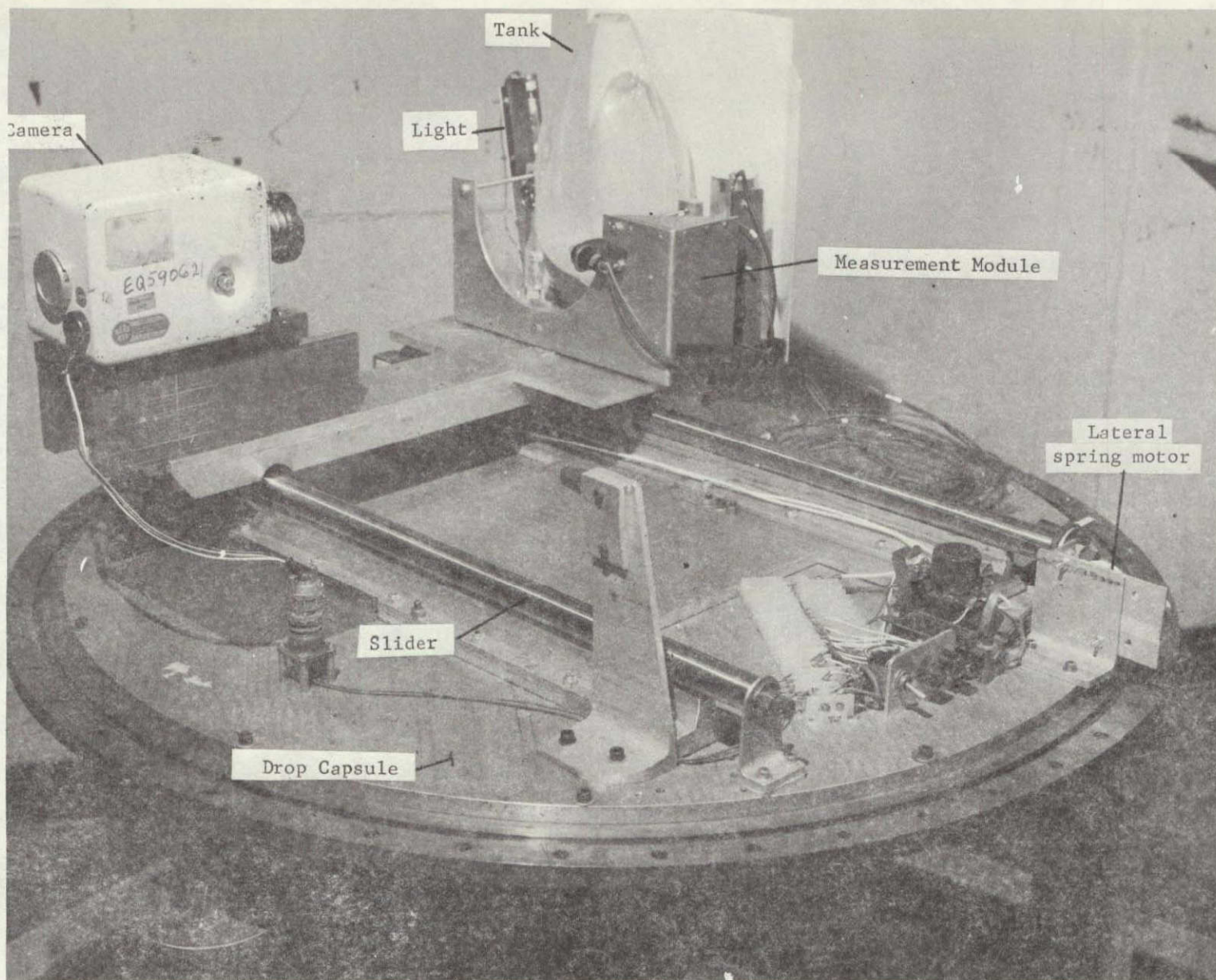
Martin Marietta's Drop Tower Test Facility was used to produce the required subscale model test conditions. This facility was developed under numerous prior test programs to be able to simulate low-g environments, and to record the motion of the liquid and the forces due to this motion. Only minor modifications were required to perform this test program.

#### 1. Test Module

The test module consists of the tank, force measuring module and a slider mechanism. The test module is shown mounted on the drop capsule in Figure II-4. Figure II-5 is a closer view of the module in which the load cells are mounted. The calibration fixture is shown installed in place of the tank.

The tanks were  $1/60^{\text{th}}$  scale models of the actual liquid oxygen tank. Figure II-6 delineates the model tank design. Two tanks were constructed; one tank had no baffles (Figure II-7), the other tank had slosh and anti-vortex baffles installed (Figures II-8 and II-9). These baffles were simplified somewhat for the models, but the key characteristics that influence the liquid motion (e.g., ring size and wall spacing) were maintained. The tanks were pressure formed in two halves using clear plastic sheet. The baffles were cut from thin plastic sheet. A support ring allowed the tank to be mounted in the measurement module at the required angle of orientation.

Three force links, two vertical and one lateral, allowed all the forces acting on the tank to be measured. Bearings at each end of the links permitted only forces along the link axis to be measured. Three flexures, perpendicular to the plane of the force links, prevent any out of plane motion of the tank. The spring constant of the flexures



ORIGINAL PAGE IS  
OF POOR QUALITY

Figure II-4 Test Module

ORIGINAL PAGE IS  
OF POOR QUALITY

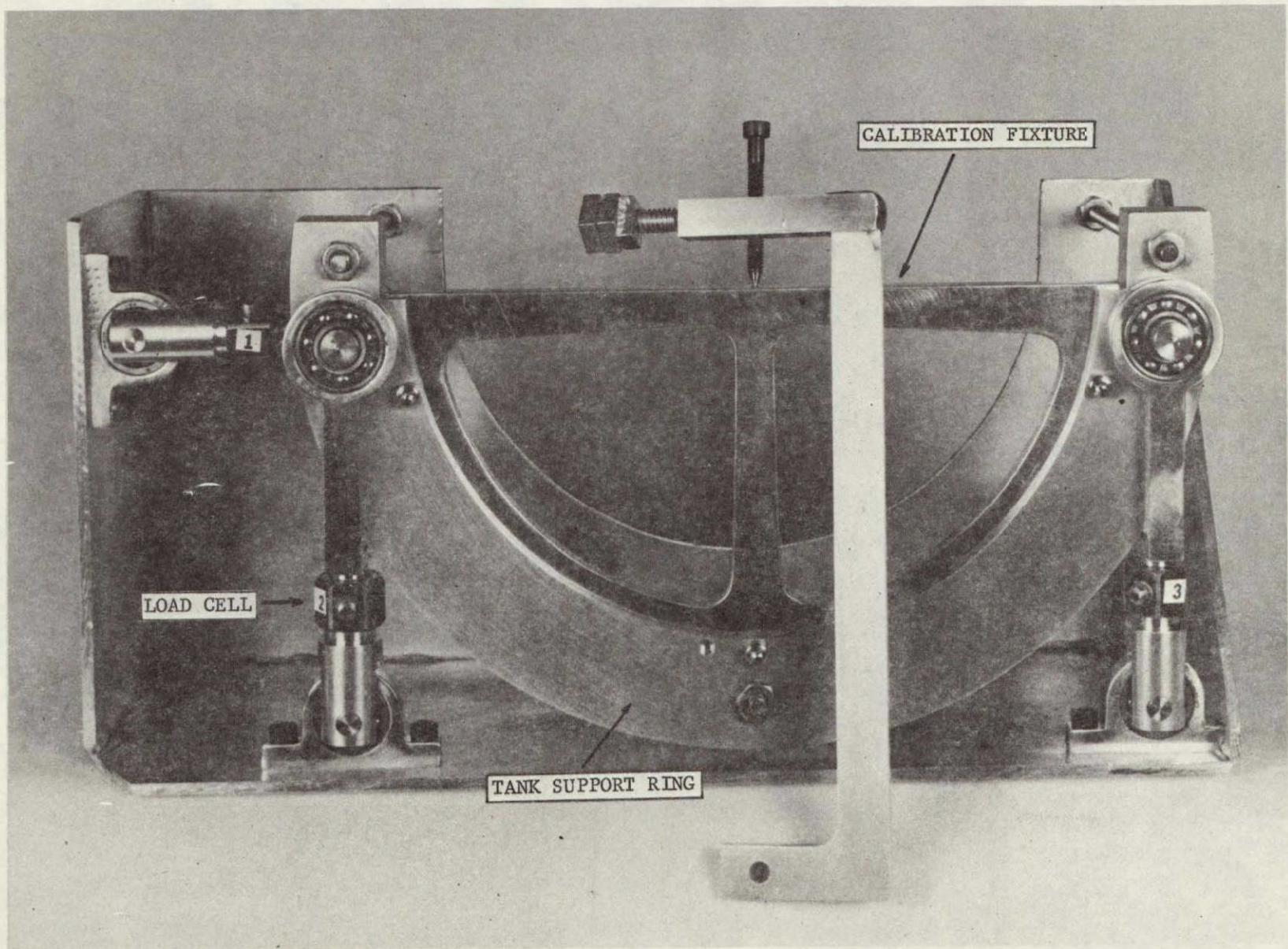
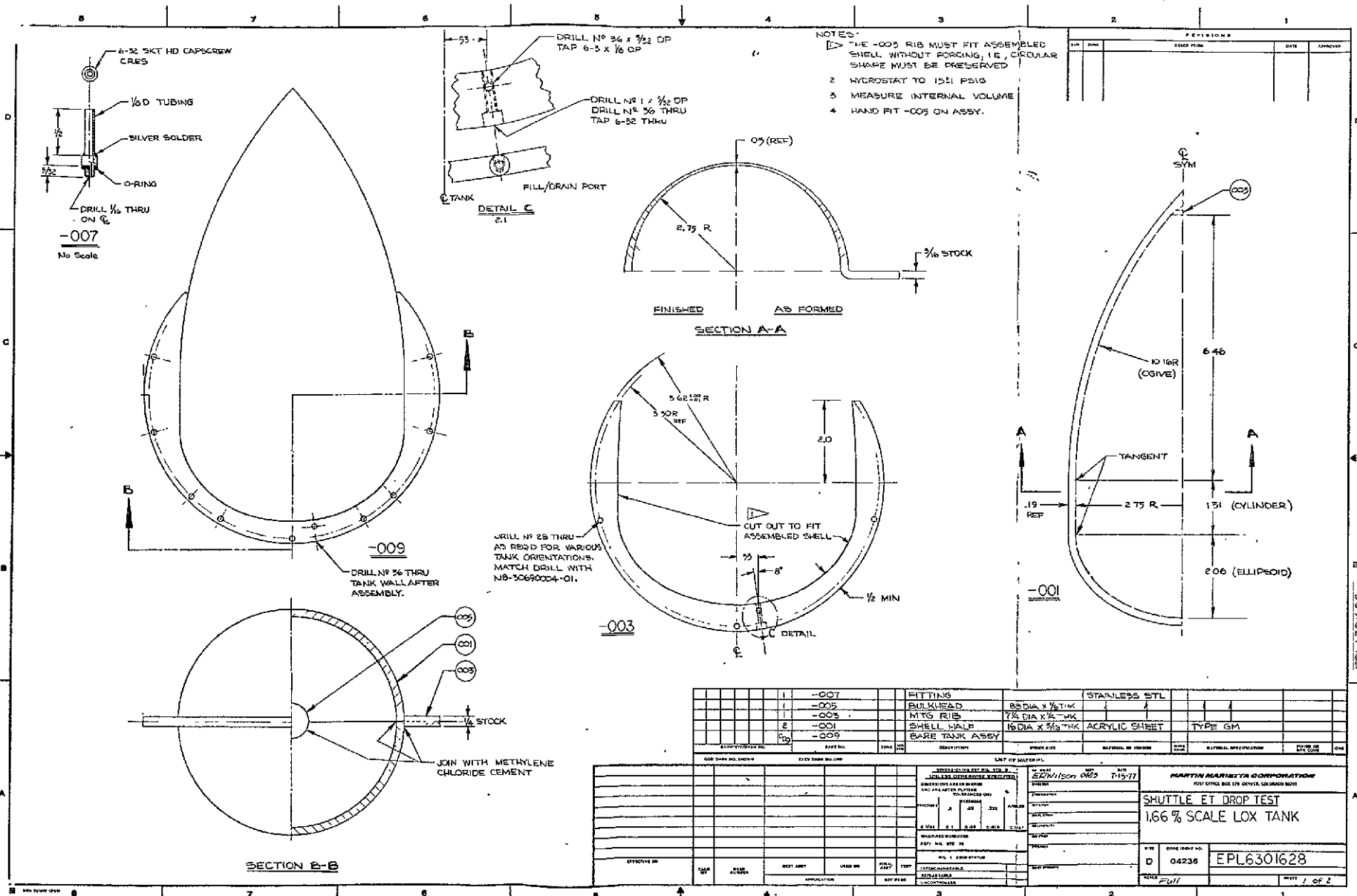


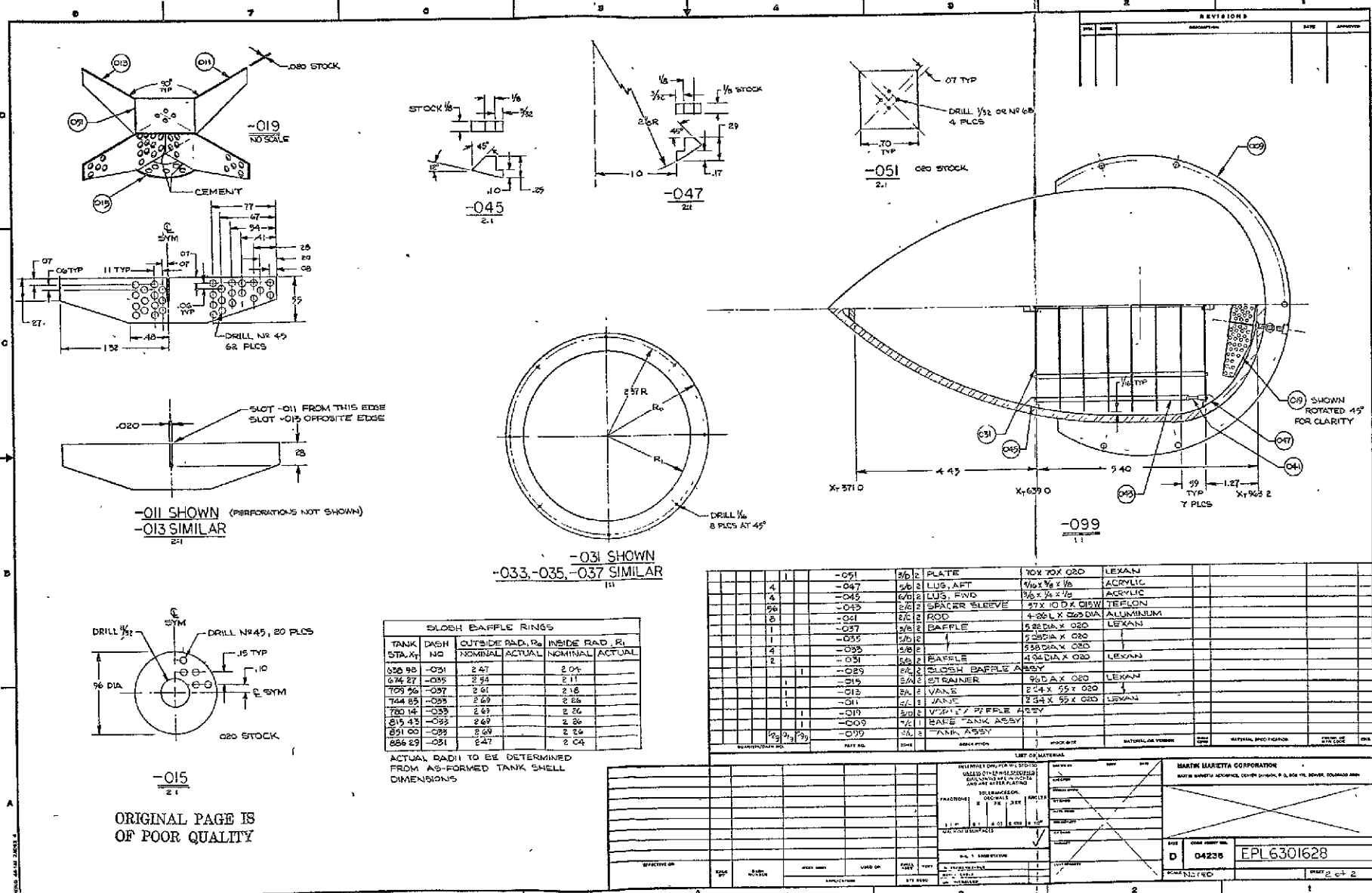
Figure II-5 Force Measurement Module with Calibration Fixture Installed



ORIGINAL PAGE IS OF POOR QUALITY

ORIGINAL PAGE IS OF POOR QUALITY

FIGURE II-6. 1/60 th SCALE MODEL DESIGN

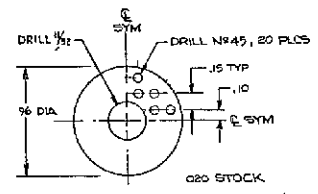


REVISIONS			DATE	APPROVED

TANK STA. #	DASH NO	OUTSIDE RAD. R <sub>o</sub> NOMINAL	ACTUAL	INSIDE RAD. R <sub>i</sub> NOMINAL	ACTUAL
626 95	-031	2.47		2.04	
624 27	-035	2.54		2.11	
703 26	-037	2.61		2.18	
744 05	-038	2.68		2.25	
780 14	-039	2.67		2.24	
815 43	-033	2.67		2.24	
851 00	-035	2.67		2.24	
856 29	-031	2.47		2.04	

ACTUAL RADII TO BE DETERMINED FROM AS-FORMED TANK SHELL DIMENSIONS

QTY	DESCRIPTION	UNIT	MATERIAL	REMARKS
4	-051	5/8" PLATE	70X 70X 020 LEXAN	
4	-047	2 LUG, APT	1/16 X 1/8 X 1/8 ACRYLIC	
4	-045	2 LUG, FWD	3/8 X 1/8 X 1/8 ACRYLIC	
2	-043	2 BRACER BLEWIE	2" X 1" O.D. X 0.010" TEFLON	
1	-041	1 ROD	4-20 L X 020 DIA ALUMINUM	
1	-037	1 BAFFLE	5.28 DIA X 020 LEXAN	
1	-035	1 BAFFLE	5.08 DIA X 020 LEXAN	
4	-033	4 BAFFLE	5.58 DIA X 020 LEXAN	
2	-031	2 BAFFLE	4.94 DIA X 020 LEXAN	
1	-029	1 SLOSH BAFFLE ASSY		
1	-019	1 STRAINER	3.02 L X 020 LEXAN	
1	-015	1 VANE	2.41 X .65 X 020 LEXAN	
1	-011	1 JAW	2.24 X .55 X 020 LEXAN	
1	-009	1 TANK ASSY		



-015  
2.1

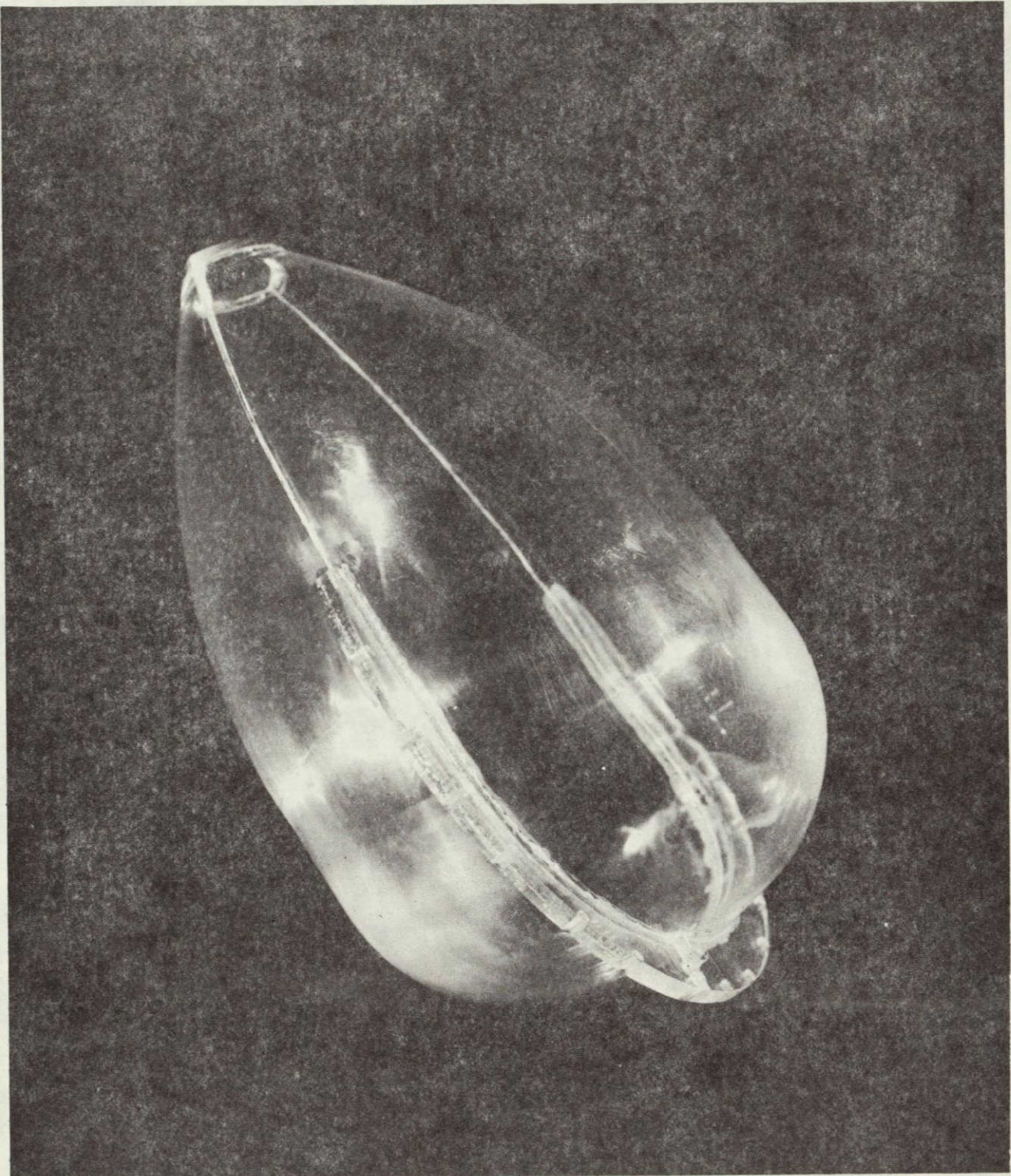
ORIGINAL PAGE IS OF POOR QUALITY

DATE	BY	CHKD	APP'D	REVISION

INTELLECTUAL PROPERTY RIGHTS RESERVED UNLESS OTHERWISE SPECIFIED THIS DOCUMENT IS UNCLASSIFIED DATE 08-14-2011 BY 60322 UCBAW/BJS	LIST OF MATERIALS PART NO. 04235 QUANTITY 1 UNIT 1 DESCRIPTION TANK ASSY	MATERIAL SPECIFICATION PART NO. EPL6301628 QUANTITY 1 UNIT 1 DESCRIPTION TANK ASSY
--	--	--

FIGURE II-6 (CONCLUDED).



*Figure II-7 Unbaffled Tank*

ORIGINAL PAGE IS  
OF POOR QUALITY

This Page Intentionally Left Blank

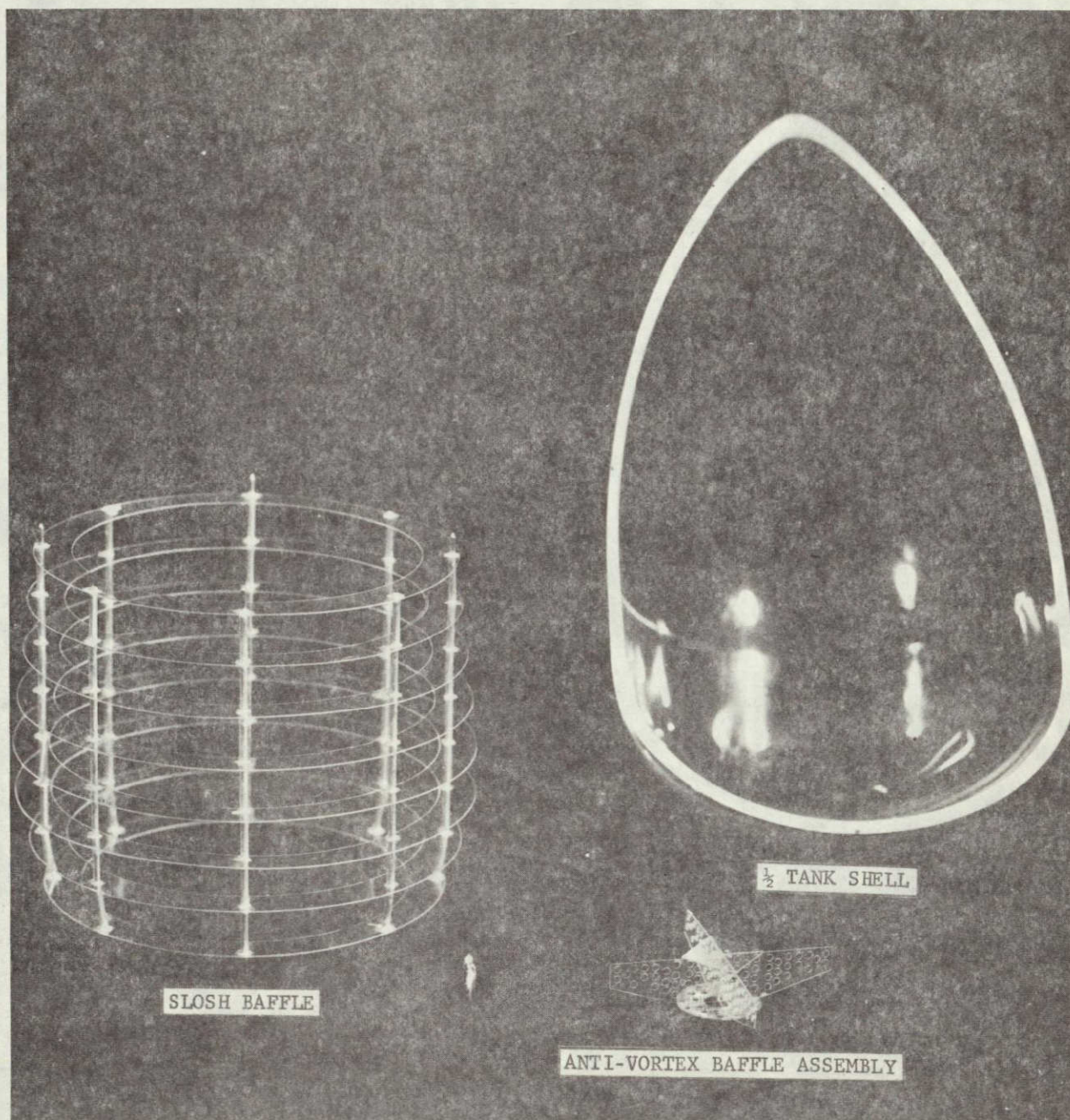
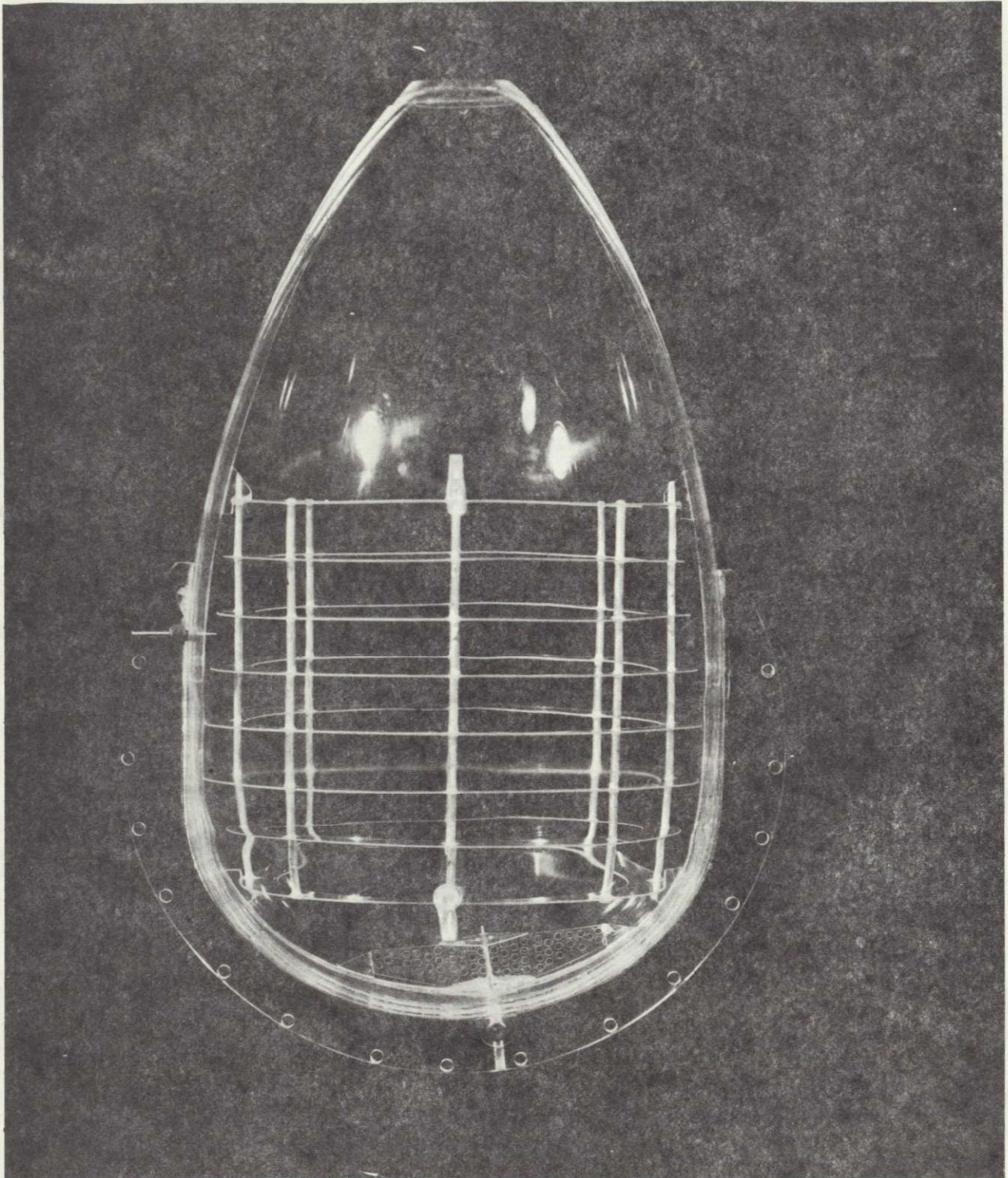


Figure II-8 Baffled Tank Prior to Assembly



*Figure II-9 Baffled Tank*

ORIGINAL PAGE IS  
OF POOR QUALITY

is much less than the spring constant of the load cells, so they do not significantly alter the forces measured by the load cells.

Linear bearings ride on two rails to provide lateral travel. An electric solenoid releases the slider at the beginning of the test, and the slider is accelerated with a constant force spring motor. A time delay relay was added to the circuit for those tests in which the application of the lateral acceleration was delayed.

The inflow of test liquid was achieved with a spring operated piston. The piston was filled and the spring compressed with a solenoid valve holding the system in this state. At the beginning of the test, the solenoid valve was opened with the same electrical signal that starts the slider. The flow from the piston was controlled by a metering valve and then entered the tank through a port at its outlet. The volumetric flowrate was set and verified prior to each test.

## 2. Drop Test Facility

The complete drop capsule is shown in Figure II-10. A simple frame is mounted over the test module to protect the instrumentation. The inflow system can be seen mounted on top of this frame. The spring motors that produce the axial acceleration of the drop capsule and a crush tube are mounted on the conical base of the drop capsule.

The total drop test system is illustrated in Figure II-11. The cable from the axial spring motor was extended and secured to the bottom of the drag shield. After releasing the drag shield from the top of the 23-meter drop tower, the slider release and inflow system were actuated. Both the lateral and axial spring motors accelerated the test module throughout the drop test. The drop capsule impacts the drag shield, with the crush tube absorbing the impact, and the drag shield lands in a bin of wheat at the end of the test. Figure II-12 is a photograph of the drop test facility.

## 3. Instrumentation

The motion of the liquid was recorded with a 16-mm Milliken DBM-3a camera mounted on the slider. The film speed was 200 frames per second (+0, -5%). Immediately before the drag shield was released, the camera was started and it was automatically stopped when the drag shield impacted the wheat.

Quartz crystal load cells (Kistler Model 912) were used to measure the liquid forces. These load cells have a capacity of 2220N in tension and 22200N in compression, providing the capability of withstanding the impact at the end of the test. Peak, high frequency accelerations of up to 160g have been measured at impact. Due to their high degree of linearity, these load cells are fully capable of measuring the small forces due to the liquid motion.

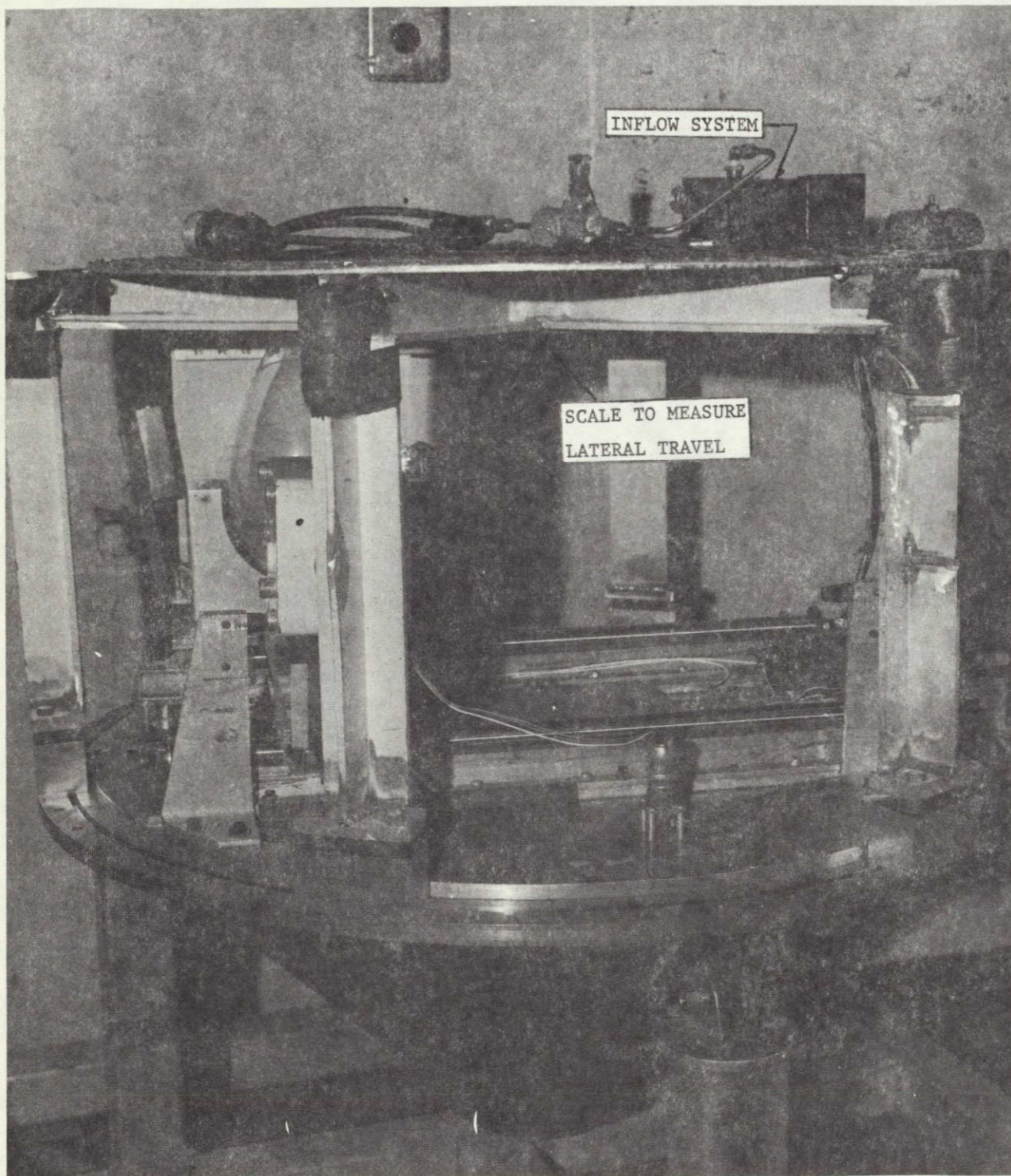


Figure II-10 Complete Drop Capsule

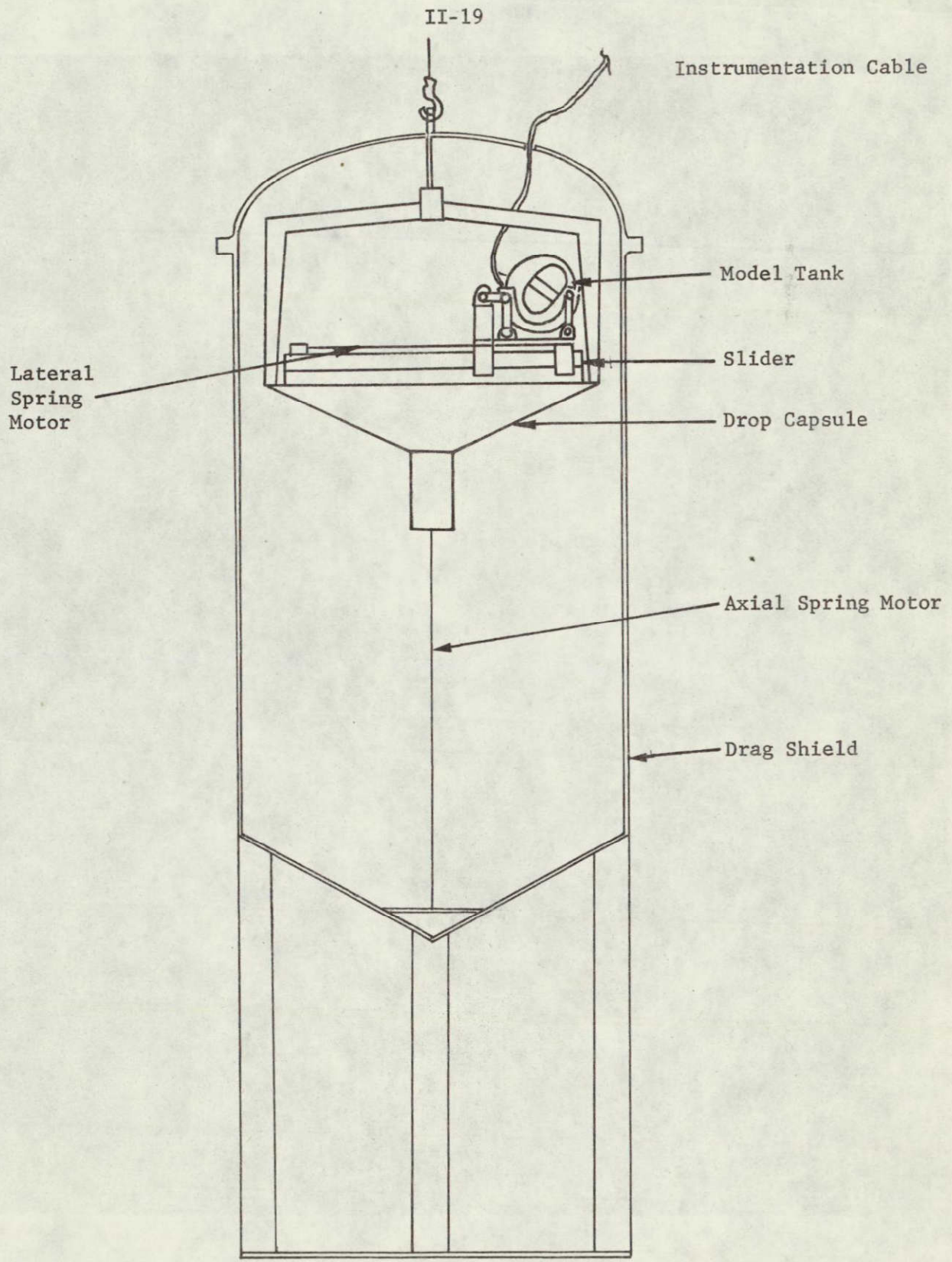
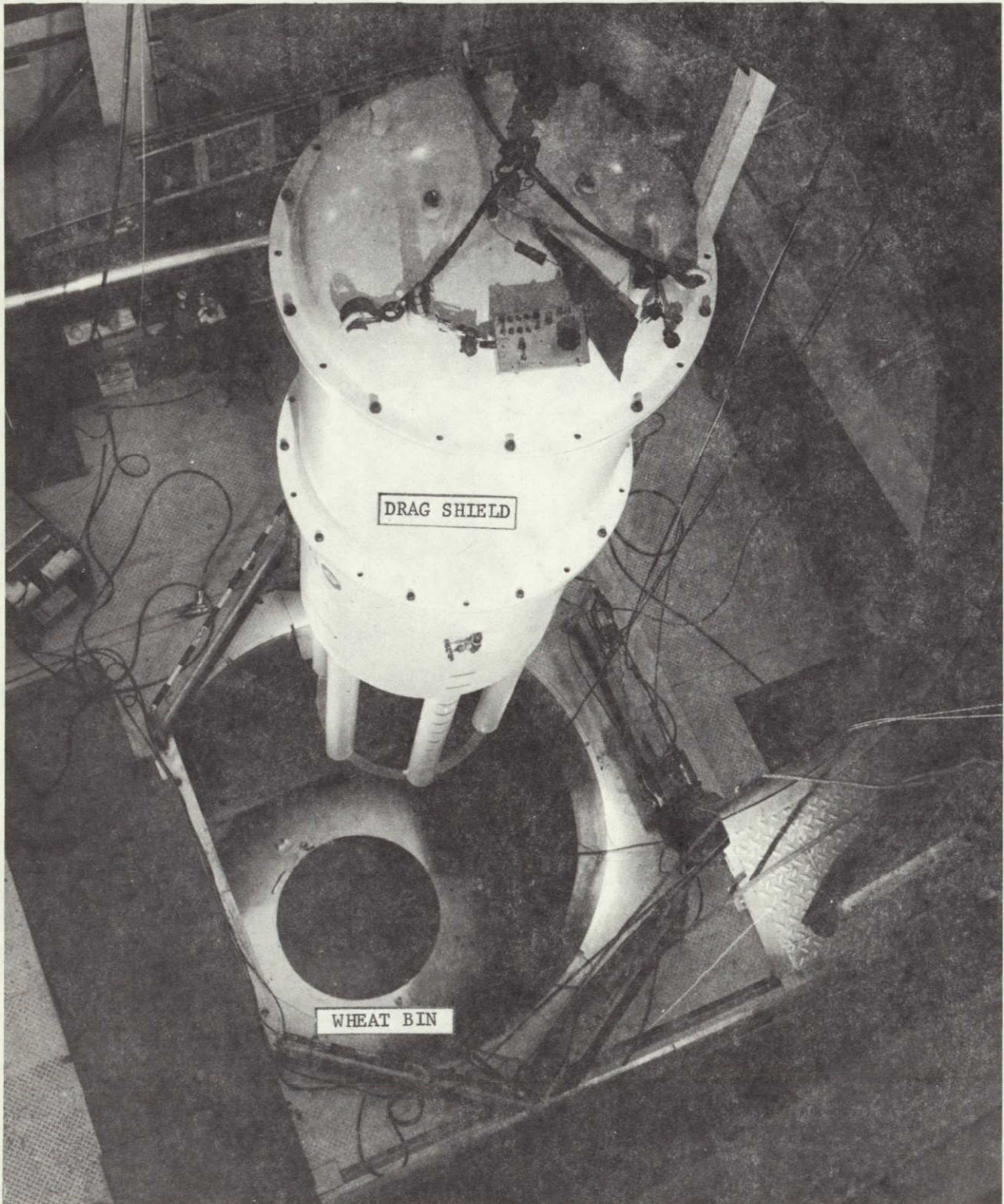


FIGURE II-11. Complete Drop Test System

ORIGINAL PAGE IS  
OF POOR QUALITY



*Figure II-12 Drop Test Facility*

The load cells were mounted in the force measuring links. Low noise cables were used to feed the output of the load cells to charge amplifiers. The charge amplifiers were located about halfway up the drop tower to minimize the motion of the cable as the drag shield falls. The amplifiers were set on long time constant and the most sensitive scale that could be accommodated, to measure the low amplitude and low frequency forces. Each charge amplifier input was momentarily grounded prior to the test, so all forces were measured with respect to zero at one-g.

The output of the charge amplifiers was fed in parallel to both a tape recorder and a chart recorder. In order to eliminate the noise produced by vibration of the camera motor, a 10 Hz low-pass filter was used in the chart recorder amplifier. An end-to-end calibration of the force measuring system was accomplished with the fixture shown in Figure II-5. Known weights were suspended from the hook at various positions with respect to the force links, and the charge amplifiers were adjusted to give the proper output.

An indicator light, that comes on at the start of the test, and a scale, both in the field of view of the camera, aid in determining the timing and lateral test accelerations. A 100 Hz signal from a time code generator was also recorded to provide a time base.

#### D. TEST CONDITIONS

Test conditions were chosen to simulate full-scale conditions during the RTLS abort. The following table delineates the accelerations on the ET during mated coast and after separation.

Sequence	ET Accelerations	
	$A_x$ (g's)	$A_z$ (g's)
Mated Coast	0.015	0.005
After Separation	0.03	0.03

Constant force spring motors were selected, based on the scaling analysis, to accelerate the model tanks. Accelerations applied to the model tanks are designated  $A_{long}$  and  $A_{lat}$  in Figure II-1. These accelerations are applied in the drop capsule coordinate system whereas the full-scale ET accelerations ( $A_x$  and  $A_z$ ) in the above table, are shown in the orbiter coordinate system (Figure II-1). The following equations transform the orbiter accelerations to the test coordinate system:

$$A_{long} = A_x \cos \gamma - A_z \sin \gamma$$

$$A_{lat} = A_x \sin \gamma + A_z \cos \gamma$$

ORIGINAL PAGE IS  
OF POOR QUALITY

During mated coast  $A_x/A_z \approx 3$ , and after separation  $A_x/A_z \approx 1$ , as seen from the preceding table. Transforming these ratios to the test coordinate system, by the above equations, and assuming,  $\gamma_{\text{nominal}} = 13^\circ$ ,  $A_x=1$ , yields;

Sequence	$A_{\text{long}}$	$A_{\text{lat}}$	$A_{\text{long}}/A_{\text{lat}}$
Mated Coast	0.90	0.55	1.64
After Separation	0.75	1.20	0.62

Due to drop tower restrictions and the desire to optimize force resolution and time scaling, these ratios of  $A_{\text{long}}/A_{\text{lat}}$  were not duplicated.

As discussed in Section II.A, a large value of acceleration improves the time scaling (simulating a larger period of full-scale time) and improves the force resolution. However, the value of lateral acceleration ( $A_{\text{lat}}$ ) that can be produced in the drop tower is limited by the travel of the slider (e.g., the desired test period). Lateral accelerations greater than 0.03g result in test times less than 1.6 sec. Experience has shown that it is desirable, based on force resolution and time scaling, not to have  $A_{\text{lat}}$  greater than 0.03g. To increase force resolution, a value of 0.09g for  $A_{\text{long}}$  has been found to be optimal, resulting in  $\sim 1.6$  seconds of test time (limited by travel within the drag shield). The majority of tests utilized this ratio.

$$A_{\text{long}}/A_{\text{lat}} = 0.09/0.03 = 3.0$$

In order to evaluate the effect of acceleration ratios on the character of the propellant motion a few other test conditions were specified. In tests 27 through 30 the longitudinal acceleration was reduced by half so that the two components were close to being equal. Tests 13 and 14 had the lateral component reduced by half. In tests 15 through 18 the lateral acceleration was delayed to simulate a change in acceleration, such as that which occurs at separation.

This approach to the simulation of the actual conditions did not duplicate the actual ratio of the acceleration components. However, it did produce liquid motion that is representative of the actual conditions, which was the primary intention of the test program. As long as there is a lateral component to the acceleration, the liquid moves along the walls of the tank rather than through the center. Changing the ratio of the accelerations primarily changes the final equilibrium position for the liquid and the rate of motion, but the basic character of the motion remains the same. The results of the tests supported this approach.

In addition to acceleration components, several other parameters were varied. The angle  $\gamma$ , which determines the initial orientation of

TABLE II-3. TEST MATRIX

Test	Fluid*	Spring Motor Force ( N )		Orientation (Degrees)	Inflow	Baffled Tank	Percent Fill
		Axial	Lateral				
1	1	130	4.4	13	Y	N	2
2	2				Y	N	2
3	1				Y	Y	2
4	2				Y	Y	2
5	1				N	N	10
6	2					N	10
7	1					Y	10
8	2					Y	10
9	1					N	2
10	2					N	2
11	1					Y	2
12	2		4.4			Y	2
13	1		1.7			Y	2
14	2		1.7			Y	2
15	1		6.7(delayed 0.5 sec)			N	2
16	1					N	10
17	1					Y	2
18	1		6.7(delayed 0.5 sec)			Y	10
19	1		4.4			Y	5
20	1					Y	15
21	1					N	5
22	1			13		N	15
23	1			30		Y	2
24	1			30		N	2
25	1			30		N	10
26	1	130		30		Y	10
27	1	67		0		Y	2
28	1	67		0		N	2
29	1	67		0		Y	10
30	1	67		0	N	N	10
31	1	130		13	Y	Y	2
32	3	130	4.4	13	N	N	10

\* Fluid 1 = FC 114B2  
 2 = FC 43  
 3 = Hexane

ORIGINAL PAGE IS  
 OF POOR QUALITY

the liquid surface was varied to simulate thrust vector dispersions. Angles of  $0^\circ$ ,  $13^\circ$  and  $30^\circ$  were used. Three test liquids were used to investigate viscosity effects: FC114B2, FC-43 and hexane. Feedline draining was investigated in tests 1 through 4 and 31. Test 31 had a decreased volumetric flow rate. In addition, the tank volume was varied, using 2, 5, 10 and 15 percent fill.

The test matrix was structured so that the influence of each of these parameters could be independently evaluated. Table II-3 delineates the actual test matrix. The accelerations achieved ( $A_{long}$  and  $A_{lat}$ ) are presented in Chapter III.

#### E. DATA REDUCTION

Data reduction encompasses two areas, which will be discussed separately: 1) calculation of applied accelerations; and 2) reduction of the measured force data.

##### 1. Applied Accelerations

The drop capsule was accelerated by constant force spring motors to provide both longitudinal and lateral acceleration. The following techniques were used to calculate the average accelerations over the test period. Strip chart and photographic data was used to determine test times and lateral travel as a function of time.

Longitudinal acceleration can be calculated by considering Figure II-13. Based on the free body diagrams, the equations of motion for the drop capsule and drag shield can be written,

$$\ddot{X}_{DC} = \frac{F}{m_2} + g$$

$$\ddot{X}_{DS} = g - \frac{F}{m_1} - \frac{D}{m_1}$$

where:  $F$  = spring force, lb

$g$  = acceleration of gravity,  $386.07 \text{ in/sec}^2$

$m_1$  = drag shield mass,  $\text{lb sec}^2/\text{in}$

$m_2$  = drop capsule mass,  $\text{lb sec}^2/\text{in}$

$D$  = aerodynamic drag acting on the drag shield, lb

The allowable travel distance,  $S$ , is known. Thus we can write:

$$S = \frac{1}{2} \ddot{X}_{DC} t^2 - \frac{1}{2} \ddot{X}_{DS} t^2$$

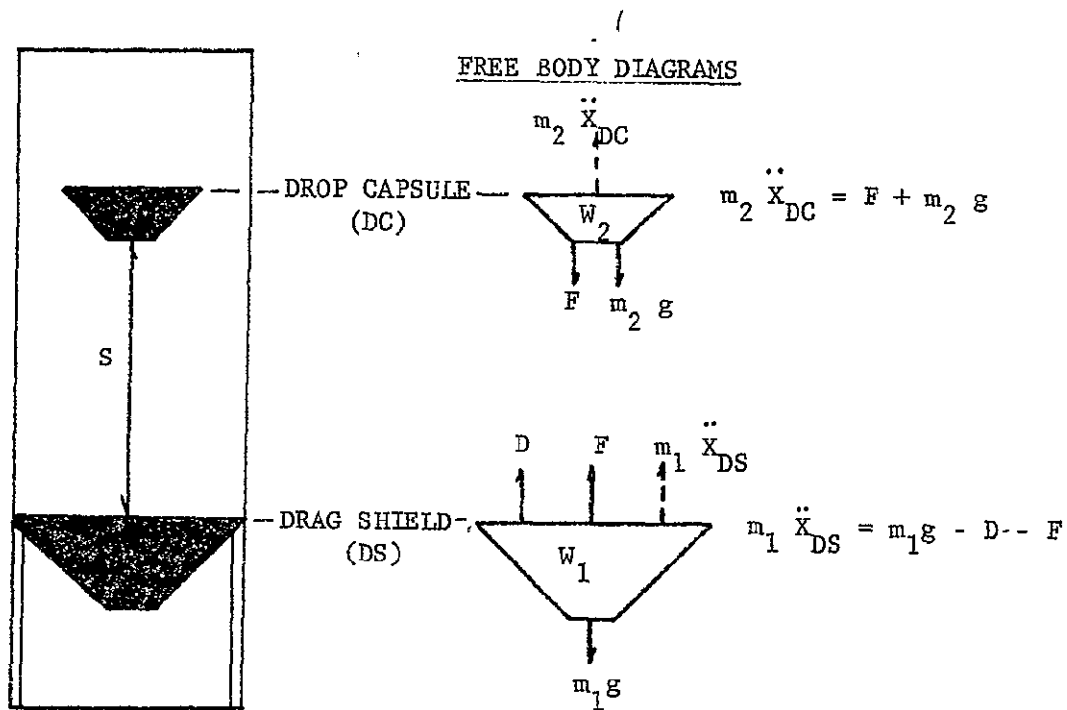


Figure II-13. Longitudinal Acceleration Calculation

Substituting for capsule and drag shield accelerations yields,

$$s = \frac{1}{2} t^2 \frac{D}{m_1} + \frac{1}{2} t^2 F g \left( \frac{1}{W_1} + \frac{1}{W_2} \right)$$

or  $s = S_D + \frac{1}{2} t^2 F g \left( \frac{1}{W_1} + \frac{1}{W_2} \right)$

where:  $S_D$  = relative travel due to drag acting on the drag shield.

The value of  $S_D$ , for a 2.1 second drop, has been previously established as  $\approx 2$  inches. Therefore, for an arbitrary test time,  $t$ , the value of  $S_D$  is,

$$S_D = 2 \frac{t^2}{(2.1)^2} = 0.4535 t^2$$

S can now be written as

$$S = 0.4535 t^2 + \frac{1}{2} t^2 F g \left( \frac{1}{W_1} + \frac{1}{W_2} \right)$$

From this expression the effective, average, acceleration of the drop capsule can be extracted.

$$A_{\text{long}} = \frac{Fg}{W_2} = \frac{2S}{t^2} - 0.9070 - \frac{386.07}{W_1} \cdot F, \text{ in/sec}^2$$

This equation was used to calculate drop capsule longitudinal accelerations,  $A_{\text{long}}$ , using as data:

S = 53.5 inches for 130 N axial motor  
 40.0 inches for 67 N axial motor

$W_1$  = 2000 lbs

F = spring motor force in lb  
 130 N = 30 lb  
 67 N = 15 lb

t = actual test time, sec

The lateral acceleration,  $A_{\text{lat}}$ , was calculated by the expression,

$$A_{\text{lat}} = \frac{2L}{t^2} = \frac{8000 L}{NF^2}, \text{ in/sec}^2$$

where: L = lateral distance traveled since drop initiation, inches

NF = number of film frames (@ 200 frames/sec) since drop initiation.

Both L and NF were acquired by reducing the high speed film data.

## 2. Force Data

A lateral force ( $F_1$ ) and two vertical forces ( $F_2$  and  $F_3$ ) were measured and recorded during the drop tests (see Figure II-5). The test data was manually scaled from oscillograph records and converted to a punched card data bank. A data reduction computer program was then used to convert the raw data to engineering units, using appropriate scale factors, based on charge amplifier sensitivities and oscillograph calibrations. The data was then smoothed to remove test fixture and camera noise by a moving average digital low pass filter set at 10 Hz. Figure II-14 depicts the shape of the filter used. An investigation was conducted to insure that this filtering did not reduce peak force levels.

Due to the lower magnitude of the lateral force measurement,  $F_1$ , and subsequent charge amplifier sensitivity increase, thermal drift was evident in the data for  $F_1$ . This drift has been measured, in bench tests, and has been shown to be linear (@  $\approx 0.0109$  lb/sec). The data reduction computer program compensated by subtracting the value  $0.0109 t$ , lb, from the  $F_1$  data.

As previously mentioned, the load cells are momentarily grounded prior to test initiation. Hence, they register "zero force" in lg prior to each drop. At the moment of drop capsule release, the transition from lg to  $A_{long}$  appears on the force data ( $F_2$  and  $F_3$ ) as a load offset. Figure II-15 shows this phenomena. Analytically, however, the lg load registers as a negative force in the longitudinal direction. To facilitate correlation between test and analytical results, the initial zero test forces were converted to negative forces, as shown in Figure II-15. The total, time zero, negative force ( $F_2 + F_3$ ) is approximately:  $(A_{long} + 386.07) * \text{mass}$  on the load cells. Force calculations in the analytical model must be adjusted by the factor  $A_{long}$  to allow direct comparison with the test data, as adjusted. The adjustment to the test data only applies to forces  $F_2$  and  $F_3$ .

To facilitate correlation of the test data with the analytical model, the data was transposed to the tank coordinate system shown in Figure II-16. The following set of equations was used to perform this transposition, based on Figure II-16.

$$F_{ZT} = (F_2 + F_3) \cos \gamma + F_1 \sin \gamma$$

$$F_{YT} = -F_1 \cos \gamma + (F_2 + F_3) \sin \gamma$$

$$M_{XT}^* = F_2 b - F_3 a - F_1 c$$

\* Moments in general are less accurate than forces since differences of like numbers are taken. Errors and noise tend to be magnified.

To facilitate analytical correlation, Table II-4 presents some important constants related to the test module.

Table II-4. Test Constants

<u>Weights</u>	
Tank support structure (on load cells)	455 gm
Unbaffled tank	351 gm
Baffled tank	377 gm
Drop capsule	175.20 Kg
<u>Tank Volumes</u>	
2% fill	50.6 cc
5% fill	127.0 cc
10% fill	253.0 cc
15% fill	379.0 cc
<u>Inflow</u>	
Tests 1, 2, 3, 4	12.50 cc/sec
Test 31	7.50 cc/sec

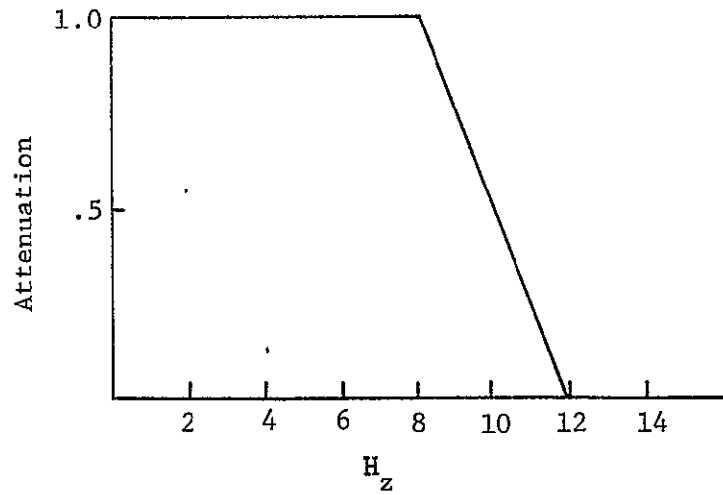


FIGURE II-14. Digital Filter Shape

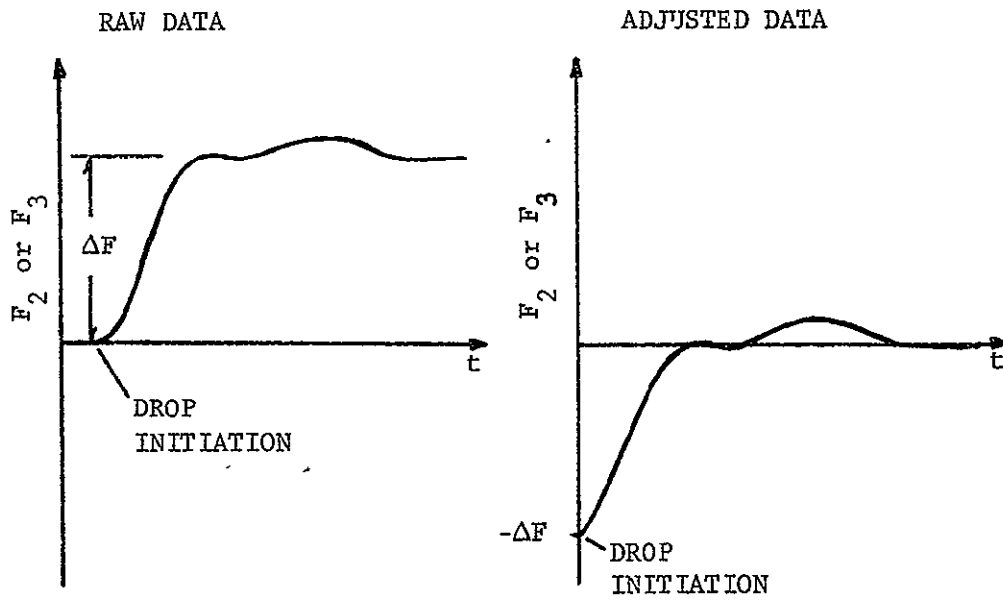
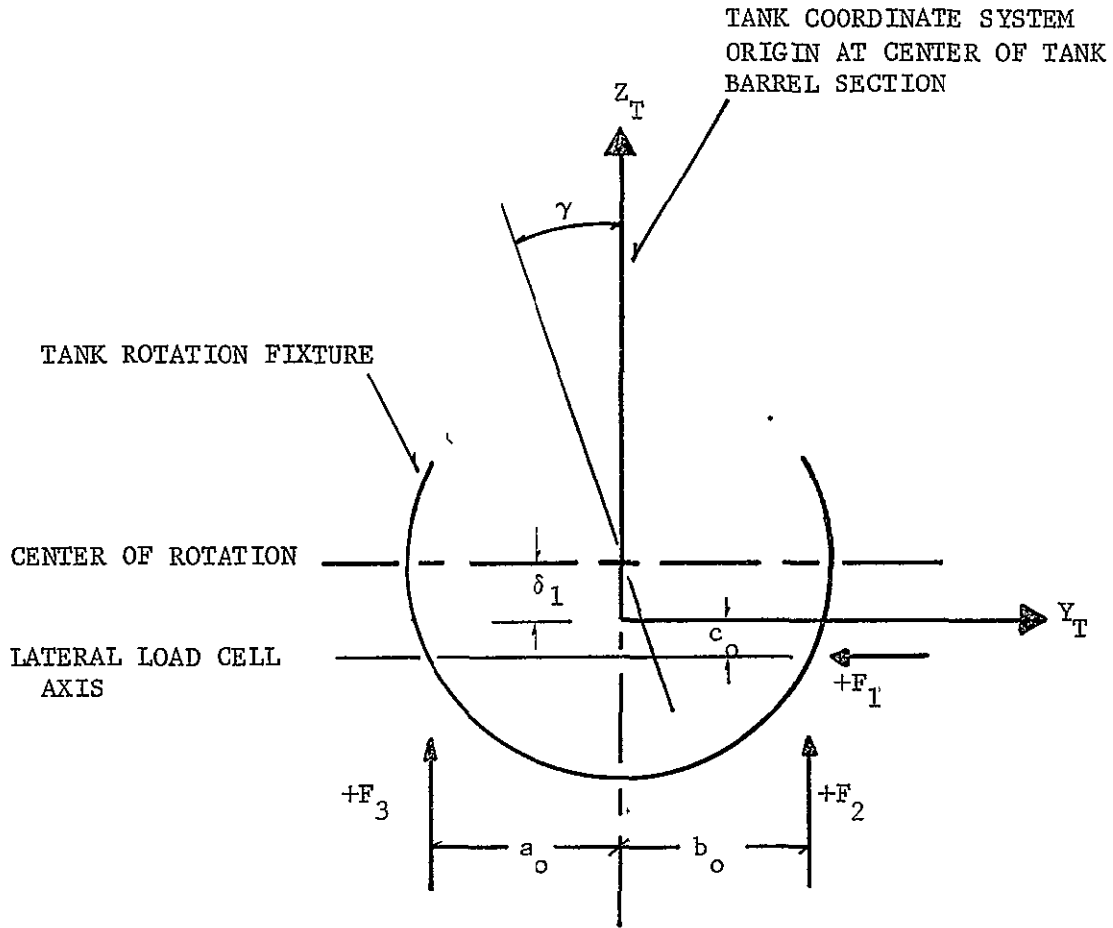


FIGURE II-15. ADJUSTMENT OF LONGITUDINAL TEST FORCES.

ORIGINAL PAGE IS  
OF POOR QUALITY.



$$a = a_o + \delta_1 \sin \gamma = 4.0 + 0.47 \sin \gamma \quad , \text{ inches}$$

$$b = b_o + \delta_1 \sin \gamma = 4.0 - 0.47 \sin \gamma \quad , \text{ inches}$$

$$c = c_o + (\delta_1 - \delta_1 \cos \gamma) = 0.08 + (0.47 - 0.47 \cos \gamma) \quad , \text{ inches}$$

$\gamma =$  angle of tank rotation

FIGURE II-16. TANK-MEASUREMENT COORDINATE SYSTEM

### III. EVALUATION OF TEST RESULTS

---

This chapter presents an evaluation of the test results. Included are discussions covering: test conditions, observations on photographed liquid motion, an evaluation of the various test parameters, and some comments on analytical correlation. Appendix A contains the measured force time histories for each test.

#### A. TEST CONDITIONS

Table III-1 tabulates the actual test conditions achieved. Lateral and longitudinal test accelerations are presented, as calculated by methods discussed in Chapter II. The tests are separated into groups indicating the primary parameters under study in each group. The effect of baffles was studied in each group. A total of 32 tests were conducted, 17 using the baffled tank and 15 using the unbaffled tank. The useful test time varied between 1.5 and 1.6 seconds.

#### B. OBSERVATIONS ON LIQUID MOTION

The film data of the test program provided an understanding of the character of propellant motion during the ET separation maneuver. These data were reviewed to determine the influence of the various test variables on the motion of the liquid. In the following paragraphs the observed effects of each of the variables is discussed.

In general, the liquid motion simulated in the testing was the reorientation from the liquid's initial position at the bottom of the tank to the ogive dome. The tests were scaled such that the most significant initial phase of the liquid motion was simulated. This included the movement of the liquid to the top of the tank and some of the subsequent dynamics. At the end of the tests there was still some liquid oscillation and turbulence, prior to establishing a quiescent, equilibrium position (based on the applied accelerations).

The liquid motion from selected tests is illustrated in Figure III-1 through III-16 with photographs made from single frames of the motion picture data. For each of the selected tests, five film frames that represent the liquid motion were chosen. The five are: (1) initial condition prior to beginning of the test; (2) 0.4 seconds from the start of the test; (3) 0.8 seconds from the start of the test; (4) 1.2 seconds from the start of the test; and (5) end of the test, which occurs about 1.6 seconds from the start of the test. In these figures the accelerations are directed as shown by Figure II-1. The direction of the lateral

TABLE III-1. TEST CONDITIONS

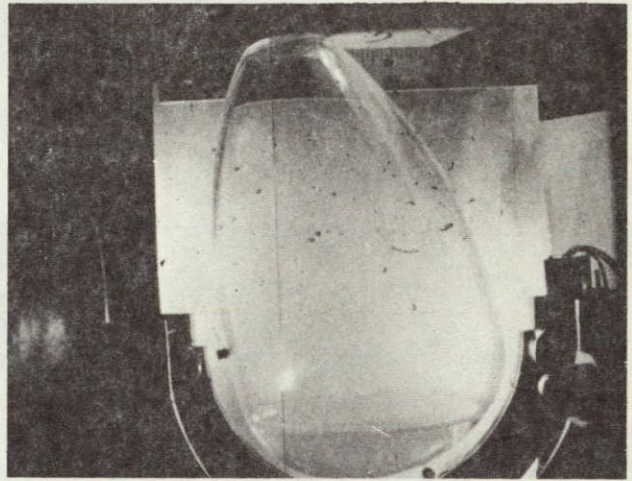
TEST	TEST # LIQUID	(g) ALONG	(g) ALAT	$\gamma^{\circ}$	LOX OUTFLOW	BAFFLED TANK	% FILL	
1	1	0.090	0.029	13	Y	N	2	
2	2	0.093	0.031	13	Y	N	2	LOX
3	1	0.093	0.031	13	Y	Y	2	outflow
4	2	0.092	0.032	13	Y	Y	2	
5	1	0.091	0.030	13	N	N	10	
6	2	0.091	0.029	13	N	N	10	
7	1	0.092	0.032	13	N	Y	10	liquid
8	2	0.092	0.032	13	N	Y	10	viscosity
9	1	0.090	0.031	13	N	N	2	
10	2	0.092	0.032	13	N	N	2	
11	1	0.092	0.034	13	N	Y	2	
12	2	0.092	0.033	13	N	Y	2	
13	1	0.088	0.014	13	N	Y	2	$A_{LAT}$
14	2	0.088	0.013	13	N	Y	2	
15	1	0.089	0-0.055*	13	N	N	2	
16	1	0.091	0-0.053	13	N	N	10	change
17	1	0.090	0-0.055	13	N	Y	2	in $A_{LAT}$
18	1	0.091	0-0.052	13	N	Y	10	
19	1	0.093	0.033	13	N	Y	5	
20	1	0.088	0.032	13	N	Y	15	% fill
21	1	0.091	0.032	13	N	N	5	
22	1	0.093	0.032	13	N	N	15	
23	1	0.091	0.034	30	N	Y	2	
24	1	0.092	0.033	30	N	N	2	$\gamma=30^{\circ}$
25	1	0.091	0.031	30	N	N	10	
26	1	0.088	0.031	30	N	Y	10	
27	1	0.043	0.033	0	N	Y	2	
28	1	0.043	0.032	0	N	N	2	$\gamma=0^{\circ}$
29	1	0.050	0.038	0	N	Y	10	$A_{LONG}$
30	1	0.042	0.032	0	N	N	10	
31	1	0.090	0.032	13	Y $\Delta$	Y	2	
32	3	0.090	0.032	13	N	N	10	special tests

# Liquid 1 = FC114B2  
 2 = FC43  
 3 = HEXANE

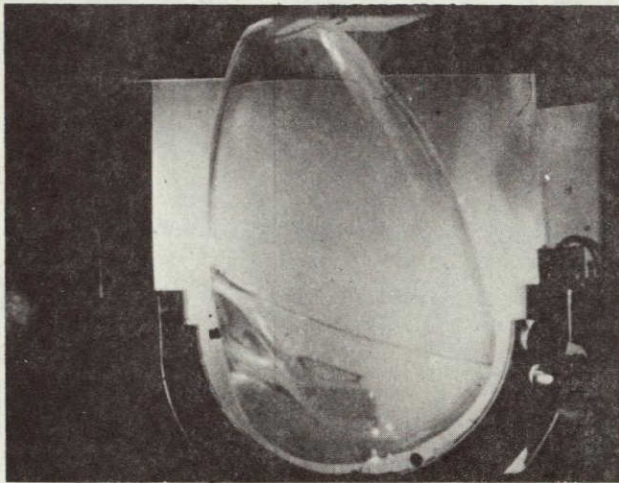
\* Lateral slider delayed  $\approx 0.5$  sec

$\Delta$  Tank outlet increased by factor of 2, flow rate reduced

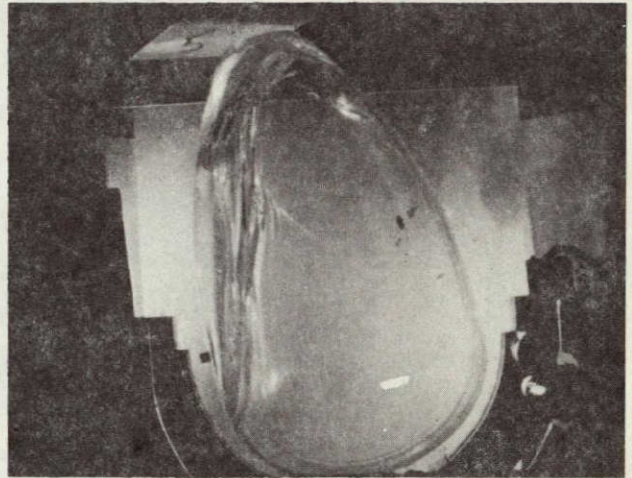
FIGURE III-1. TEST 5, FC-114B2  
 $\gamma = 13^\circ$ , 10% FILL



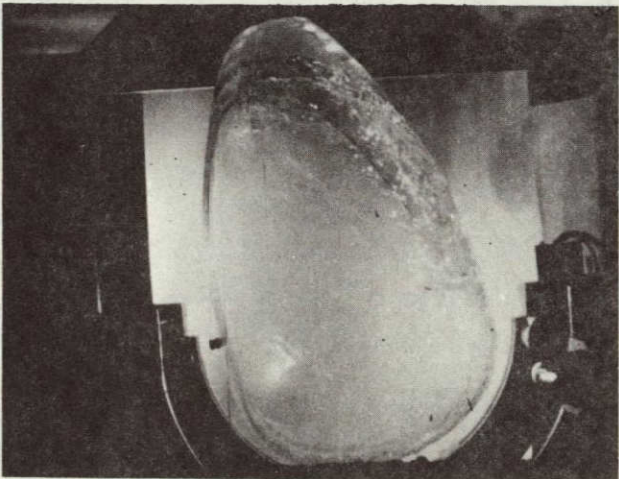
T= 0.0 SEC



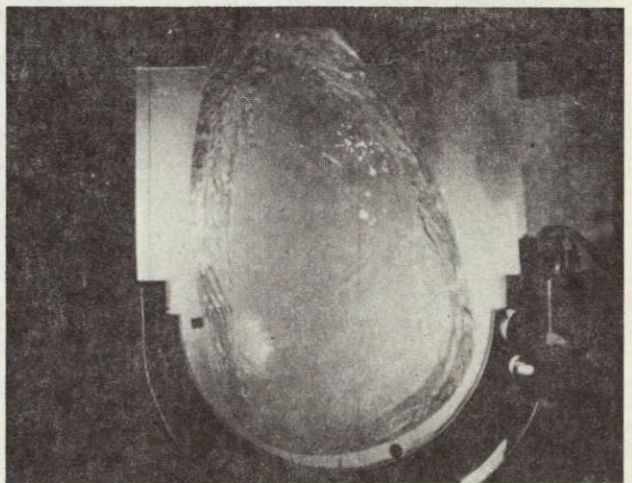
T= 0.4 SEC



T= 0.8 SEC



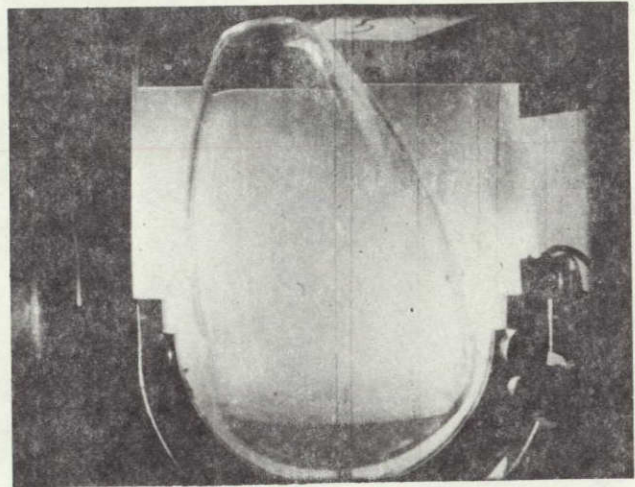
T= 1.2 SEC



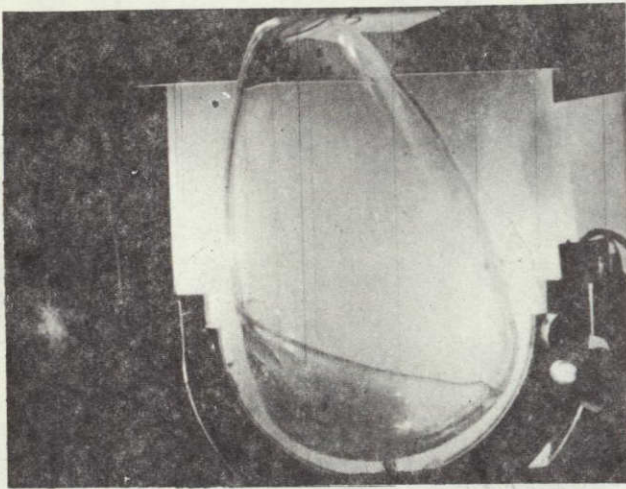
T= 1.6 SEC

ORIGINAL PAGE IS  
OF POOR QUALITY

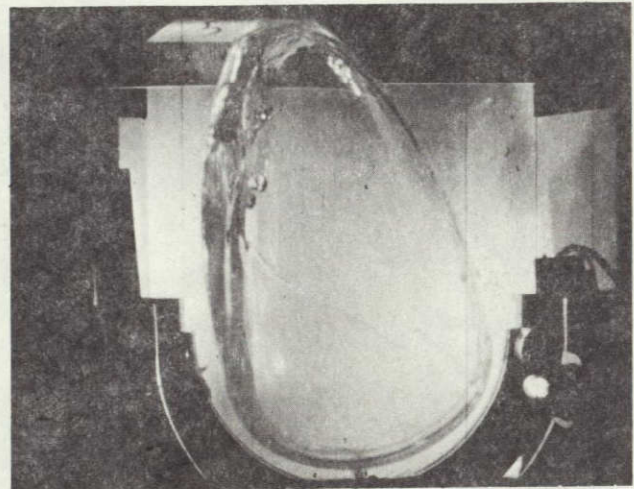
FIGURE III-2. TEST 6, FC-43  
 $\gamma = 13^\circ$ , 10% FILL



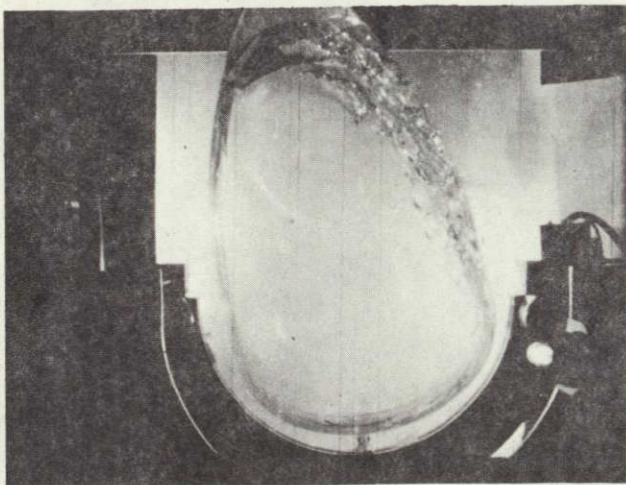
T= 0.0 SEC



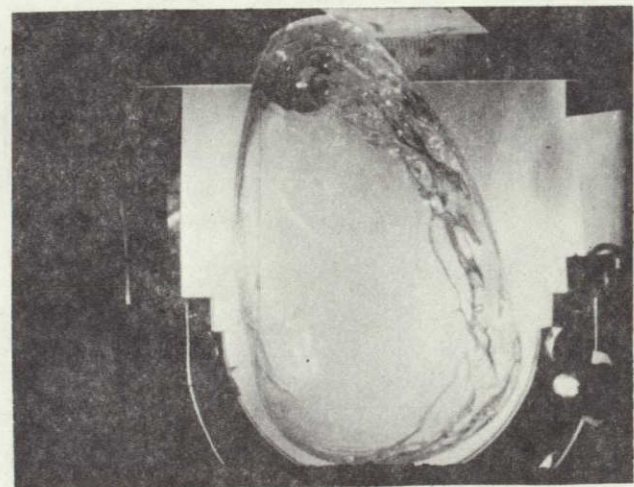
T= 0.4 SEC



T= 0.8 SEC

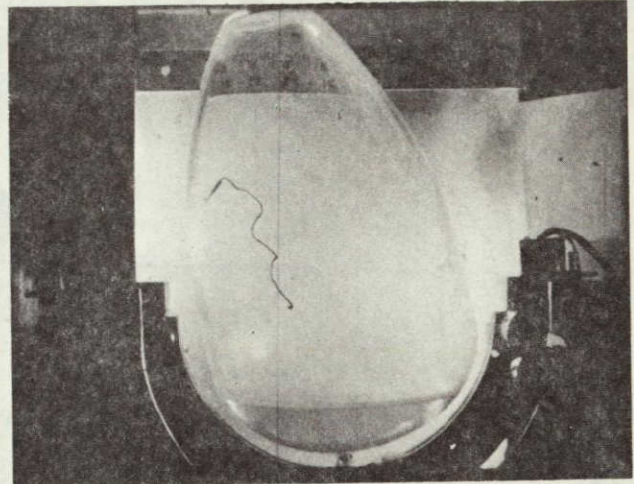


T= 1.2 SEC

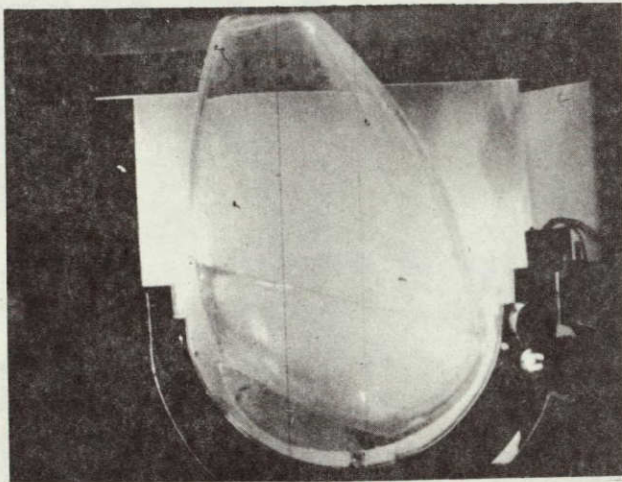


T= 1.6 SEC

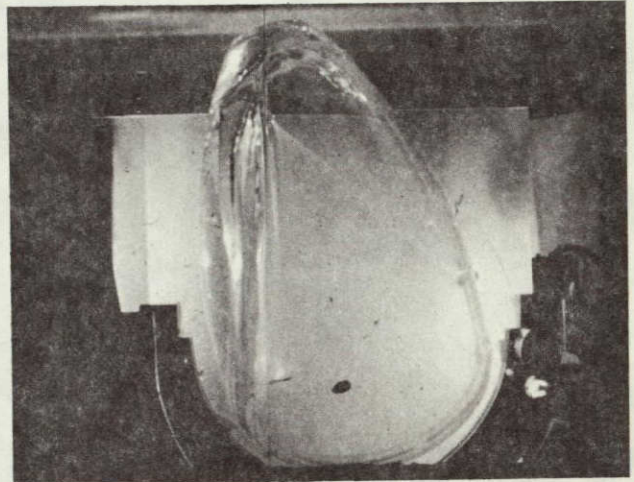
FIGURE III-3. TEST 32, HEXANE  
 $\gamma = 13^\circ$ , 10% FILL



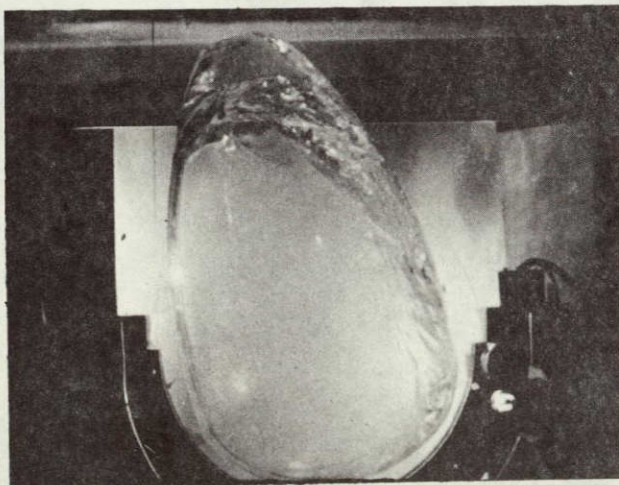
T= 0.0 SEC



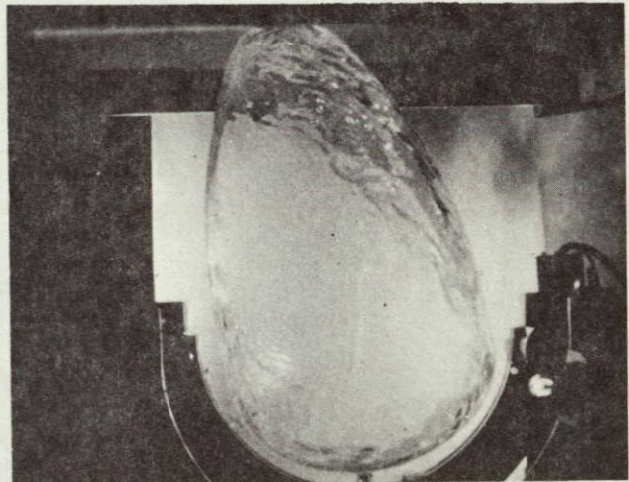
T= 0.4 SEC



T= 0.8 SEC

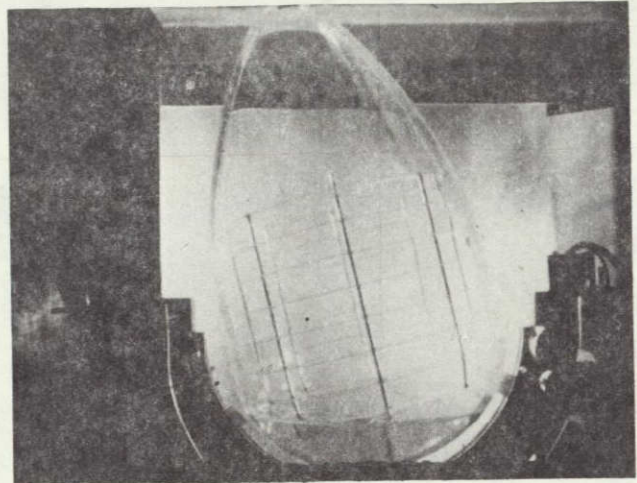


T= 1.2 SEC

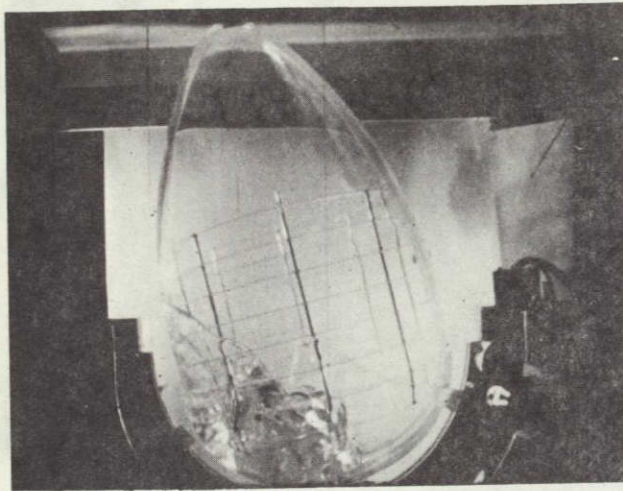


T= 1.6 SEC

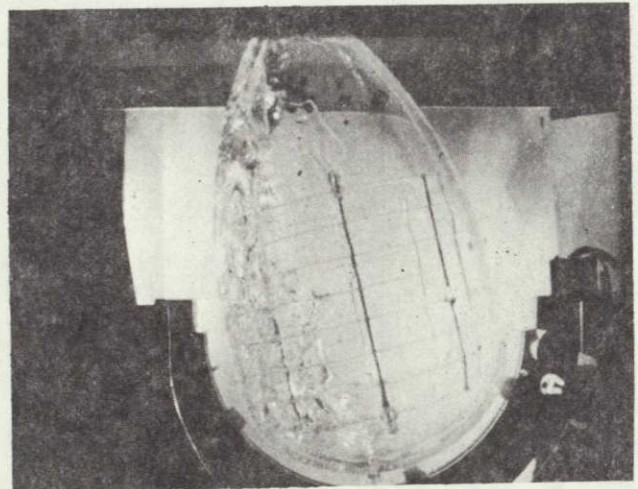
FIGURE III-4. TEST 7, FC-114B2  
 $\gamma = 13^\circ$ , 10% FILL



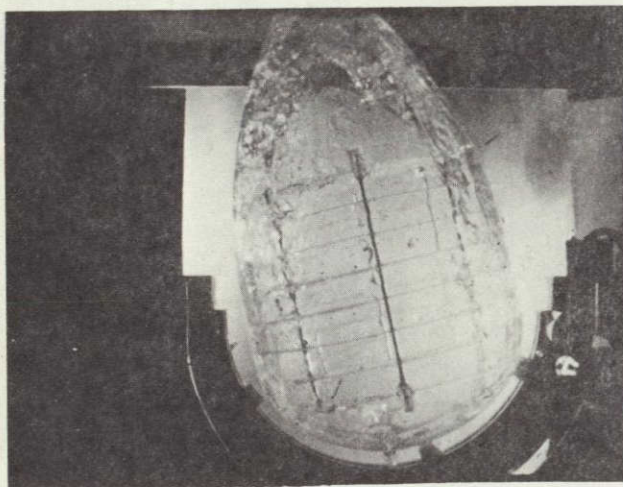
T= 0.0 SEC



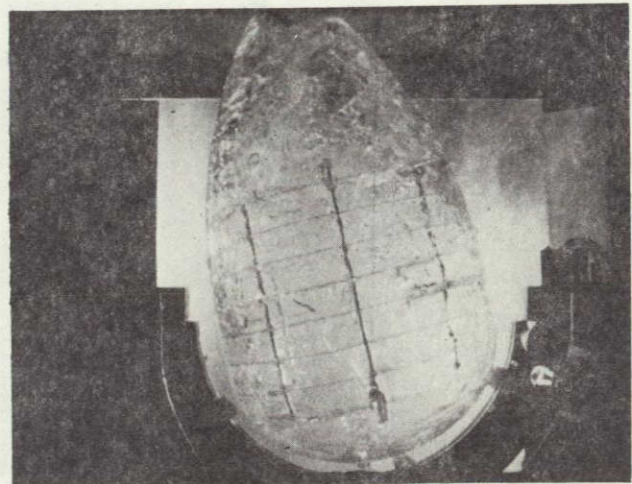
T= 0.4 SEC



T= 0.8 SEC



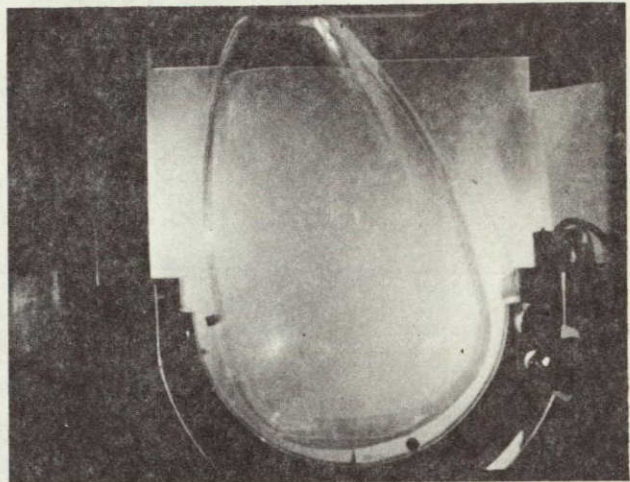
T= 1.2 SEC



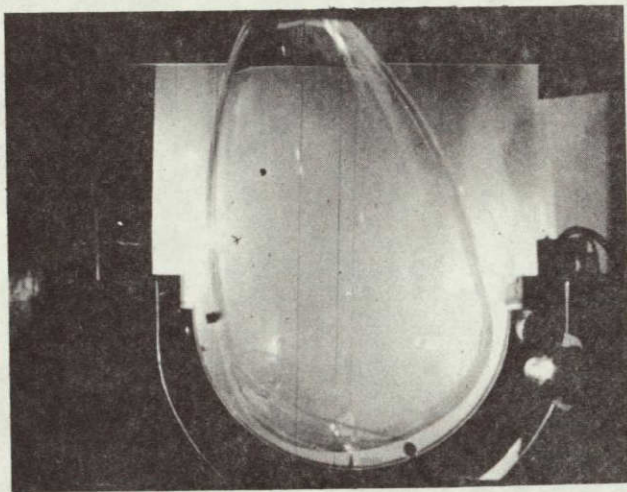
T= 1.6 SEC

ORIGINAL PAGE IS  
OF POOR QUALITY.

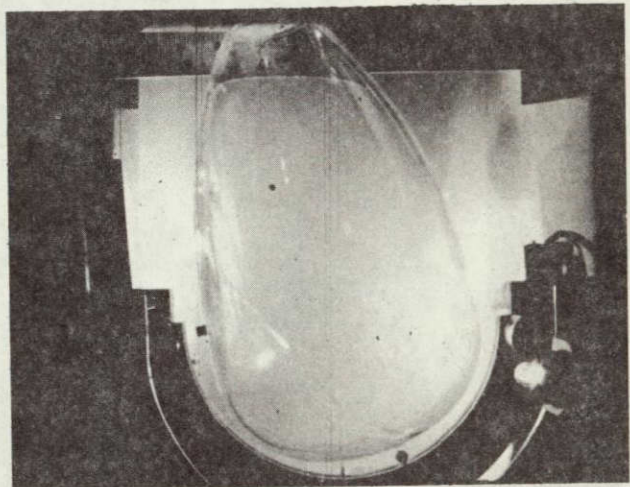
FIGURE III-5. TEST 9, FC-114B2  
 $\gamma = 13^\circ$ , 2% FILL



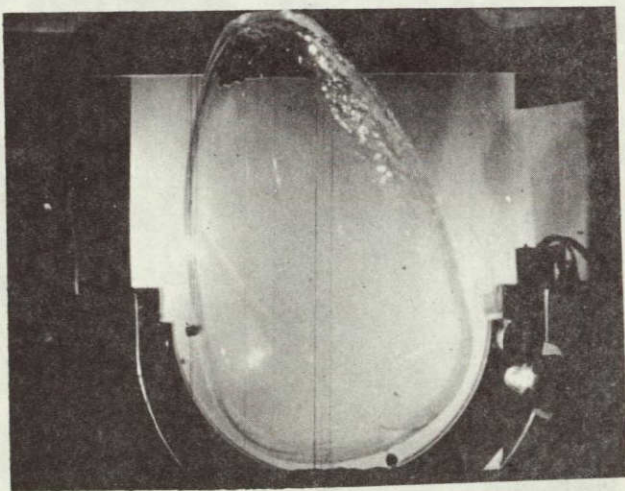
T= 0.0 SEC



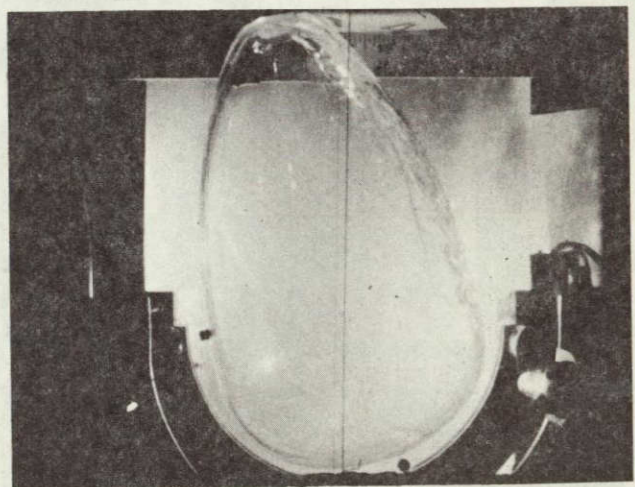
T= 0.4 SEC



T= 0.8 SEC

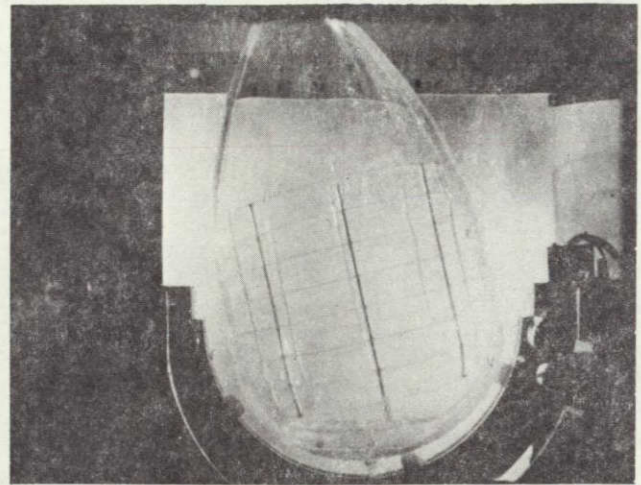


T= 1.2 SEC

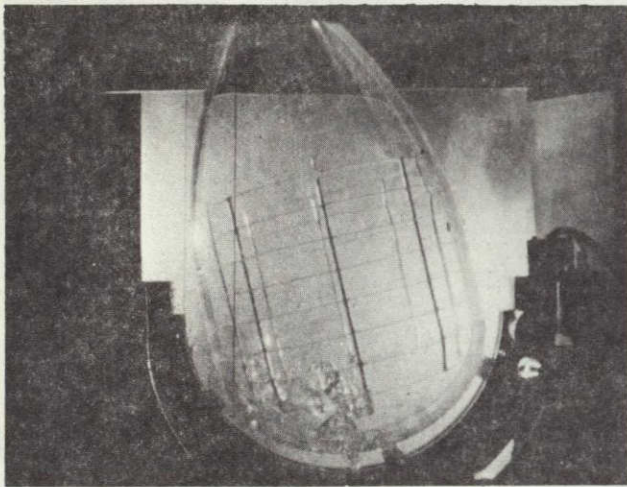


T= 1.6 SEC

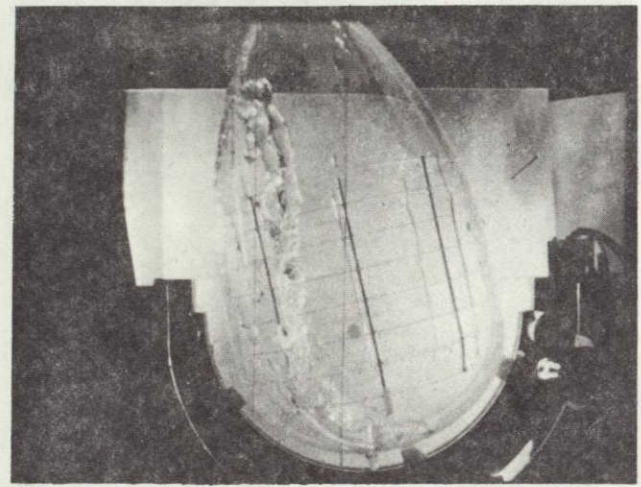
FIGURE III-6. TEST 11, FC-114B2  
 $\gamma = 13^\circ$ , 2% FILL



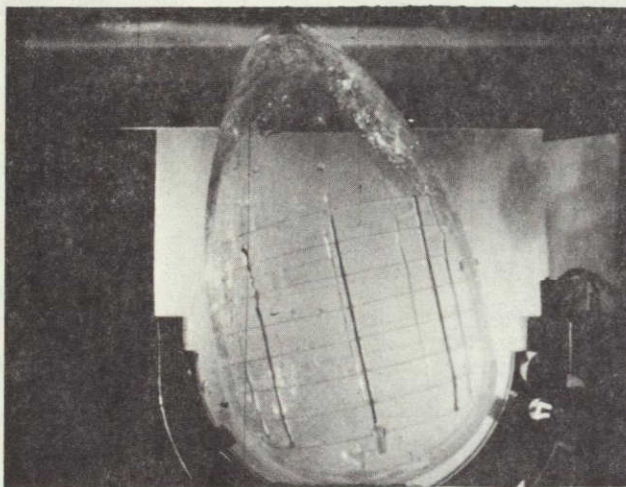
T= 0.0 SEC



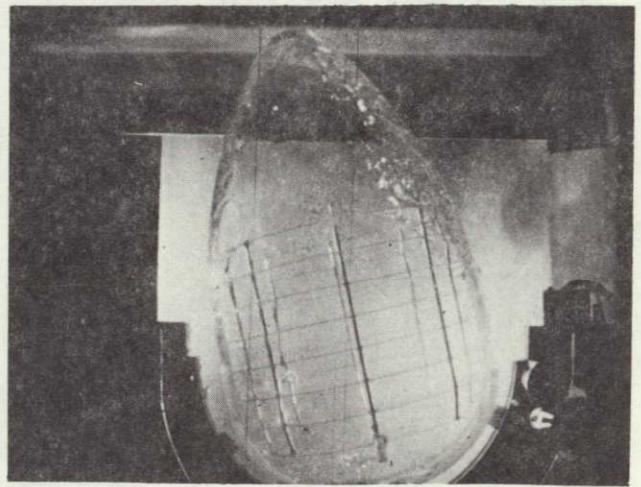
T= 0.4 SEC



T= 0.8 SEC



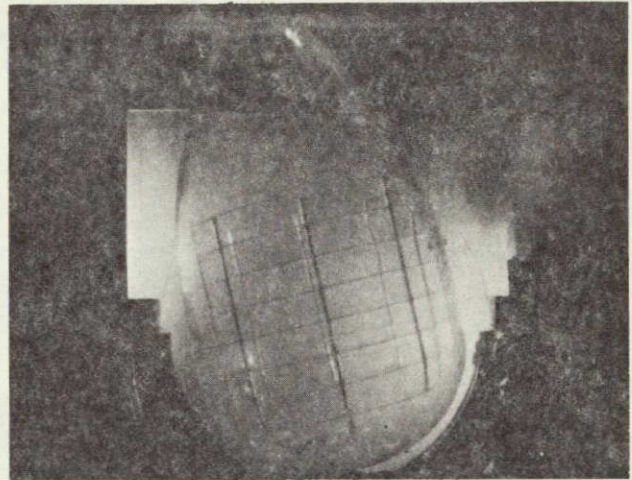
T= 1.2 SEC



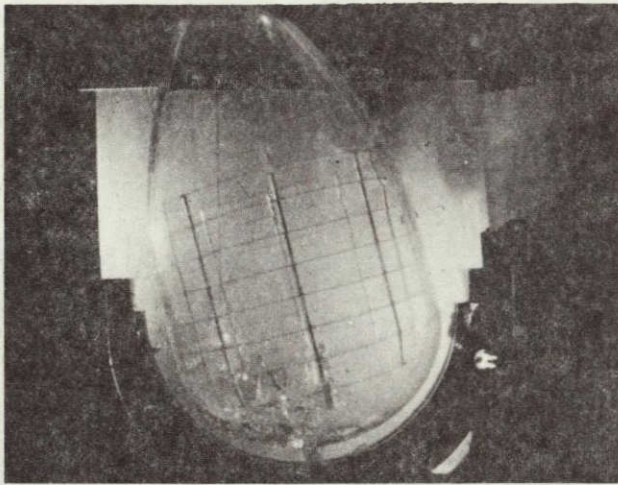
T= 1.6 SEC

ORIGINAL PAGE IS  
OF POOR QUALITY

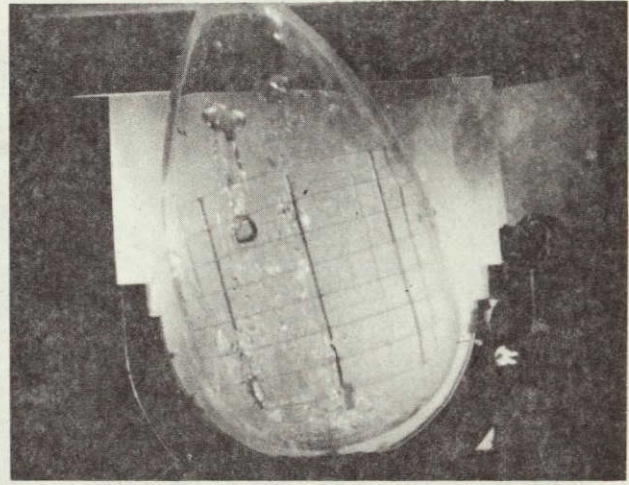
FIGURE III-7. TEST 13, FC-114B2  
 $\gamma = 13^\circ$ , 2% FILL



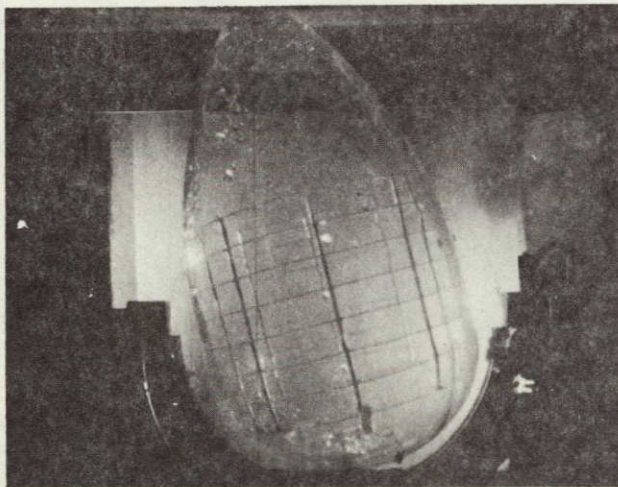
T= 0.0 SEC



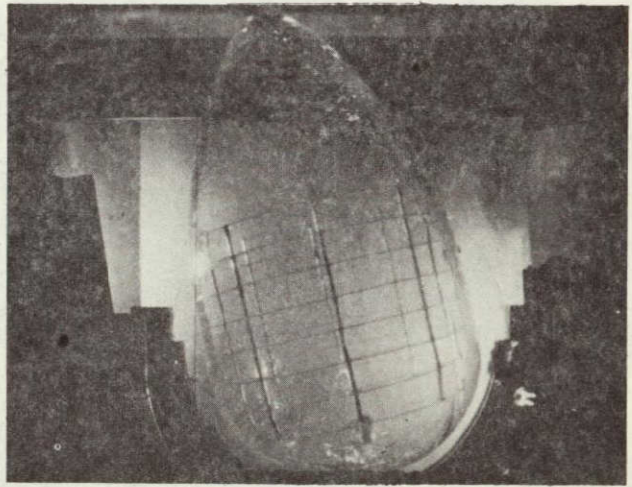
T= 0.4 SEC



T= 0.8 SEC

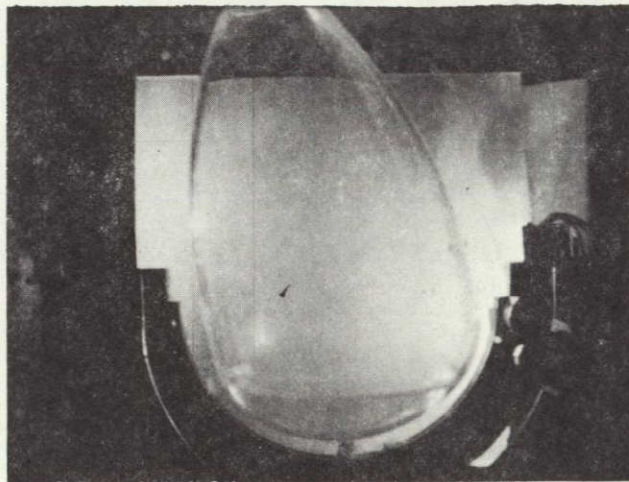


T= 1.2 SEC

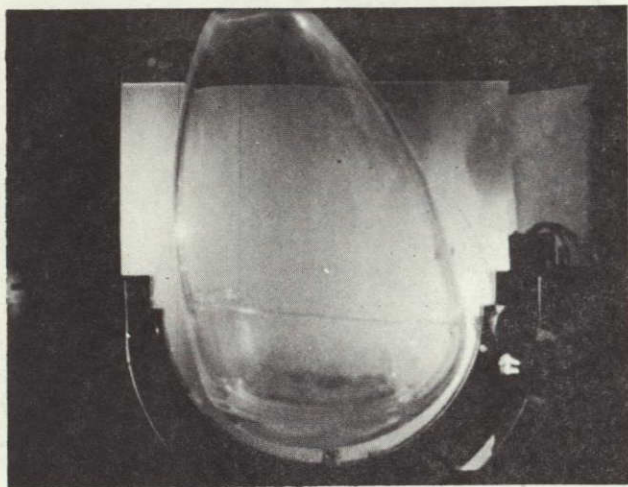


T= 1.6 SEC

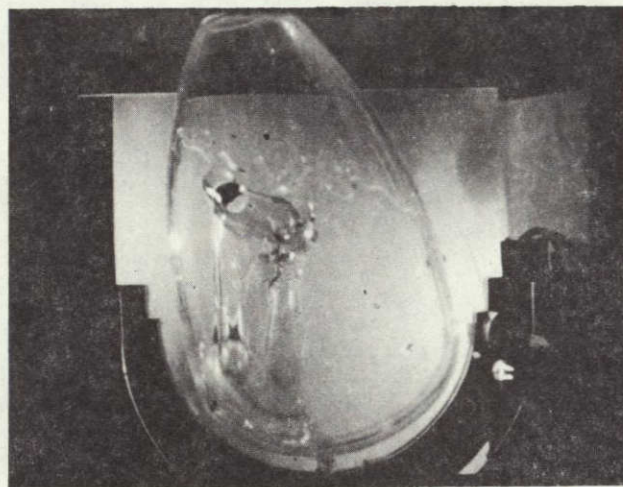
FIGURE III-8, TEST 16, FC-114B2  
 $\gamma = 13^\circ$ , 10% FILL



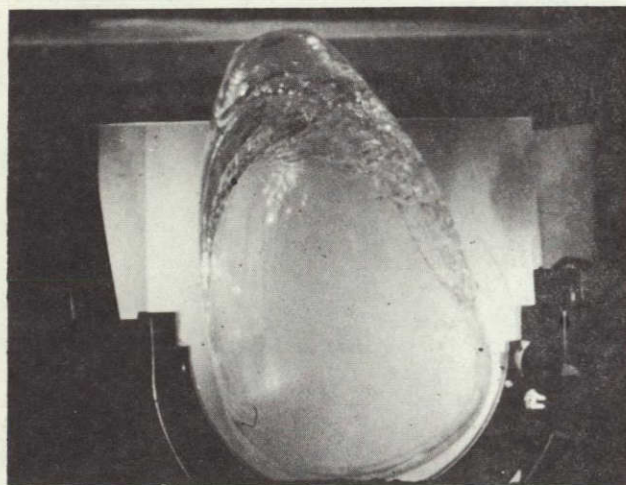
T= 0.0 SEC



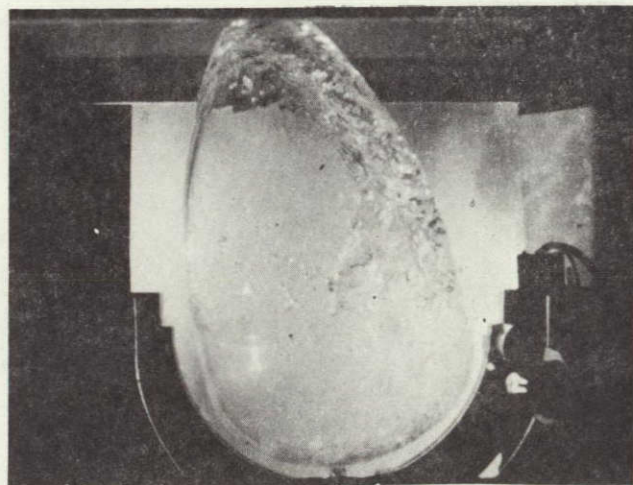
T= 0.4 SEC



T= 0.8 SEC



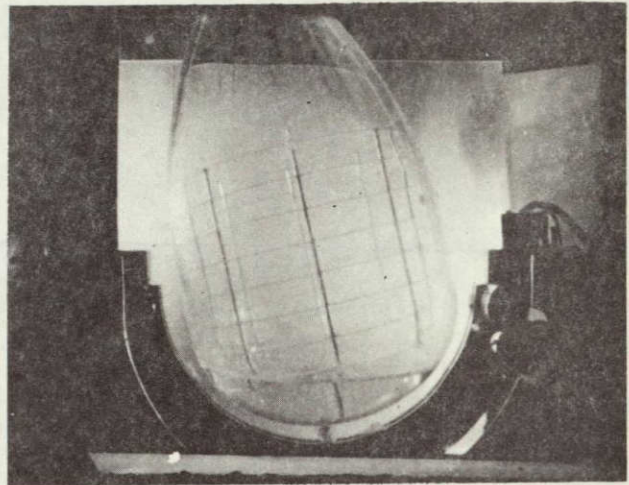
T= 1.2 SEC



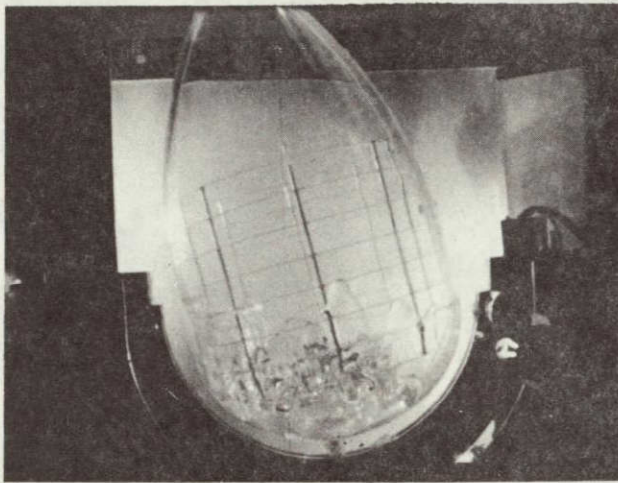
T= 1.6 SEC

ORIGINAL PAGE IS  
OF POOR QUALITY

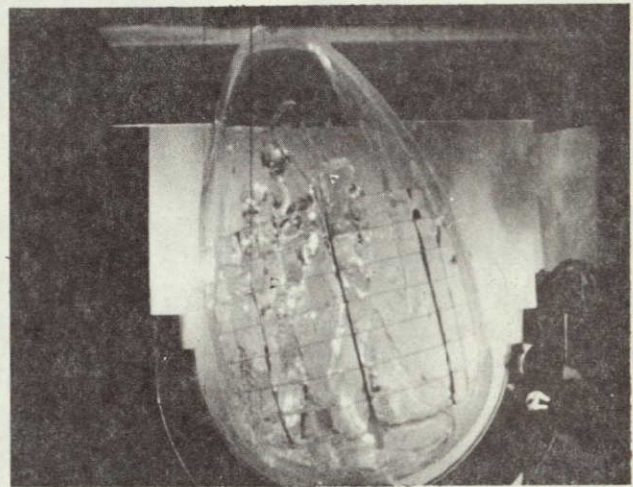
FIGURE III-9. TEST 18, FC-114B2  
 $\gamma = 13^\circ$ , 10% FILL



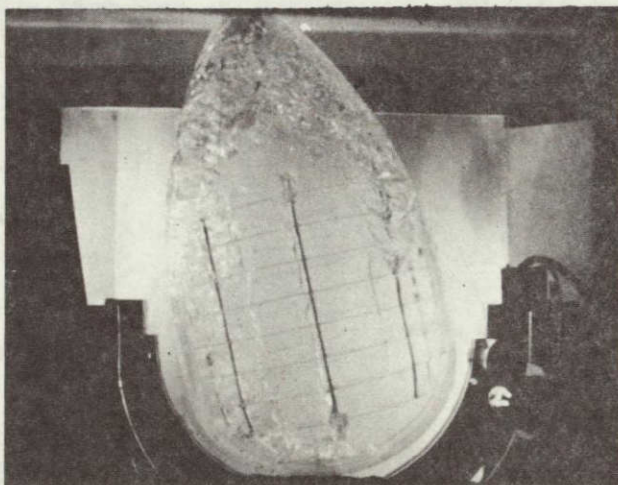
T= 0.0 SEC



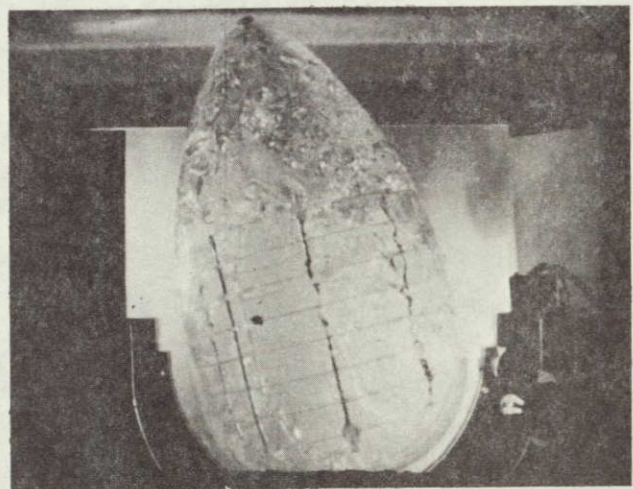
T= 0.4 SEC



T= 0.8 SEC

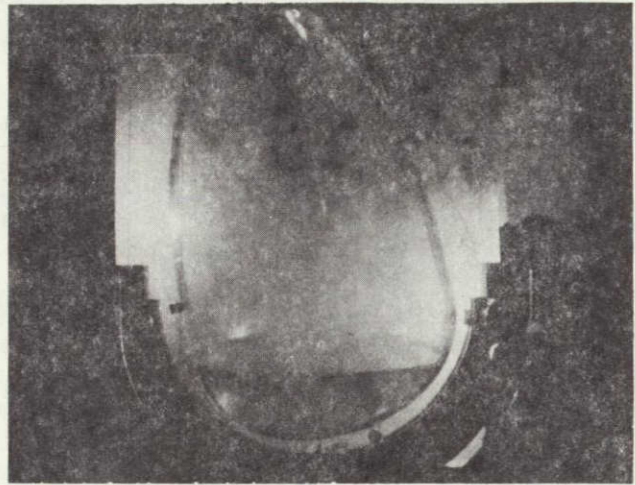


T= 1.2 SEC

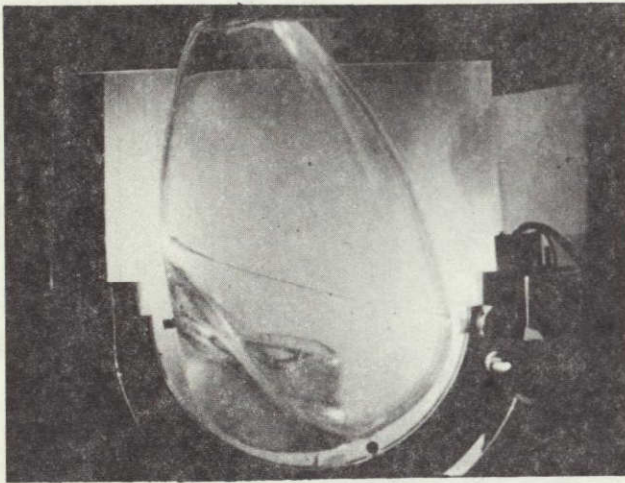


T= 1.6 SEC

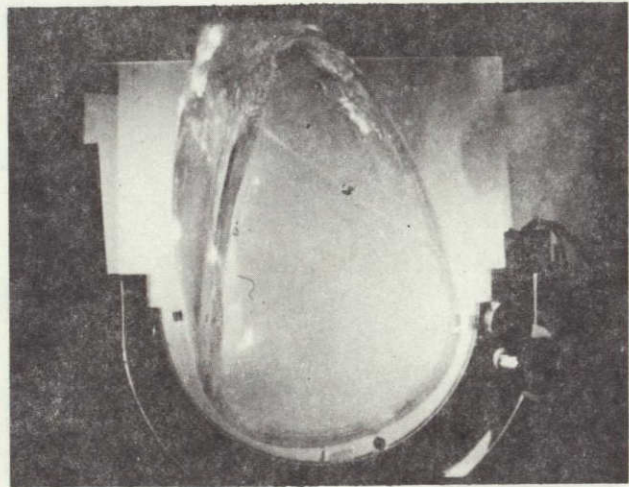
FIGURE III-10. TEST 22, FC-114B2  
 $\gamma = 13^\circ$ , 15% FILL



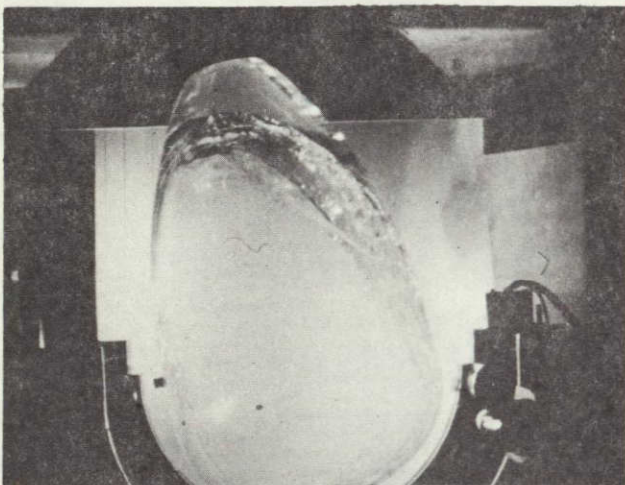
T= 0.0 SEC



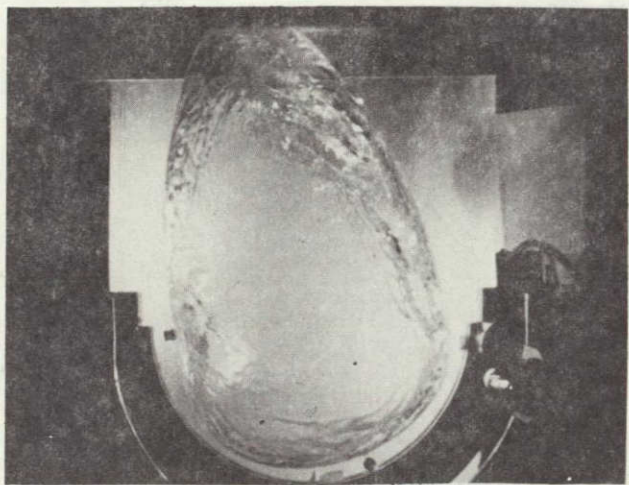
T= 0.4 SEC



T= 0.8 SEC

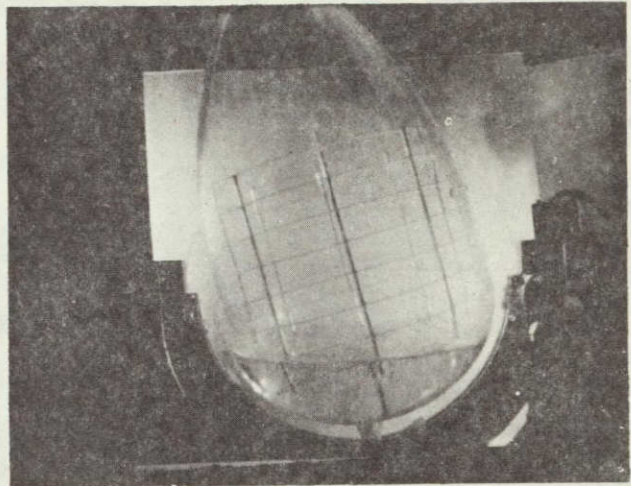


T= 1.2 SEC

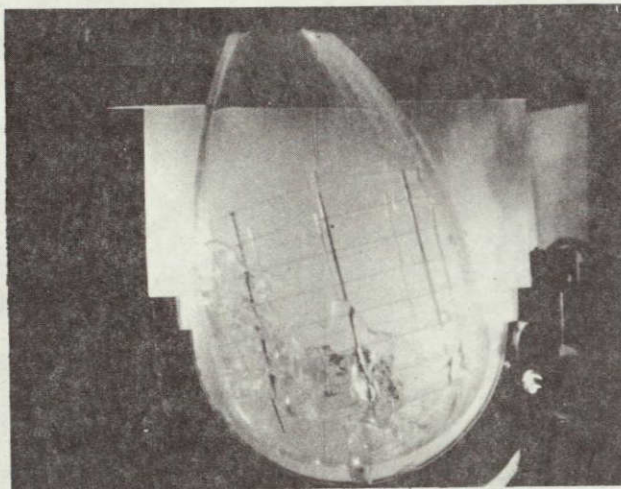


T= 1.6 SEC

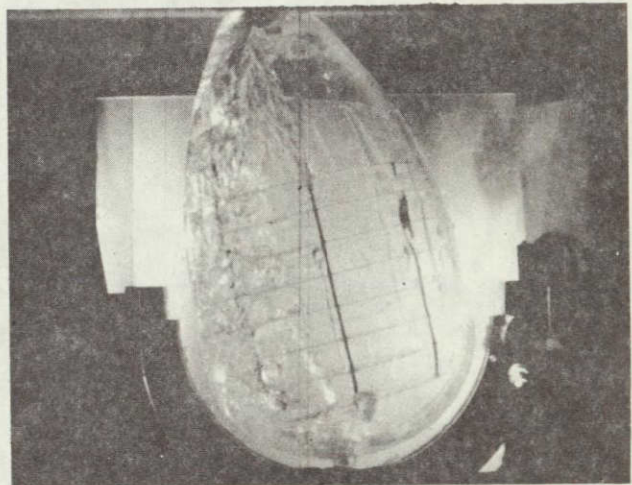
FIGURE III-11. TEST 20, FC-114B2  
 $\gamma=13^{\circ}$ , 15% FILL



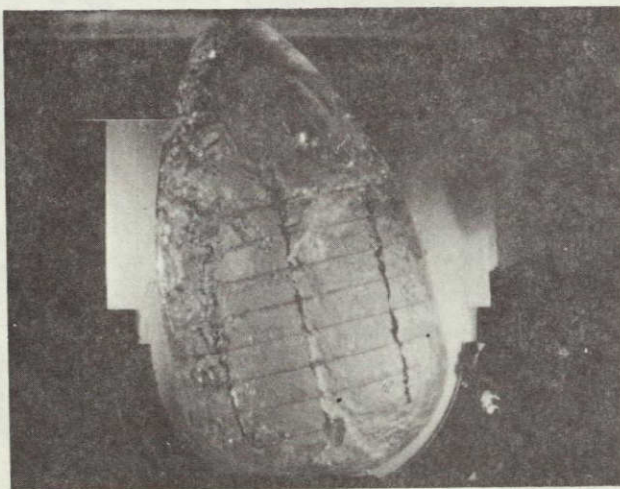
T= 0.0 SEC



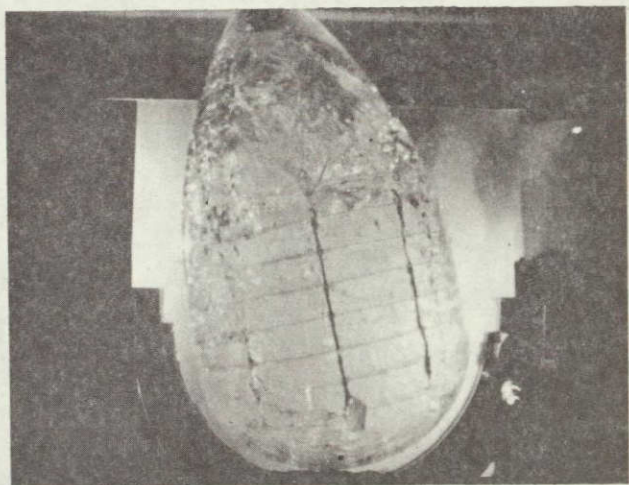
T= 0.4 SEC



T= 0.8 SEC



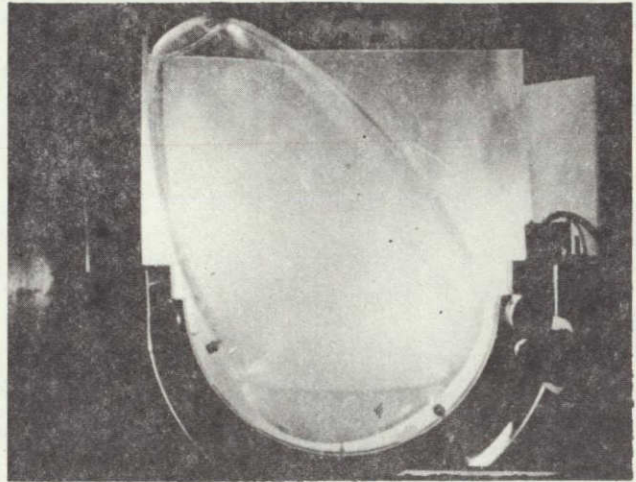
T= 1.2 SEC



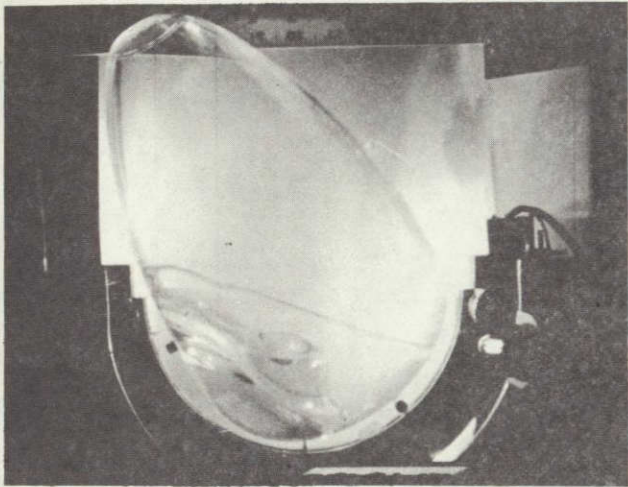
T= 1.6 SEC

ORIGINAL PAGE IS  
OF POOR QUALITY.

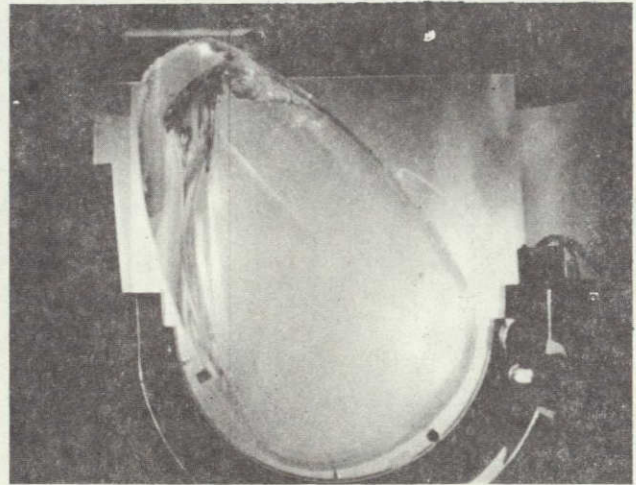
FIGURE III-12. TEST 25, FC-114B2  
 $\gamma = 30^\circ$ , 10% FILL



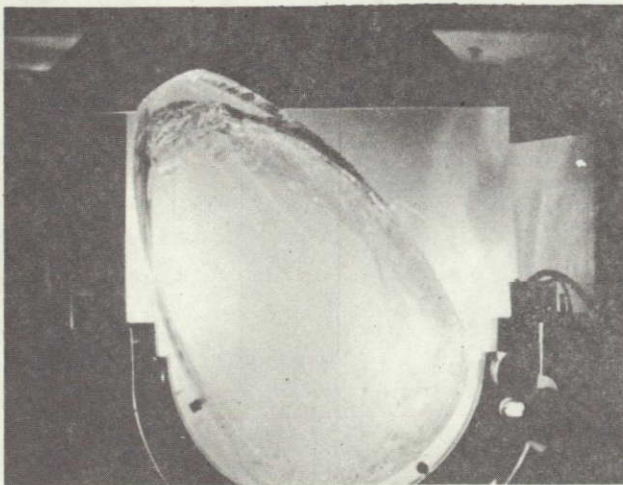
T= 0.0 SEC



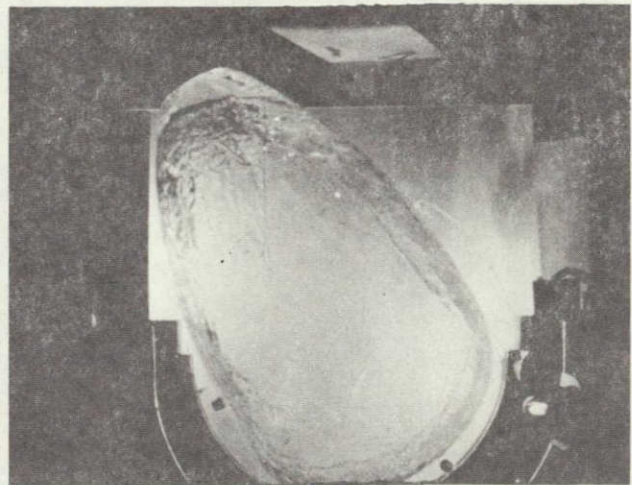
T= 0.4 SEC



T= 0.8 SEC

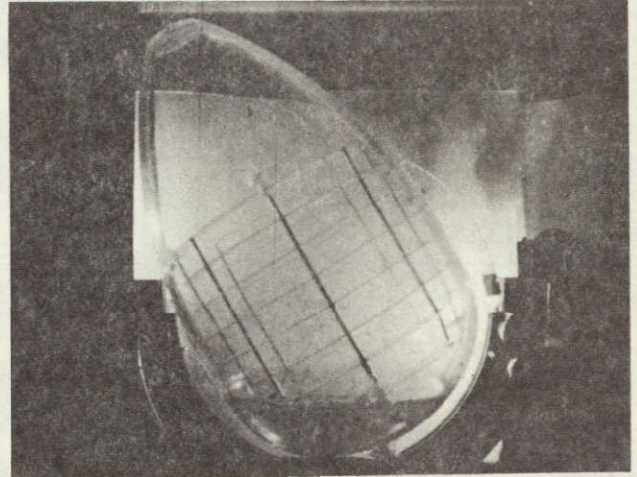


T= 1.2 SEC

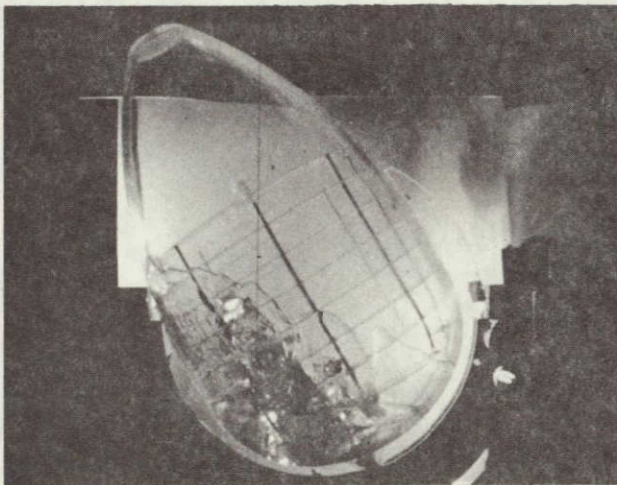


T= 1.6 SEC

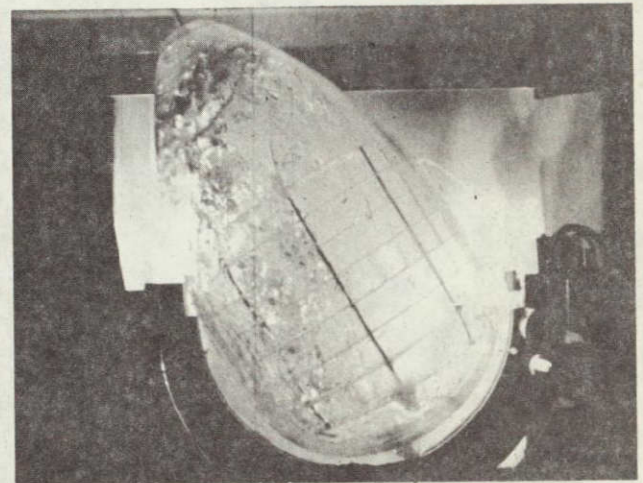
FIGURE III-13. TEST 26, FC-114B2  
 $\gamma = 30^\circ$ , 10% FILL



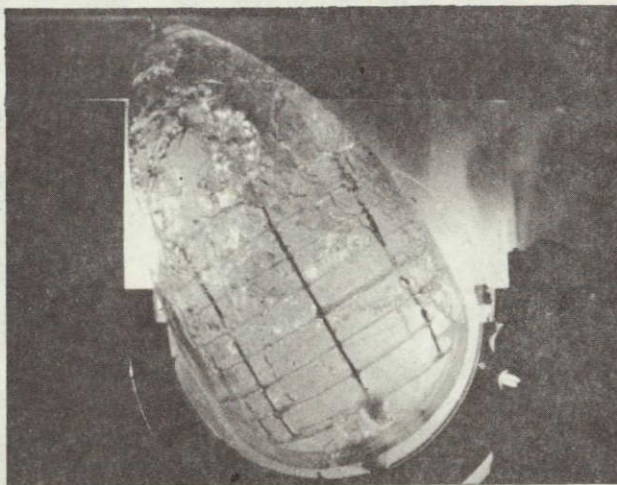
T= 0.0 SEC



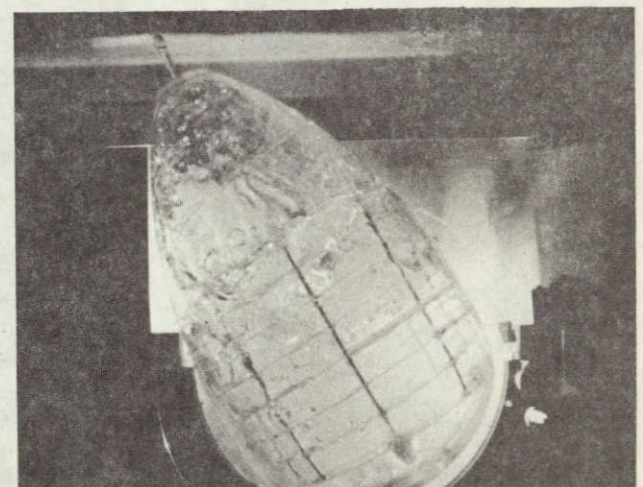
T= 0.4 SEC



T= 0.8 SEC



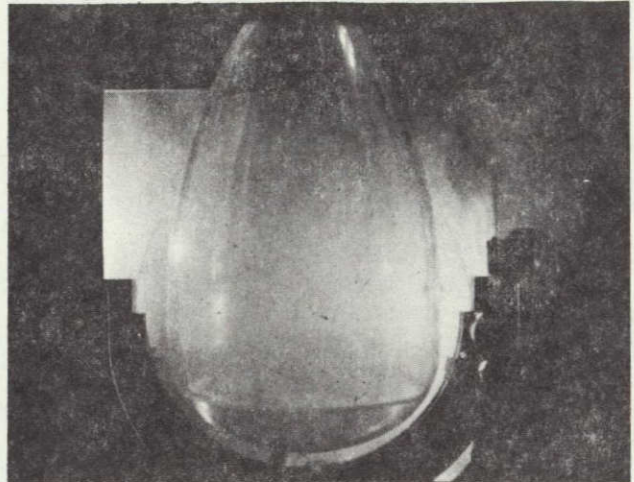
T= 1.2 SEC



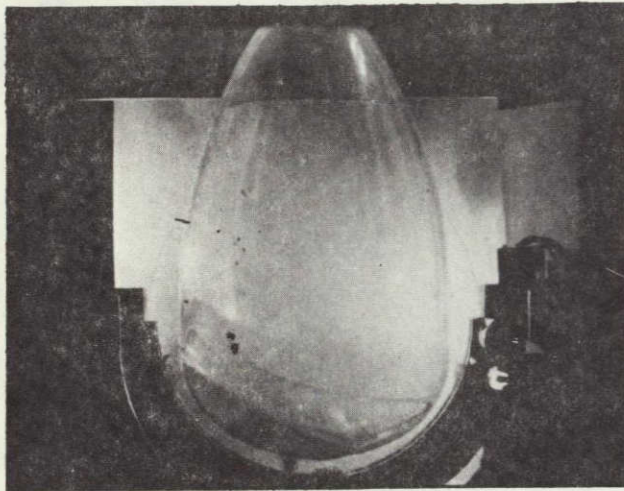
T= 1.6 SEC

ORIGINAL PAGE IS  
OF POOR QUALITY

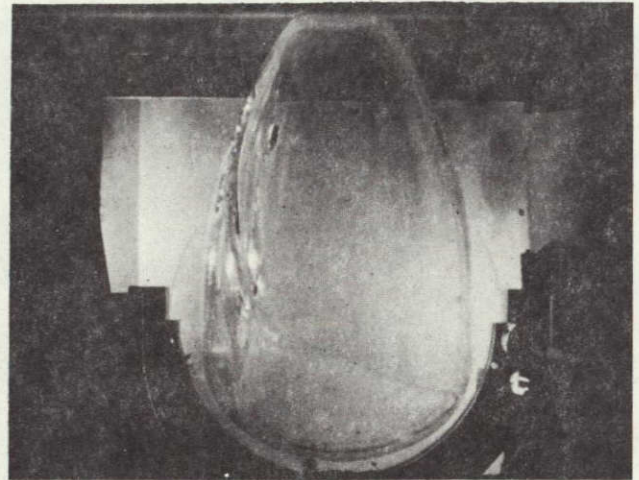
FIGURE III-14. TEST 30, FC-114B2  
 $\gamma = 0^\circ$ , 10% FILL



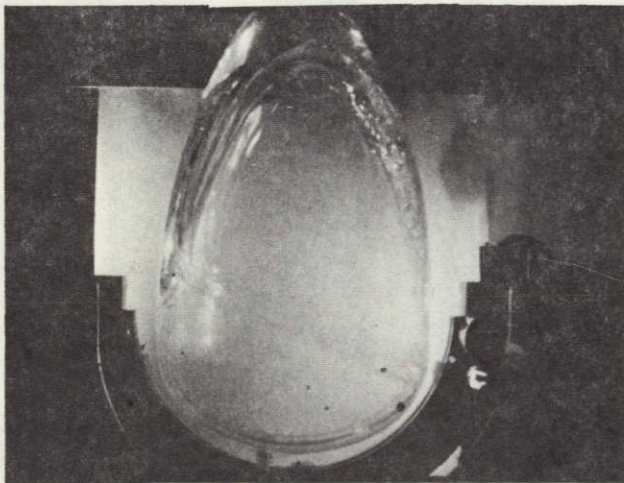
T= 0.0 SEC



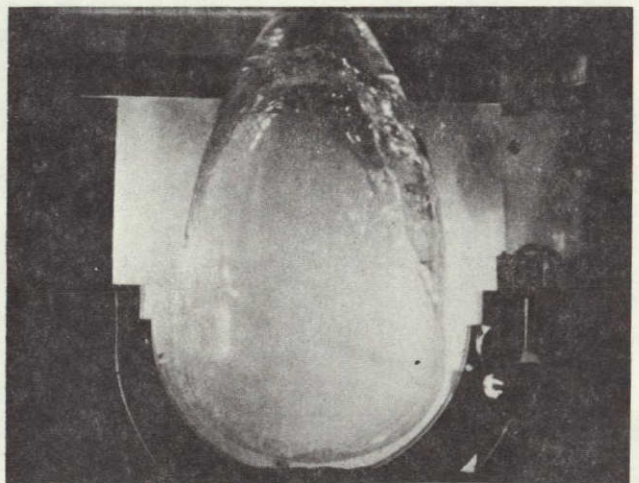
T= 0.4 SEC



T= 0.8 SEC

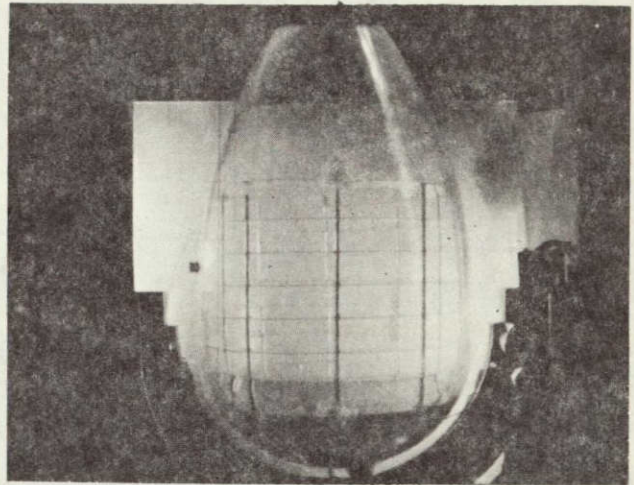


T= 1.2 SEC

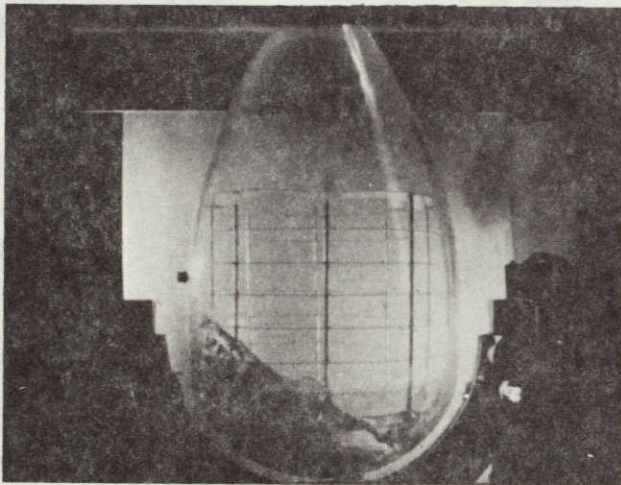


T= 1.6 SEC

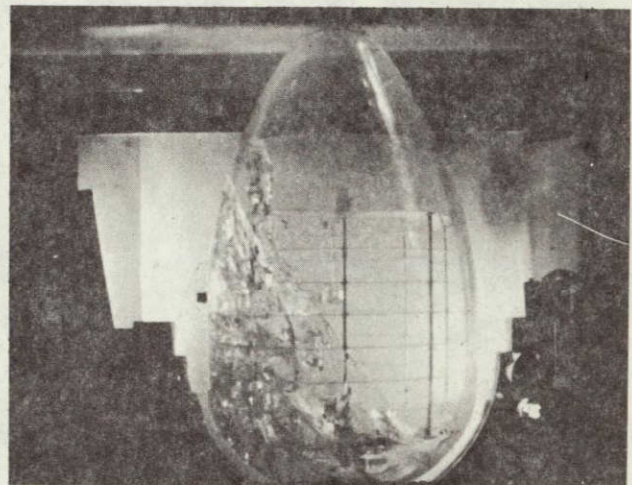
FIGURE III-15. TEST 29, FC-114B2  
 $\gamma = 0^\circ$ , 10% FILL



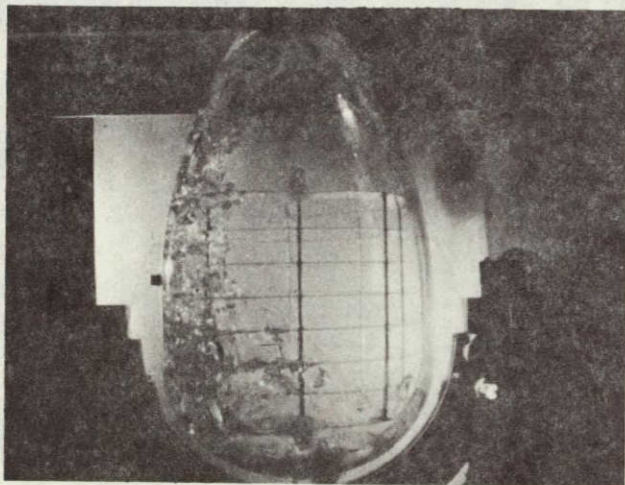
T= 0.0 SEC



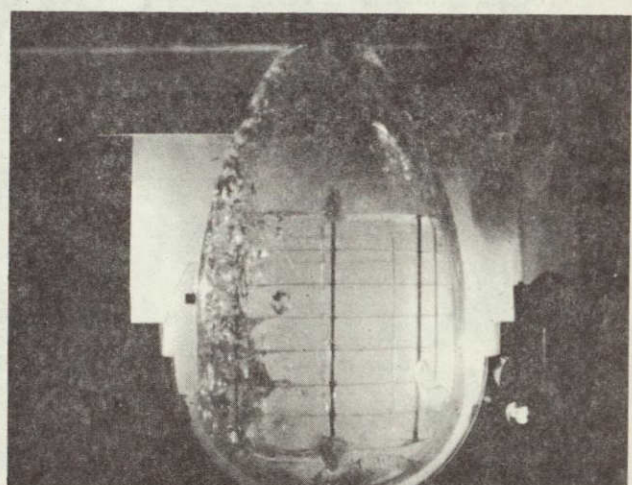
T= 0.4 SEC



T= 0.8 SEC

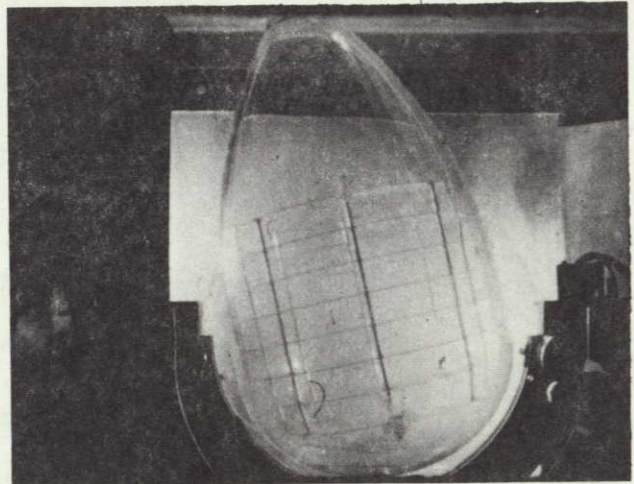


T= 1.2 SEC

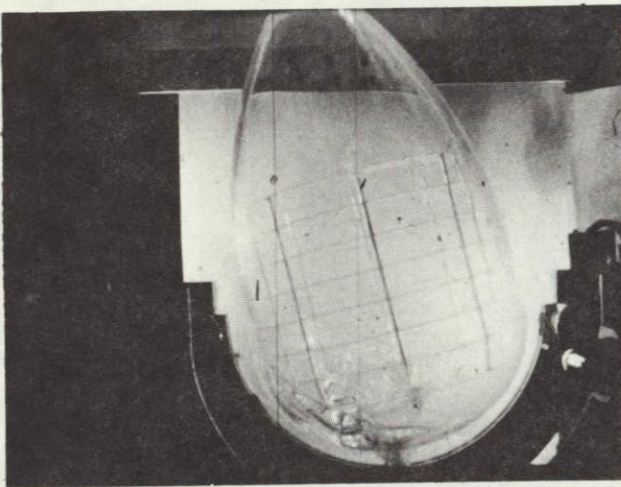


T= 1.6 SEC

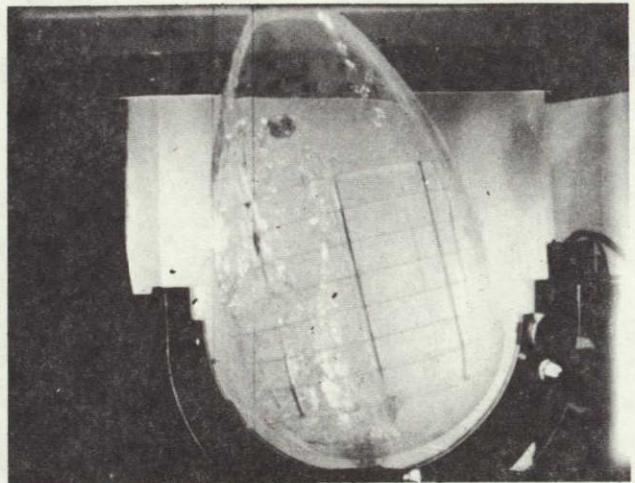
FIGURE III-16. TEST 31, FC-114B2  
 $\gamma = 13^\circ$ , 2% FILL  
LOX LINE OUTFLOW  
INTO TANK



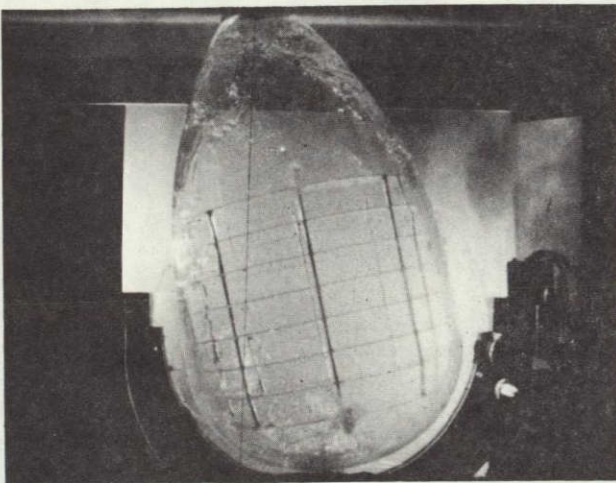
T= 0.0 SEC



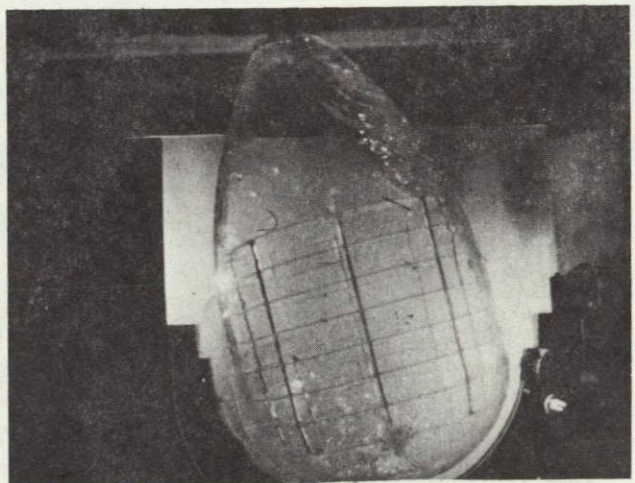
T= 0.4 SEC



T= 0.8 SEC



T= 1.2 SEC



T= 1.6 SEC

ORIGINAL PAGE IS  
OF POOR QUALITY

component of the acceleration is to the right in the photographs. The drop capsule was accelerated downward, producing the axial acceleration component.

#### 1. Liquid Motion in the Bare Tank

All of the tests that were performed are closely interrelated, such that each test can be compared to another that differs by the change of a single variable. The most basic test condition is represented by test number 9. For that test, the bare tank was used, the larger accelerations were applied and FC-114B2, the preferred test liquid, was used. The most typical conditions at ET separation were simulated; a  $13^{\circ}$  orientation angle, a 2% fill volume, and no draining of the feedline.

The liquid motion during this test was typical of that observed during prior test programs (References 9 and 10) using more conventional tank geometries (i.e., spherical tanks and cylindrical tanks with hemispherical domes). It has been found that when there is a lateral component of the acceleration, which may be small in comparison to the axial component, the liquid moves along one side of the tank.

During test 9 the liquid moved up along the left side of the tank in response to the axial and lateral acceleration components (Figure III-5). The flow of liquid began as a thin film and the liquid layer thickened as more liquid began to move. The leading edge of the liquid reached the top of the tank and its momentum carried it down the right side of the tank. As the motion of the leading edge continued, it was slowing, since the axial acceleration opposed the motion. By the end of the test it had reached the bottom of the tank. At that point the liquid was distributed around the tank, but most of it was located on the right side and was beginning to return and collect at the final equilibrium position near the top of the tank. The flow of the liquid was smooth and uniform as it circulated around the tank.

At the beginning of the test there was some tendency for the liquid to move through the center of the tank, as was evident from the hump that formed in the center of the liquid. This hump, which is usually called a Taylor instability, forms because the motion of the liquid along the wall is not rapid enough in comparison to the bulk liquid motion produced by gravity forces. This instability did not persist for very long, since the lateral acceleration caused it to join the flow along the wall and it disappeared.

a. Influence of Fill Volume - Tests 21, 5 (Figure III-1) and 22 (Figure III-10) can now be compared with the above described test 9 to see the influence of the fill volume. These tests had 5, 10 and 15 percent fill, respectively; all other test parameters remained constant. In general, the manner of liquid motion in all four tests was very similar, with the liquid circulating smoothly around the tank along the wall. Therefore, only the differences between the tests will be discussed.

As the liquid volume was increased, the distance the leading edge had traveled by the end of the test also increased. At 15% volume the leading edge passed through the top of the tank, returned down the right side of the tank, passed through the bottom and was again accelerated along the left side of the tank, reaching the top and joining the collected liquid well before the end of the test. At 10% the leading edge completely circled the tank once and was just reaching the top of the tank when the test ended. At 5% it circled the tank and reached the ogive portion of the dome, short of the top.

One reason for this influence of the liquid volume is that the distance between the initial liquid position and the top of the tank decreases as the volume of liquid increases. The contribution of this factor is small, because the reduction in that distance also means the liquid is initially accelerated over a shorter distance. The primary influence of fill volume was the thickness of the liquid layer that was moving along the wall which increased as the liquid volume increased. This factor reduced the influence of the boundary layer and its viscous resistance, in slowing the liquid flow.

It has been shown that the velocity of the liquid's leading edge, under such flow conditions, is approximately 0.88 times the free-fall velocity (Reference 11). When the distance and acceleration were taken into account for each of these tests (5, 9, 21, 22), it was found that the time required for the leading edge of the liquid to reach the top of the tank was the closest to the free-fall condition at volumes of 10% and 15%. At 2% the leading edge was 35% slower than would be predicted based on free-fall, due to the observably thinner liquid layer.

The motion of the leading edge generally involves only a small volume of liquid. At the 2% volume, however, essentially all the liquid is involved in flow characteristic of the leading edge. At the larger volumes, the leading edge flow is only a small fraction of the total liquid motion. Following the leading edge, the remaining liquid continues to flow to the top of the tank. As the leading edge continues to recirculate, the remaining liquid does not achieve as much momentum, so its overshoot at the top of the tank is less. Liquid that has passed through the top comes to rest and returns to the top along the right side of the tank. This overshoot is damped and the liquid gradually collects at its final equilibrium position. A portion of the leading edge, however, may completely circle the tank.

Another significant influence of the fill volume was noted in the way the liquid moved through the tip of the ogive upper dome. At a 2% fill there was a smooth flow of the liquid through the dome. At the larger volumes, with 15% being the most pronounced, the flow through the dome occurred as a filling and emptying of the tip of the ogive. At one point with the 15% volume, most of the liquid had collected in the top of the ogive dome, but then the momentum of the liquid caused some emptying as the liquid recirculated. This effect is due to the tank geometry. Since the liquid must be sharply turned at the top of

the dome and then begin to decelerate, the dome fills faster than it can empty. This phenomena does not occur with a hemispherical dome because a much smoother turning of the liquid occurs.

It has been observed that the damping of the liquid is significantly increased when the liquid must turn a sharp corner. Hemispherical domes do little to damp the liquid motion. A previous test program demonstrated that liquid motion in flat-ended cylindrical tanks was significantly damped as it passed through the sharp corners at the tank ends (Reference 12). A similar influence due to the ogive dome would be expected.

b. Influence of Viscosity - Test 5 (Figure III-1), with 10% volume, was selected to be repeated with the other two test liquids, as Test 6 (FC-43, Figure III-2) and Test 32 (Hexane, Figure III-3). As discussed under the scaling analysis, these three test liquids allow the influence of viscosity on the liquid motion to be evaluated. The FC-114B2 gave the largest Reynolds number (least influence of viscosity), FC-43 gave the lowest Reynolds number, and hexane was intermediate. The scaling analysis had indicated that the influence of viscosity on liquid velocity, during reorientation, should be negligible if the Reynolds number is greater than 50; a requirement that all three test liquids satisfy under the selected test conditions. The velocity of the liquid center of mass was used in defining the Reynolds number.

There were some definite differences between the three tests. The thin leading edge of the liquid flow is most sensitive to the influence of viscous effects. These effects can be observed by comparing the relative motion of the leading edges in the three tests. During the initial motion of the liquid, the leading edges reached the top of the tank in the order of increasing viscosity. The leading edge of the FC-114B2, with the lowest kinematic viscosity, was the first to reach the top of the tank, the hexane took only a slightly longer time and the FC-43 was last to arrive. Even though the kinematic viscosities of the two fluorocarbons differed by a factor of 10, the time to reach the top of the tank differed by only 7%.

As the leading edge of the liquid circled the tank during these three tests, the gap between the two fluorocarbons continued to lengthen. The FC-114B2 circled the tank and reached the top again at the end of the test, while the FC-43 was just above the barrel section after circling the tank. The leading edge of the hexane stayed close to the FC-114B2 until returning to the bottom of the tank. As the hexane passed through the bottom of the tank it slowed, falling behind the position of the FC-43 at the same elapsed time. The hexane caught up with the FC-43 on the left side of the tank and the hexane was slightly ahead of the FC-43 at the end of the test.

The velocity of the leading edge as it recirculates back through the bottom of the tank is influenced by the interaction of two liquid layers. One layer is the recirculating leading edge of the liquid and the other is from liquid that is still moving from the bottom of the

tank, including some liquid that initially began to move up the right side of the tank. As these two layers interact, the wetting characteristics of the liquid, as determined by surface tension and contact angle, will influence the motion of the leading edge. With such interaction, the viscous effects may no longer be the factor determining the liquid velocity, causing the observed differences in the motion of the leading edges in the three tests.

While viscosity causes some differences in the rate of motion of the liquid leading edge, there was very little difference in the bulk motion of the three liquids. The variation of the forces of the liquid on the tank with time were also found to be very similar, especially between the two fluorocarbons since they have similar densities (the force data is discussed in detail later in this chapter). This indicates that on a bulk basis, viscous forces have a negligible effect supporting conclusions of the scaling analysis.

The basic test conditions of Test 9 were also repeated in Test 10, with the exception that the FC-43 was the test liquid. This pair of tests permits the influence of viscous effects at a 2% fill volume to be observed. The leading edge of the liquid reached the top of the tank in essentially the same time with both liquids, but at the end of the test the FC-114B2 was ahead of the FC-43. No other difference between the two tests were noted. It may be that the effects of a small liquid volume, as previously discussed, overwhelm any influence of the change in viscosity.

c. Influence of Tank Orientation - In two of the unbaffled tank tests the tank was oriented at  $30^{\circ}$ , instead of the baseline  $13^{\circ}$ . Since the drop capsule accelerations were not changed, the change in the angle causes the Z component of the acceleration to be increased with respect to the X component when referenced to the tank axes (refer to Figure II-1).

At a 2% fill volume, tests 9 (the baseline) and 24 can be compared. At a 10% fill volume, tests 5 (Figure III-1) and 25 (Figure III-12) can be compared. In both comparisons, the resulting bulk liquid motion is essentially the same. There are only slight differences on the bulk liquid position at equal points in time. Apparently small changes to the tank orientation angle do not significantly change the motion of the liquid relative to the tank.

## 2. Liquid Motion in the Baffled Tank

All of the above discussed tests, performed with the bare tank, were repeated using the baffled tank. The smooth manner of liquid motion observed in the bare tank tests was no longer possible with the baffles present. As the liquid interacted with the baffles, turbulence was produced and the recirculation of the liquid was interrupted.

The baseline test (Test 9), using the bare tank, can be compared to Test 11 (Figure III-6) with the baffled tank. With the baffles, a

portion of the liquid still moved along the left side of the tank as it did with the bare tank. At the 2% fill volume the liquid that reoriented along the wall was a layer thin enough to pass freely under the baffles. The leading edge of this wall flow moved at the same velocity and reached the top of the tank after the same interval as it did in the bare tank (Test 9).

Unlike the bare tank test, some of the liquid in the baffled tank reoriented through the central part of the tank. Streams and drops of liquid formed around the anti-vortex baffle, over the tank outlet. These streams elongate, join and move through the tank, left of the centerline, but to the right of the ring baffles. After these streams thinned out, smaller drops of liquid continued to detach from the anti-vortex baffle throughout the test. Most of the liquid was reoriented through the center of the tank and only a small portion moved along the wall.

The anti-vortex baffle is the cause of this manner of liquid motion. The baffle significantly reduces the influence of the lateral acceleration that was acting to displace the liquid to the side of the tank. This influence of the anti-vortex baffle was most pronounced at the 2% fill level, when the initial liquid orientation almost covered the baffle. Therefore, the axial acceleration moved the liquid through the central region of the tank. The anti-vortex baffle slowed this liquid, so the formation of the streams are delayed. The thin layer of liquid that flowed along the tank wall reached the top of the tank before the streams in the center of the tank, even though the wall flow is strongly influenced by viscous effects.

The central flow impacted the tank wall near the top of the ogive, joining the wall flow. All of the liquid then flowed along the wall, through the top of the tank and down the right side. Due to the small liquid volume there was very little interaction as the liquid reached the ring baffles on the right side of the tank. At the end of the test the liquid position was essentially the same in both the bare and baffled tank tests, being distributed over the right side of the tank. A small quantity of liquid was retained by the anti-vortex baffle throughout the test.

a. Influence of Fill Volume - Test 7, with a 10% fill level and baffles (Figure III-4), can now be compared with Test 11 (2%, baffles) and Test 5 (Figure III-1, 10%, no baffles). At 10% volume the ring baffles had a much stronger influence on the liquid motion and the anti-vortex baffle had very little influence, compared to the test at 2% volume. The motion of the liquid was basically the same as observed with the same volume in the bare tank, but the ring baffles create turbulence within the liquid.

In Test 7 the liquid reoriented along the left side of the tank. With the anti-vortex baffle initially submerged, it produced some distortion of the initial liquid motion, but did not produce any motion through the central region of the tank, as it did at 2% volume. The

initial instability in the center of the liquid was a number of bumps, instead of the single hump observed in the bare tank.

As the liquid flowed past the ring baffles, its depth was sufficient to cause considerable interaction. The turbulence produced can be readily observed in the photographs. Some drops broke loose from the liquid surface. After the liquid passed through the top of the tank it had achieved some velocity prior to reaching the baffles on the right side of the tank. When this flow hit the right side baffles, some of it could pass under the baffles, while some of the liquid was deflected off the upper baffle and shot across to the left side of the tank. The baffles reduced the recirculation that occurred in the bare tank tests. Some of the liquid was retained within the ring baffles, following the initial flow along the left side of the tank. Even though there was no recirculation as occurred in the bare tank, the liquid volume was still distributed over most of the tank at the end of the test. It was difficult to discern if the baffles had increased the rate at which the liquid achieved its equilibrium position.

The filling and draining of the top of the ogive, that was observed with the bare tank, was not evident in the baffled tank. The baffles did not slow the movement of the leading edge of the liquid, since it passed under the baffles. The leading edge reached the top of the tank at essentially the same time in both the bare and baffled tanks for 10% fill. The force data, discussed in Section III.C, provided the best indication of the influence of the baffles on the rate of the bulk motion of the liquid.

The baffled tank tests at 5% volume (Test 19) and 15% volume (Test 20, Figure III-11) can also be compared with the similar bare tank test. Motion similar to that described above for 10% volume was observed and the comparisons between the bare and baffled tank tests were also the same. The motion observed at 2% volume was a special case for both the baffled and bare tank tests.

b. Influence of Viscosity - Test 12 (2%, baffled) and Test 8 (10%, baffled) were performed using FC-43 as the test liquid. These tests can be compared to the previously described baffled tank tests (all of which were performed using FC-114B2) to determine the influence of the liquid viscosity. The differences in the rate of motion of the liquid leading edge, observed in the bare tank tests, was also noted in the baffled tank tests. The leading edge of the more viscous FC-43 always traveled a shorter distance during the test than did the FC-114B2.

In Test 12, a large quantity of liquid was retained at the anti-vortex baffle. Viscosity influenced the rate at which the FC-43 drained around and through the anti-vortex baffle. Otherwise the liquid motion observed in similar FC-43 and FC-114B2 tests exhibited the same characteristics.

c. Influence of Tank Orientation - Two of the baffled tank tests were performed with a 30° inclination, rather than the usual 13° inclination. One test was with a 2% volume (Test 23) and the other was with a 10% volume (Test 26, Figure III-13).

At the 2% volume the larger inclination angle caused some differences in the liquid motion. At 13° the liquid moving through the central region impacted the top of the tank on the left side. With a 30° angle, the liquid still reoriented through the center of the tank, but it impacted slightly to the right of center. This slight change in the impact point was enough to alter the interaction of the wall flow, central flow and the damping of the liquid such that there was no recirculation of the liquid. This resulted in most of the liquid being collected at the top of the tank at the end of the test.

At the 10% volume, differences due to the change in inclination were not significant.

### 3. Effect of Acceleration Magnitude

Some of the above described tests were repeated with a reduced value of the lateral or axial acceleration. The purpose of these tests was to investigate any influence of the acceleration magnitude on the liquid motion. In some tests the application of the lateral component of the acceleration was delayed for 0.5 sec and then applied for the remaining 1.1 seconds. This simulated the change in acceleration that would occur when the external tank separates from the orbiter.

In Tests 13 (Figure III-7) and 14 the force exerted by the lateral spring motor was reduced from 4.4 N to 1.7 N with the axial force remaining at 130 N. Both tests were performed with the baffled tank and a 2% volume, one test using FC-43 and the other FC-114B2. With the smaller lateral acceleration more of the liquid reoriented through the center of the tank. The motion of the liquid was essentially along the tank centerline. The liquid impacted the top center of the tank, while impact was to the left of center with the larger lateral force. Impacting in the center resulted in little overshoot of the liquid, so it was well collected at the top of the tank by the end of the test. This effect is due more to the tank geometry and the point of impact of the central liquid flow, and only indirectly due to the magnitude of the lateral acceleration.

With FC-43 as the test liquid in Test 14 the liquid motion was basically the same as that described above for test 13, with the exception of the previously described effect of viscosity on the leading edge of the wall flow. In Test 14, very little liquid flowed along the left wall. The viscous effects slowed the flow so that the leading edge did not reach the top of the tank during the test.

In Tests 27 through 30 the force of the axial spring motor was reduced from 130 N to 67 N, with the lateral force remaining at 4.4 N. The orientation of the tank was also changed from the usual 13° to 0°. These changes made the acceleration components as close to equal as

possible within the limitations of the test system and without reducing the test duration.

These four tests were compared with similar tests as follows:

Test 27 and Test 11 (2%, baffles)  
 Test 28 and Test 9 (2%, no baffles)  
 Test 29 (Figure III-15) and Test 7 (Figure III-4), (10%, baffles)  
 Test 30 (Figure III-14) and Test 5 (Figure III-1), (10%, no baffles)

These comparisons show that the character of the liquid motion remained the same in all four cases. The rate of motion was slowed due to the lower acceleration, so the bulk liquid has just reached the top of the tank at the end of the test. Changing the angle of orientation from  $13^{\circ}$  to  $0^{\circ}$  did not alter the motion; the same conclusion obtained for changes from  $13^{\circ}$  to  $30^{\circ}$  (see Sections III.A.1c and III.A.2c).

In Tests 15 through 18 the application of the lateral acceleration was delayed for 0.5 seconds. In addition a larger lateral acceleration was used. The following comparisons were made:

Test 15 and Test 9 (2%, no baffles)  
 Test 16 (Figure III-8) and Test 5 (Figure III-1) (10%, no baffles)  
 Test 17 and Test 11 (2%, baffles)  
 Test 18 (Figure III-9) and Test 7 (Figure III-6) (10%, baffles)

While there was only a longitudinal acceleration acting, an instability formed in the center of the liquid surface. In the bare tank this instability was columnar in form, with the column being hollow at the top. In the baffled tank the instability consisted of streams and drops of liquid. It took some time for these instabilities to form, so the motion lagged that observed in the tests with no delay. Most of the liquid moved through the center of the tank in this instability.

Once the lateral acceleration began to act, the instability was displaced to the left side of the tank, joining the flow along the wall. The velocity of the leading edge was also slowed because very little liquid flowed up the wall. When the instability joined the wall flow near the top left side of the ogive, the leading edge of the wall flow and the tip of the instability were both at the same position in the tank.

After the instability and the wall flow joined, the motion was then the same as observed in the undelayed cases. The motion in the delayed cases continued to lag due to the initial slow response.

#### 4. Effect of Liquid Inflow

In Chapter II the influence of feedline draining was evaluated. While it was found that draining of the feedline could occur, the rate of draining is slow. The amount of liquid added to the residual tank

volume, due to feedline draining, is not sufficient to alter the basic character of the reorientation. To show this was true, a worst case situation was simulated in Tests 1 through 4. During these tests a volume of liquid equivalent to the feedline volume flowed into the tank.

In one-g with the liquid in the tank located over the tank outlet, inflow of that volume of liquid only resulted in some turbulence in the liquid. However, in the low-g environment of the test, the inflowing liquid was a jet that impinged on the top of the tank. With the anti-vortex baffle present, this jet was deflected toward the sides of the tank. Inflow at this high rate significantly disturbed the motion of the liquid and added to its momentum.

The result was that these tests were not realistic simulations of the influence of feedline draining. The velocity of the liquid leaving the feedline should not be any greater than the velocity of the residual liquid moving away from the tank outlet, since the acceleration is the only driving force. Therefore, the draining should not accelerate or disturb the liquid in the tank, but only add to its volume.

For Test 31 the tank outlet diameter was enlarged and the volumetric flow rate of the inflow system was decreased to reduce the liquid inflow velocity and give a more realistic simulation of feedline draining. The inflow quantity was equivalent to 55% of the feedline volume so this was still a very conservative simulation. Test 31 (Figure III-16) was compared with Test 11 (Figure III-6) to determine any influence of the inflow.

The inflow still caused some disturbance of the liquid, but most of it was dissipated by the anti-vortex baffle. Liquid can be seen continuing to enter the tank and joining the other liquid as it reorients. Based on the film data, there are no other observable differences due to the inflow.

### C. PARAMETER EFFECTS ON REORIENTATION FORCES

This section presents an evaluation of the effect parameters varied in the test program have on reorientation forces. Comparison force plots are presented to demonstrate the effects of baffles, test liquid viscosity, and percent fill volume. The effects of LOX inflow are also discussed. In general, force trends are more easily evaluated for the higher fill volume tests. This is due to the greater magnitude of the forces produced.

#### 1. Comparisons of Baffled and Unbaffled Test Data

Figures III-17 through III-24 present comparison of reorientation forces between the unbaffled and baffled tanks for similar test conditions. Figures III-17 and III-18 are for FC-43 at 2% and 10% fill

ORIGINAL PAGE IS  
OF POOR QUALITY.

volumes. Figures III-19 through III-22 are for FC-114B2 at fill volumes of 2%, 5%, 10% and 15% respectively. Figure III-17 through III-22 represent the nominal  $\gamma$ ,  $13^\circ$ . Figure III-23 presents forces for FC-114B2 (10% fill) at  $\gamma=30^\circ$ . For reference, Figure III-24 is a comparison of the Tests 16 and 18, which have a step change in acceleration at  $\approx 0.5$  seconds. The forces are presented in the tank coordinate system as shown in Figure II-16. Photographs of several of these tests are presented in Figures III-1 through III-16.

A study of Figures III-17 through III-22, as well as Figures III-1 through III-16, shows that the baffles add turbulence to the reorienting liquid resulting in a much lower reorientation velocity. This can be indirectly observed in the plots of Fz. As the fluid reorients, two forces are exerted on the tank: 1) the D'Alembert acceleration force ( $ma$ ); and 2) a centripetal acceleration force ( $mV^2/R$ ). The peak in the Fz force (@  $\approx 0.9$  sec) is primarily due to the centripetal component. In all comparisons the baffled tank results in a lower peak value. The Fy force also reflects this trend at  $\approx 0.8$  seconds. In the case of Fy a negative spike appears since the liquid reaches maximum velocity on the left side of the tank ( $-Y_T$  direction) just prior to reaching the tip of the ogive.

The Fy plots also reveal another point of interest. The baffled tank cases exhibit a larger negative value for a longer period of time. This is probably due to entrapment of liquid by the baffles and the slower velocity.

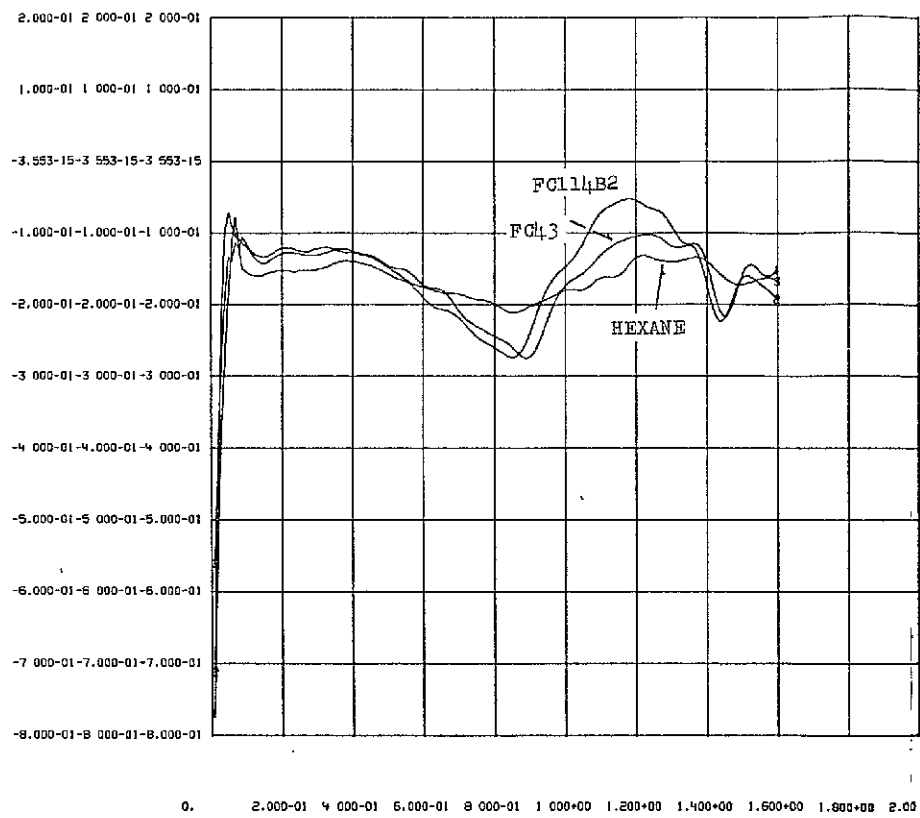
In general, the characteristics of the baffled and unbaffled tests are very similar. The force trends exhibit peaks and valleys which almost overlay each other, except for magnitude. A slight time shift is noted in the baffled cases due to the lower reorientation velocities. Figures III-23 and III-24 exhibit similar trends.

Section B of this chapter discussed the fact that the 2% fill volume exhibited unusual reorientation characteristics due to the anti-vortex baffle. The bulk of the liquid reoriented interior to the baffles instead of along the wall and impacted the tank wall just below the ogive tip. Due to the small forces in the 2% fill cases, no unusual characteristics can be observed in the force data (Figures III-17 and III-19). Trends appear similar to the larger fill volume cases.

## 2. Effects of Liquid Viscosity

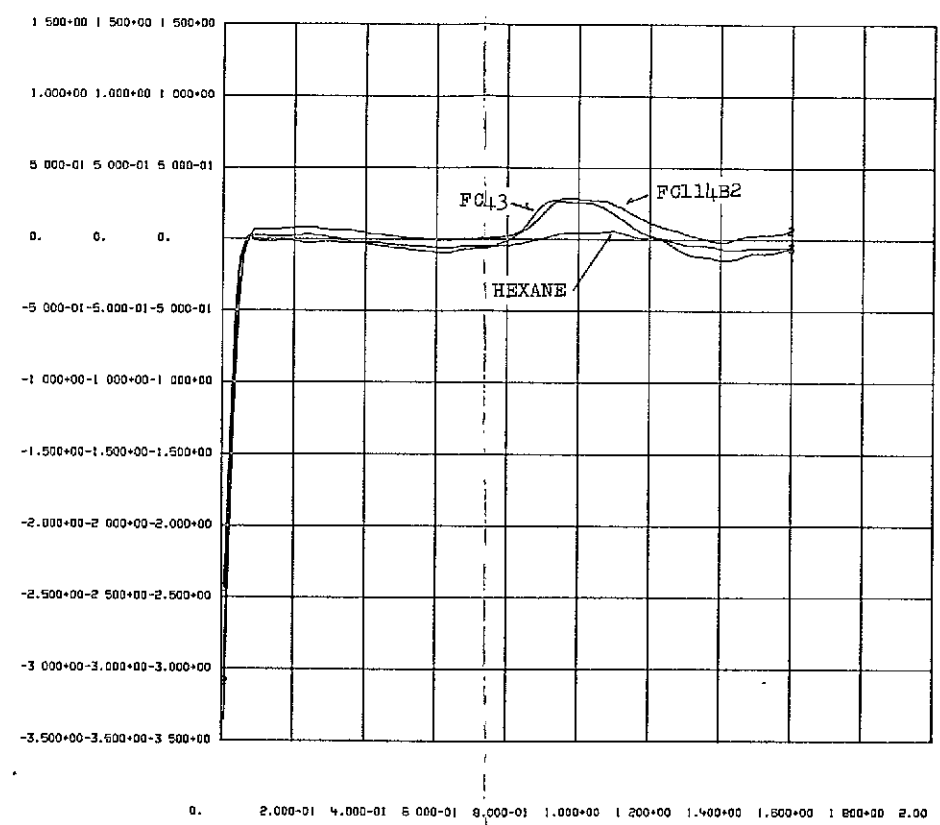
Figure III-25 presents Fy and Fz for Tests 5, 6 and 32: 10% fill,  $\gamma=13^\circ$ , unbaffled tank. The forces for all three test liquids are shown. Absolute magnitude comparisons cannot be made due to the different liquid densities. If viscosity has an effect on forces it would most likely be in the phasing of force peaks. FC-43 is over eight times as viscous as FC-114B2, and almost twenty times as viscous as hexane. However, the results are somewhat inconclusive. No clear trend presents itself in Figure III-25. The Fy plot supplies the most information. The negative

This Page Intentionally Left Blank



TEST32	TEST06	TEST05	FY(LB)	VS	T(SEC)
3	2	1			

CMP2A1 02N077 UNBAFFLED VISCOSITY COMPARISON FY

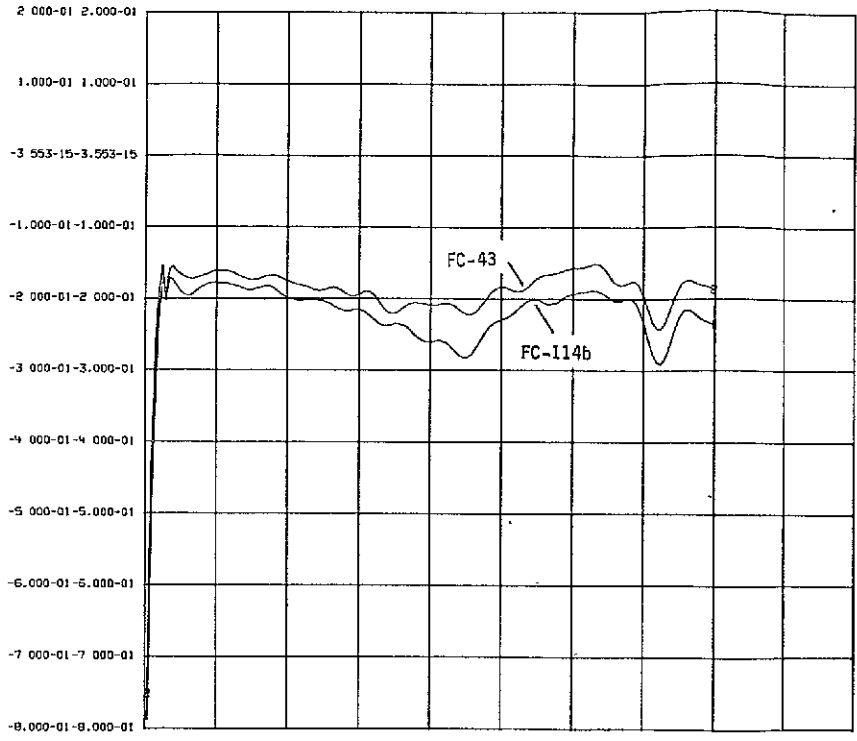


TEST32	TEST06	TEST05	FZ(LB)	VS	T(SEC)
3	2	1			

CMP2A1 02N077 UNBAFFLED VISCOSITY COMPARISON FZ

FIGURE III-25. COMPARISON TEST5/TEST6/TEST32  
 $\gamma = 13^\circ$ , 10% FILL

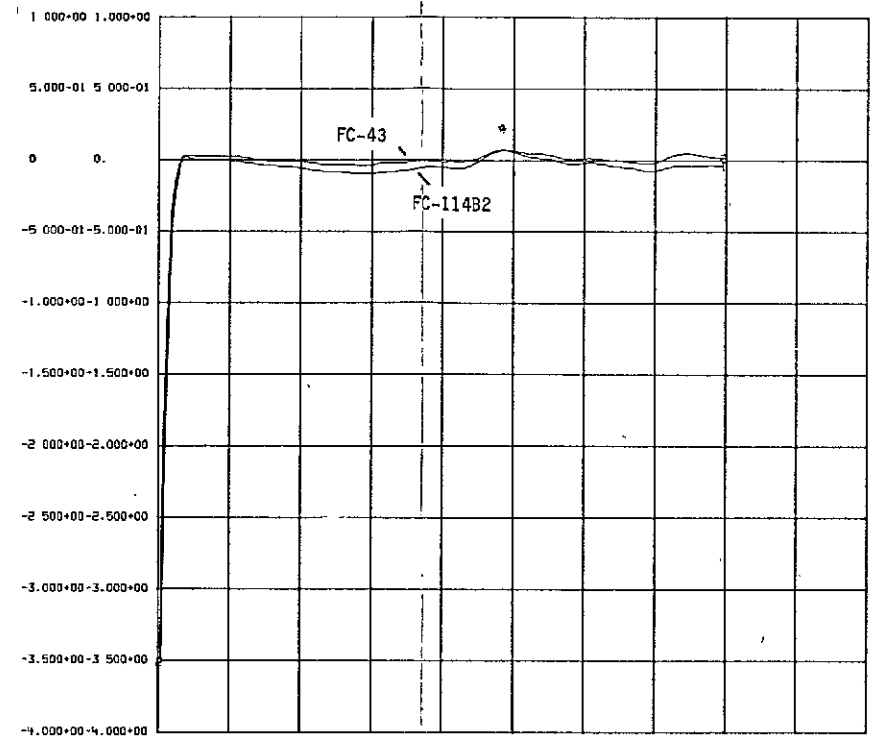
ORIGINAL PAGE IS  
 OF POOR QUALITY



0. 2.000e-01 4.000e-01 6.000e-01 8.000e-01 1.000e+00 1.200e+00 1.400e+00 1.600e+00 1.800e+00 2.000e+00

TEST08	TEST07	FY(LB)	VS	T(SEC)
2	1			

CH2801 03X077 BAFFLED VISCOSITY COMPARISON FY



0. 2.000e-01 4.000e-01 6.000e-01 8.000e-01 1.000e+00 1.200e+00 1.400e+00 1.600e+00 1.800e+00 2.000e+00

TEST08	TEST07	FZ(LB)	VS	T(SEC)
2	1			

CH2801 03X077 BAFFLED VISCOSITY COMPARISON FZ

FIGURE III-26. COMPARISON TEST7/TEST8  
 $\gamma = 13^\circ$ , 10% FILL

C-8

Fy peak for FC-114B2 occurs slightly ahead of the peak for FC-43, time-wise. This indicates, perhaps, that the less viscous FC-114B2 is moving a little faster than the FC-43. In general, however, viscosity does not seem to have an appreciable effect on force trend characteristics. As discussed in Section III.B it may have some effect on recirculation.

Figure III-26 is a comparison of Tests 7 and 8 (FC-43, FC-114B2); 10% fill,  $\gamma = 13^\circ$ , baffled tank. Once again there appears to be no appreciable difference due to viscosity.

### 3. Effects of Percent Fill Volume

Experience from other propellant motion studies has indicated that fill volume does not alter the basic character of the propellant motion. Results from this study verify that conclusion (with the possible exception of the 2% baffled case). Figures III-27 and III-28 present comparisons for unbaffled tests at 2%, 5%, 10% and 15% fill volumes. The unbaffled cases are shown because their larger forces make trend identification easier.

Larger fill volumes have larger force peaks and peak sooner than smaller volumes. Smaller volumes must traverse a longer distance to reach the same relative point in the tank, resulting in a peak time delay. Figures III-27 and III-28 exhibit these characteristics.

### 4. LOX Inflow

Due to the small force magnitude in the 2% fill cases, no effect of LOX inflow on the force trends could be identified. As discussed in Chapter II, LOX inflow would add a very small percentage of liquid to the tank during RTL separation. It is felt that inflow is not an important parameter to be considered in simulations of the RTL abort. The tests conducted were very conservative and even so did not result in noticeable force differences.

## D. ANALYTICAL CORRELATION

The primary objective of this study was to develop a data base for use in validating JSC's analytical simulation of large amplitude propellant slosh during the RTL abort. An evaluation of current modeling techniques has been conducted based on the 1/60<sup>th</sup> scale model test results.

Martin Marietta has developed, under a previous NASA contract (Reference 9), a large amplitude slosh model (LAMPS) similar to JSC's SVDS slosh model. The analog portrays the propellant as a point mass moving on an ellipsoidal constraint surface. The constraint surface formulation was modified to be consistent with JSC's formulation. The surface is a distorted ellipsoid defined by the following equation,

$$\left(\frac{Y_E}{b}\right)^2 + \left(\frac{Z_E}{a_0 - a_1 \frac{Z_E}{a_0}}\right)^2 = 1$$

where:  $a_0 = a_{fwd} (1 + a_1)$

$$a_1 = \frac{a_{aft} - a_{fwd}}{a_{aft} + a_{fwd}}$$

$b$  = semi-minor axis of the ellipse

$a_{fwd}$  = semi-major axis of the ellipse representing the forward part of the tank

$a_{aft}$  = semi-major axis of the ellipse representing the aft part of the tank

The coefficients  $a_{fwd}$ ,  $a_{aft}$  and  $b$  are defined by the static propellant cm location obtained by analytically rotating the tank in a lg field. Figure III-29 delineates the model concept.

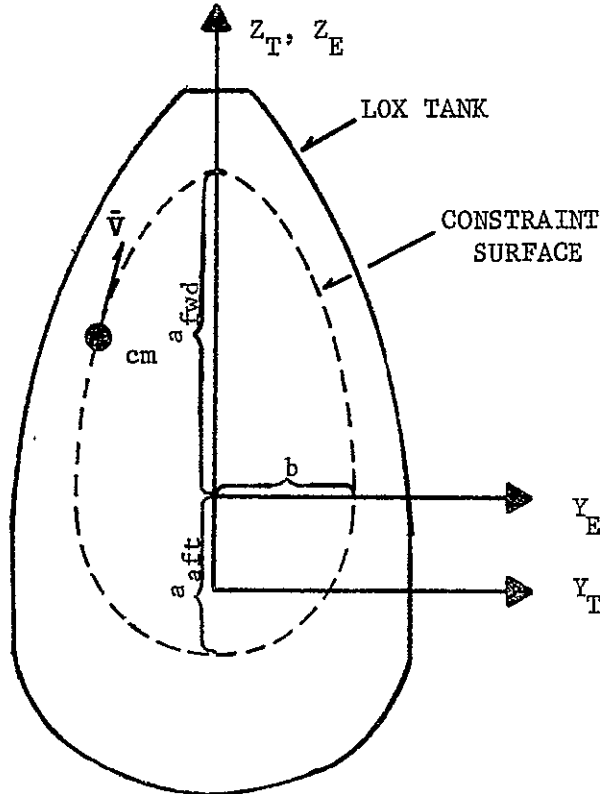


Figure III-29. Analytical Model Concept

The LAMPS model was successfully correlated in Reference 10 to test data obtained using a model tank with a short barrel section and hemispherical domes. The total force exerted by the moving propellant, on the tank, can be expressed conceptually as,

$$F = \frac{m V^2}{R} + m A$$

where:  $m A$  = D'Alembert acceleration force

$$\frac{m V^2}{R} = \text{centripetal acceleration force}$$

It was found that fairly good correlation could be obtained by adjusting the centripetal acceleration component of force with an empirically derived effective mass factor,  $f_m$  ( $f_m \leq 1.0$ ).

$$F = f_m \frac{m V^2}{R} + m A$$

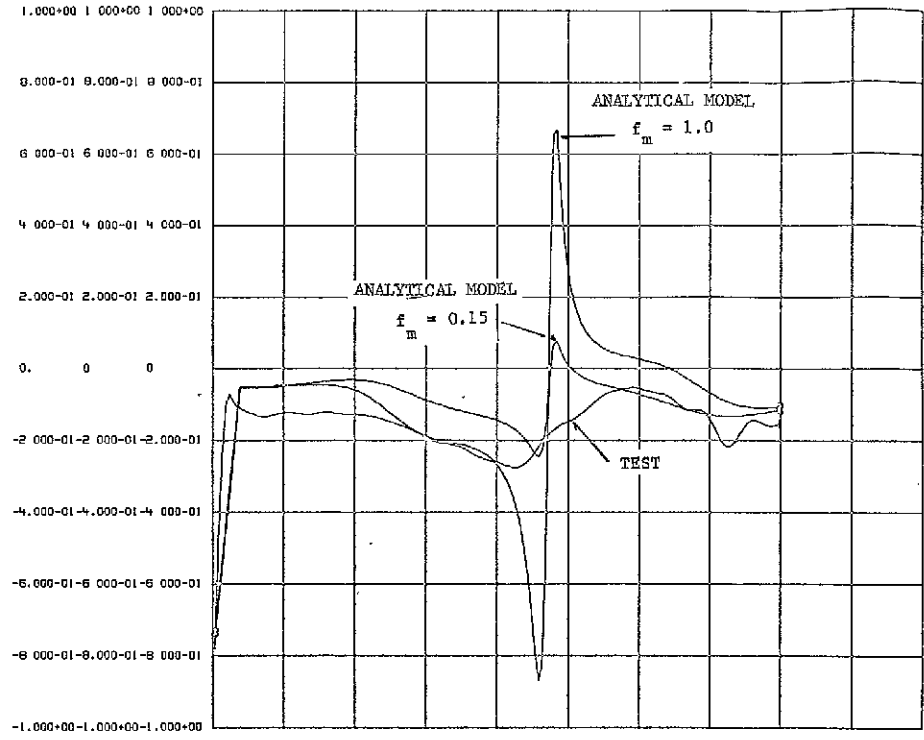
This effective mass factor is an attempt to account for the expansion and contraction of the propellant surface area. The centripetal acceleration force acts normal to the fluids velocity vector. Hence, surface expansion results in a smaller equivalent mass acting at the fluid cm, as in the point mass model. Examination of Figures III-1 through III-16 reveals this phenomena. In previous studies, the effective mass factor has been empirically derived as a function of tank fill volume.

The effective mass concept was used in attempting to correlate the modified LAMPS program with the 1/60th scale model drop tower test data. Figure III-30 shows a sample correlation attempt. It is apparent from the correlation (or lack of correlation) that a single point mass model is not adequate to represent propellant reorientation forces in a tank with the geometry of the ET LOX tank. The measured forces maintain their peak values over a larger period of time than the analytical point mass model. It is felt that better correlation can be achieved through the use of a multiple mass model. JSC has made some cursory runs with their SVDS slosh model using multiple masses and achieved promising results. Phase II of this contract will concentrate on developing a multiple mass approach to simulation which can be used with confidence in full-scale simulations of the Shuttle RTLS abort.

ROBOUT FRAME  
1

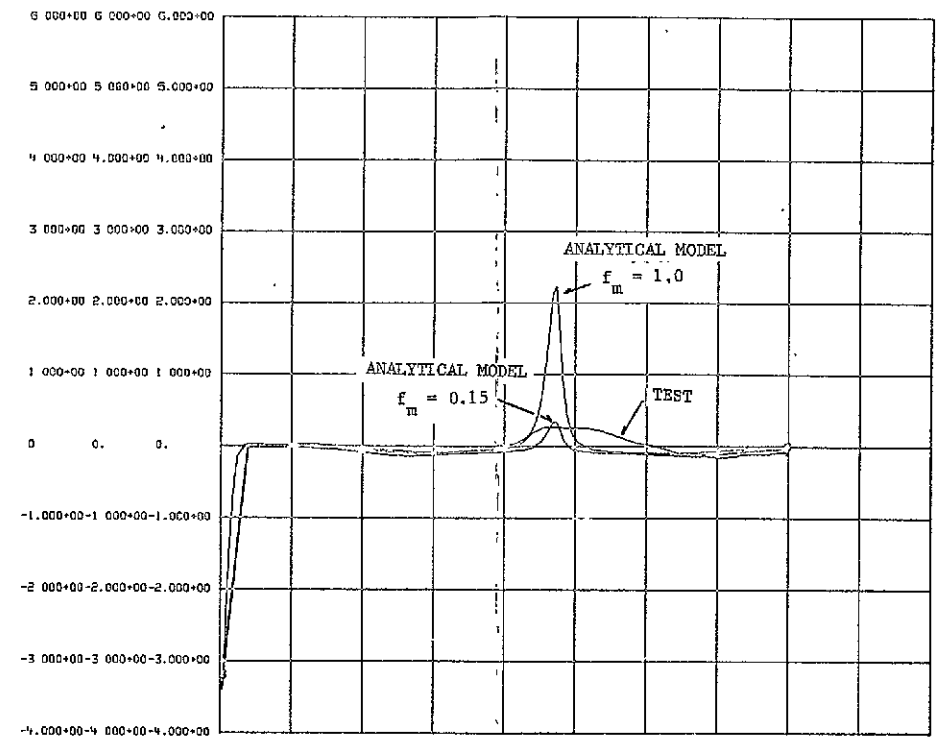
ROBOUT FRAME  
2

III-44



0. 2.000-01 4.000-01 6.000-01 8.000-01 1.000+00 1.200+00 1.400+00 1.600+00 1.800+00 2.00

TEST05 TEST05 TEST05 FY(LB) VS T(SEC)  
3 2 1 C/P4A1 06N077 TEST ANALYTICAL COMPARISON FY



0. 2.000-01 4.000-01 6.000-01 8.000-01 1.000+00 1.200+00 1.400+00 1.600+00 1.800+00 2.00

TEST05 TEST05 TEST05 FZ(LB) VS T(SEC)  
3 2 1 C/P4A1 06N077 TEST ANALYTICAL COMPARISON FZ

FIGURE III-30. TEST/ANALYTICAL CORRELATION

ORIGINAL PAGE IS  
OF POOR QUALITY

#### IV. CONCLUSIONS AND RECOMMENDATIONS

---

Evaluation of the motion picture data lead to the following conclusions regarding the character of liquid motion observed during the tests.

In the unbaffled tank, liquid motion was basically the same as observed with more conventional tank geometries in previous test programs. The lateral acceleration component causes the liquid to reorient along the side of the tank. Overshoot and recirculation occur before the liquid achieves its final equilibrium position. At low liquid volume (2%) viscous effects slow the liquid motion. At larger fill volumes (10%, 15%) the liquid accumulates in the upper ogive before recirculation takes place. Liquid viscosity influences the velocity of the leading edge of the reorienting liquid, but does not alter the velocity of the bulk liquid. Small changes to tank orientation ( $\gamma$ ) did not alter the basic character of the liquid motion.

The primary effect of the slosh baffles was to cause the reorienting flow to be very turbulent. At small volumes (2%) the anti-vortex baffle caused most of the liquid to reorient through the center of the tank, rather than along the side.

Changes in the magnitude of the acceleration components did not significantly alter the manner of liquid motion. When the application of the lateral component was delayed, the liquid moved through the center of the tank, joining the wall flow after application of the lateral acceleration. Inflow of liquid, simulating feedline draining, does not alter the liquid motion.

- R.1 NASA should proceed with low-g testing of a 10% scale model of the ET LOX tank. This testing is necessary to further assess; 1) the effects of Reynolds number on reorientation; 2) the effect of the anti-vortex baffle on the reorientation character and forces for low fill volumes; and 3) upward scaling to the full-scale ET.

The single point mass analog in NASA's SVDS computer simulation is inadequate to represent the propellant interaction forces during reorientation. A multiple mass simulation appears to be a promising alternative.

- R.2 Studies should be initiated to develop a multiple mass analog to simulate propellant motion during the RTLS separation; correlated with the available test data.

Fluid reorientation forces measured in this study were similar in character to those measured in previous studies. The slosh baffles affect both the magnitude and time phasing of the measured forces; compared to the bare tank. Further study and simulations of the actual ET/orbiter separation are required before the implications of the baffles on RTLS separation are fully understood.

The effect of viscosity on the reorientation forces appears to be small. However, implementation of Recommendation 1 (R.1) will further clarify any effects. LOX inflow does not appear to be a significant parameter in the simulation of large amplitude propellant reorientation during RTLS separation.

V. REFERENCES

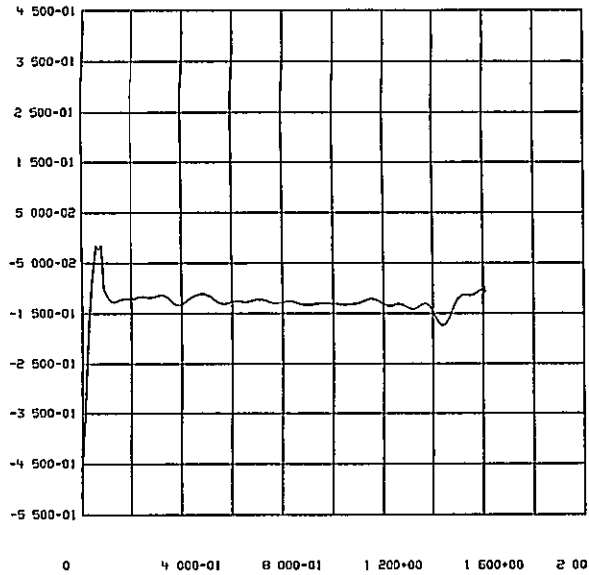
---

1. J. F. McCarthy, Jr.: "Zero-G Propulsion Problems", in Jet, Rocket, Nuclear, Ion and Electric Propulsion: Theory and Design, W.H.T. Loh (ed), Springer-Verlag, New York, 1968.
2. R. C. Weast, Ed: "Handbook of Chemistry and Physics", 53rd Edition, The Chemical Rubber Company, Cleveland, Ohio, 1972.
3. J. J. Jasper: "The Surface Tension of Pure Liquid Compounds", J. of Physical and Chemical Reference Data, Volume 1, No. 4, 1972.
4. T. A. Coney: "Surface Tension, Viscosity and Density Measurements of Two Fluorocarbon Solvents", NASA TM X-1862, NASA Lewis Research Center, Cleveland, Ohio, August 1969.
5. "FC-114B2, Dibromotetrafluoroethane", Freon Technical Bulletin B-4B, E. I. DuPont de Numours and Company, Wilmington, Delaware.
6. T. E. Bowman: "Cryogenic Liquid Experiments in Orbit, Volume I: Liquid Settling and Interface Dynamics", NASA CR-651, Martin Marietta Corporation, Denver, Colorado, December 1966.
7. D. G. Stephens: "Experimental Investigations of Liquid Impact in a Model Propellant Tank", NASA TN D-2913, NASA Langley Research Center, Hampton, Virginia, October 1965.
8. G. B. Wallis: "One Dimensional Two-Phase Flow", McGraw-Hill Book Company, 1969.
9. R. L. Berry and J. R. Tegart: "Experimental Study of Transient Liquid Motion in Orbiting Spacecraft, Interim Report", MCR-75-4, Martin Marietta Corporation, Denver, Colorado, February 1975.
10. R. L. Berry and J. R. Tegart: "Experimental Study of Transient Liquid Motion in Orbiting Spacecraft, Final Report", MCR-76-11, NASA-CR-144213, Martin Marietta Corporation, Denver, Colorado, February 1976.
11. T. E. Bowman: "Sheet of Liquid Flowing Down a Wall", The Physics of Fluids, Volume 14, No. 7, July 1971, pp. 1578-1579.
12. J. R. Tegart and R. L. Berry: "Propellant Motion in Compartmented Tanks", 0482-76-MS1, Martin Marietta Corporation, Denver, Colorado, May 1976.

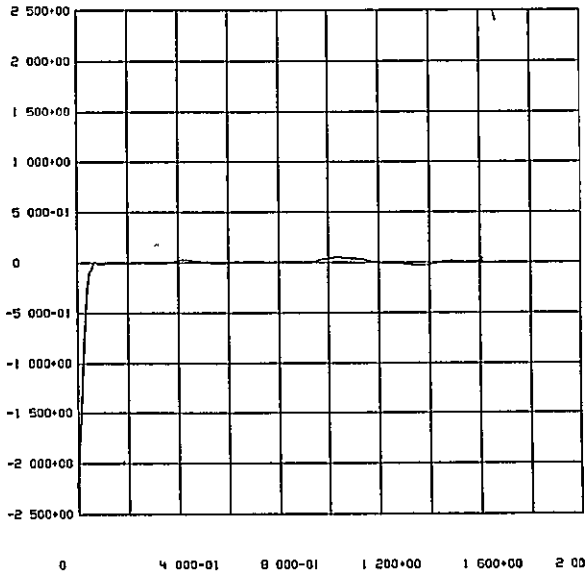
## APPENDIX A - FORCE TIME HISTORIES

---

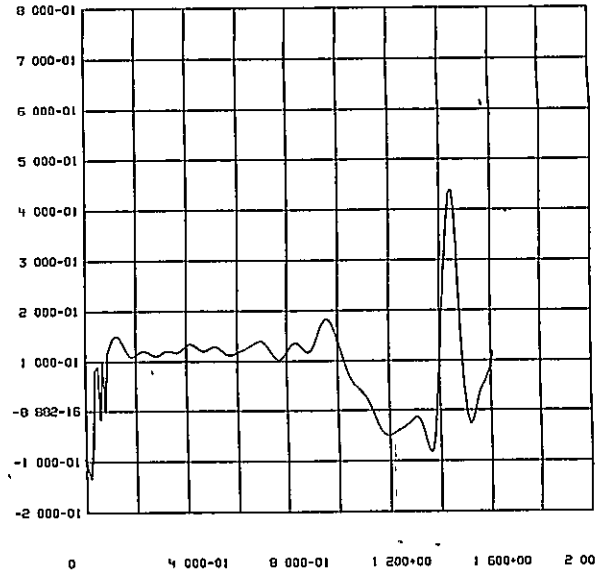
This appendix presents the measured force time histories for all 32 tests. For each test there are three plots:  $F_y$ ,  $F_z$ , and  $M_x$ . The forces are presented in the tank coordinate system.



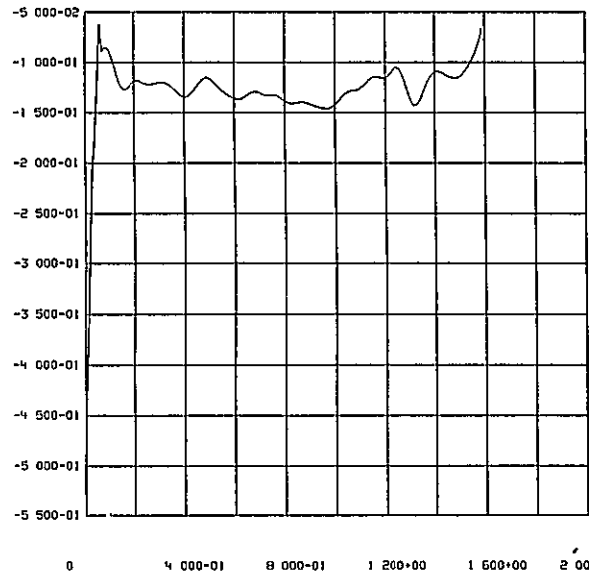
FY(LB) VS T(SEC)  
1 TEST01 140C77 RAW DATA TANK TRIAD



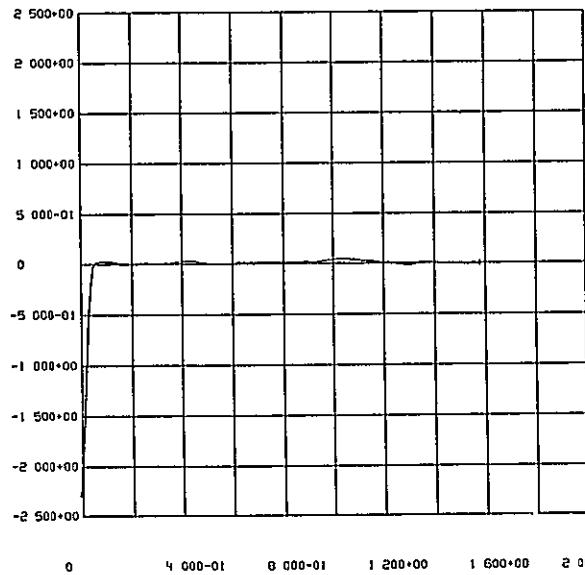
FZ(LB) VS T(SEC)  
1 TEST01 140C77 RAW DATA TANK TRIAD



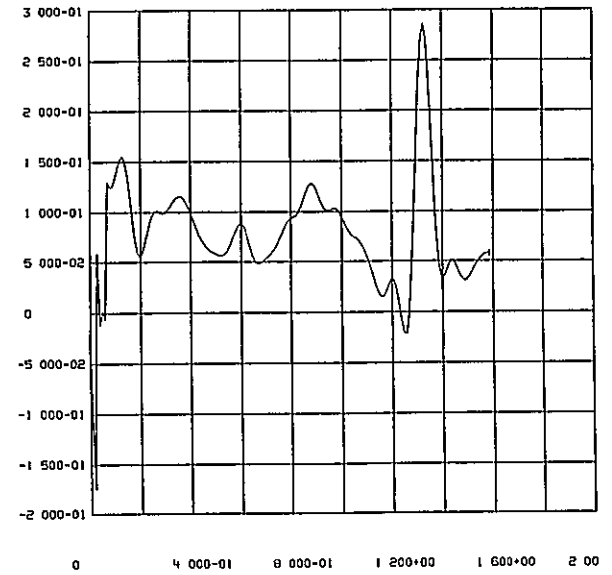
MX(1P) VS T(SEC)  
1 TEST01 140C77 RAW DATA TANK TRIAD



FY(LB) VS T(SEC)  
1 TEST02 140C77 RAW DATA TANK TRIAD



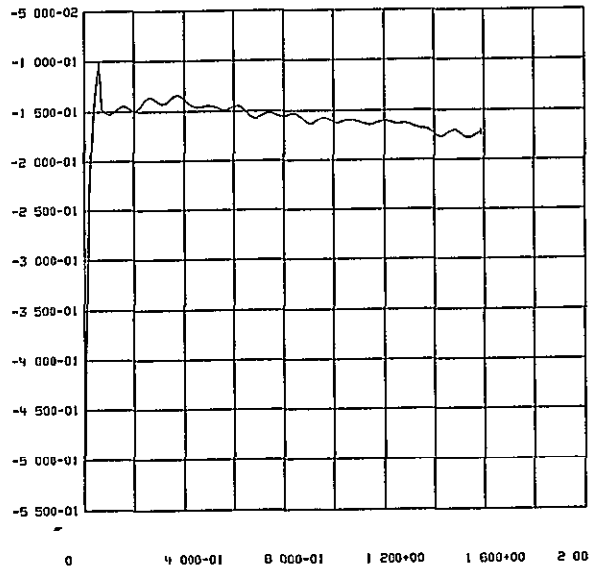
FZ(LB) VS T(SEC)  
1 TEST02 140C77 RAW DATA TANK TRIAD



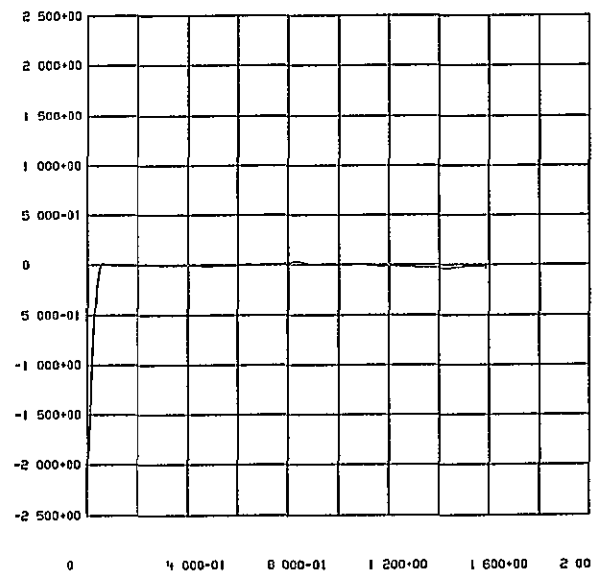
MX(1P) VS T(SEC)  
1 TEST02 140C77 RAW DATA TANK TRIAD

A-2

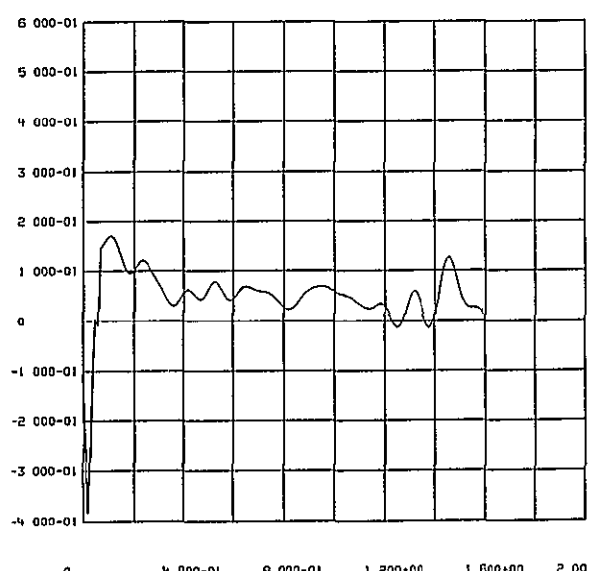
ORIGINAL PAGE IS  
OF POOR QUALITY



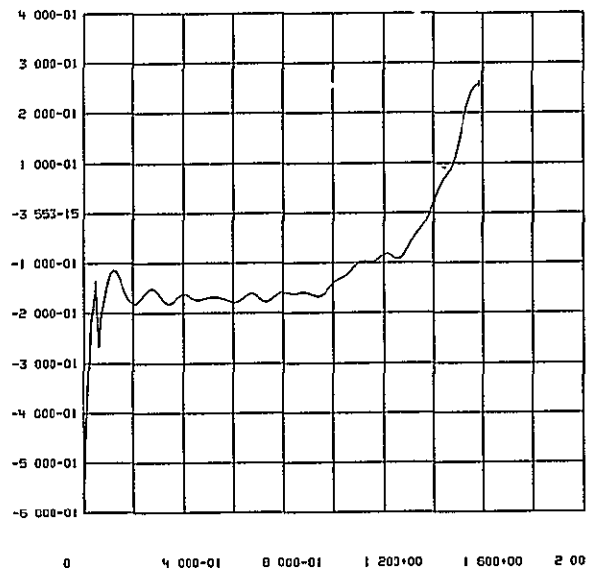
FY(LB) VS T(SEC)  
1 TEST03 03N077 RAW DATA TANK TRIAD



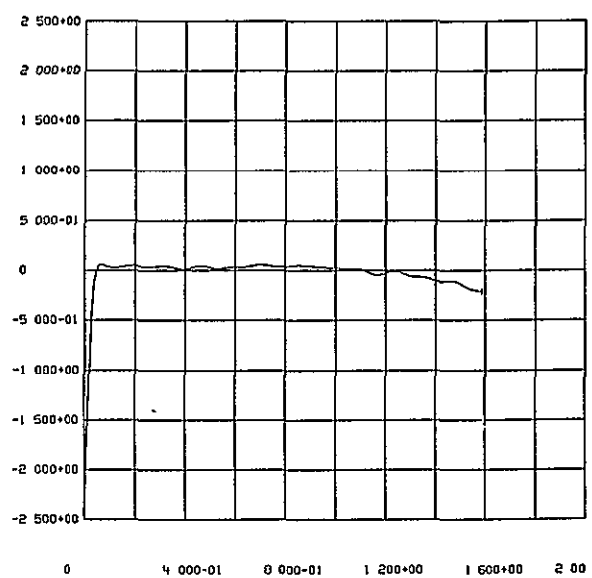
FZ(LB) VS T(SEC)  
1 TEST03 03N077 RAW DATA TANK TRIAD



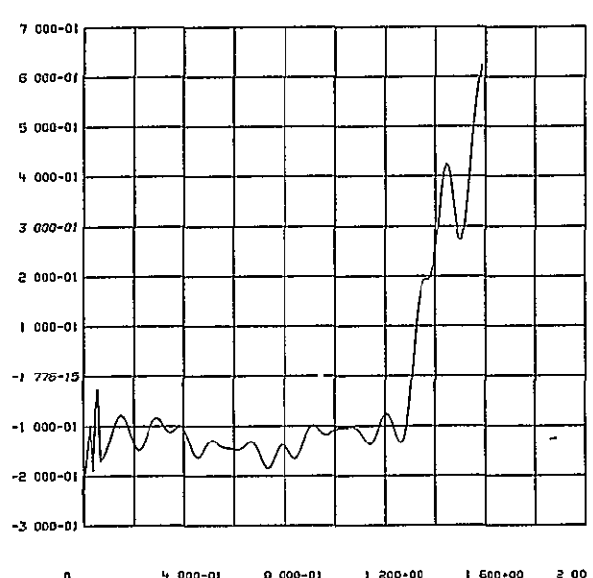
HX(IP) VS T(SEC)  
1 TEST03 03N077 RAW DATA TANK TRIAD



FY(LB) VS T(SEC)  
1 TEST04 03N077 RAW DATA TANK TRIAD

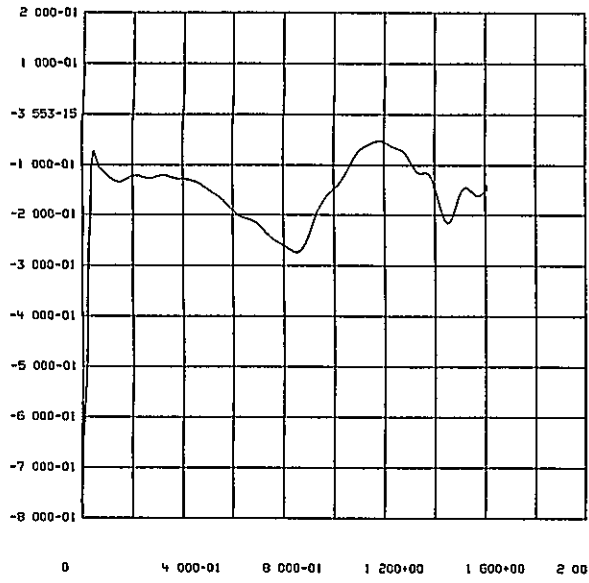


FZ(LB) VS T(SEC)  
1 TEST04 03N077 RAW DATA TANK TRIAD

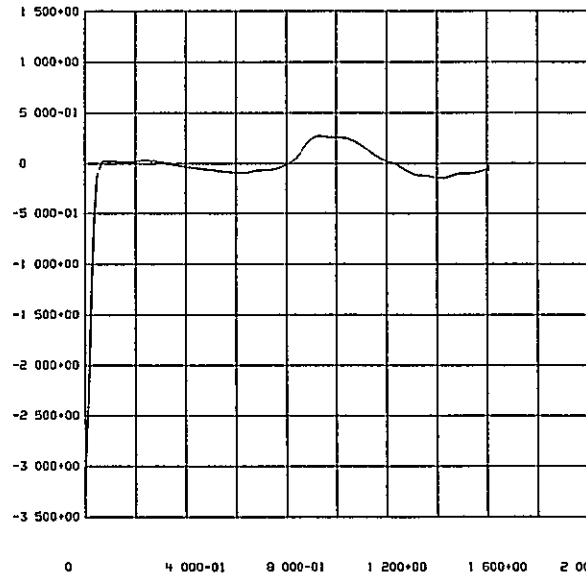


HX(IP) VS T(SEC)  
1 TEST04 03N077 RAW DATA TANK TRIAD

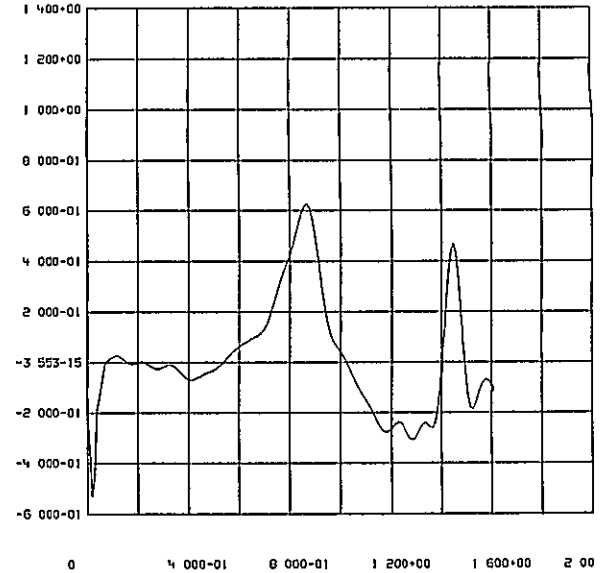
4-3



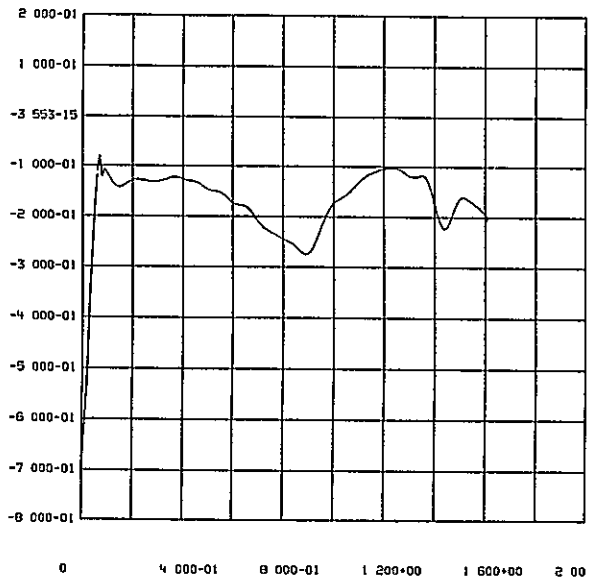
FY(LB) VS T(SEC)  
 1 TEST05 140C77 RAW DATA TANK TRIAD



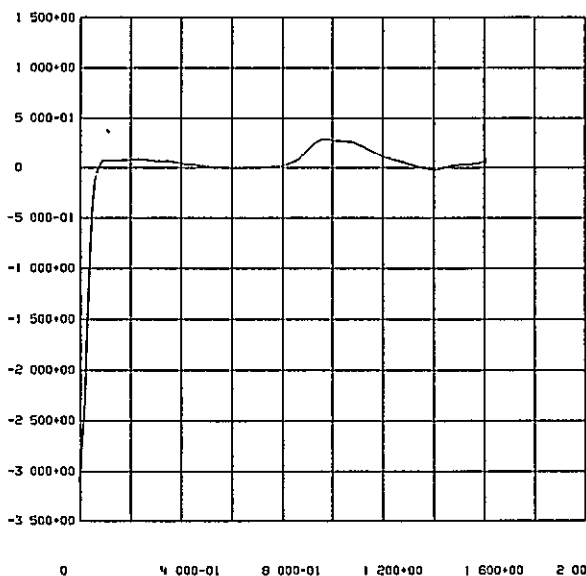
FZ(LB) VS T(SEC)  
 1 TEST05 140C77 RAW DATA TANK TRIAD



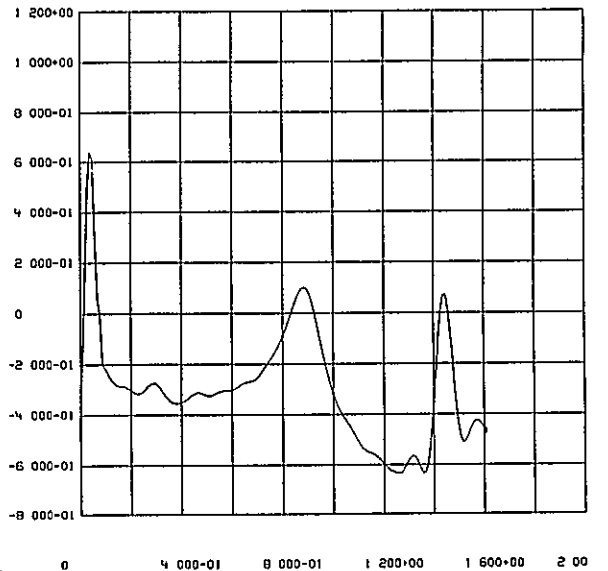
MX(IP) VS T(SEC)  
 1 TEST05 140C77 RAW DATA TANK TRIAD



FY(LB) VS T(SEC)  
 1 TEST06 140C77 RAW DATA TANK TRIAD

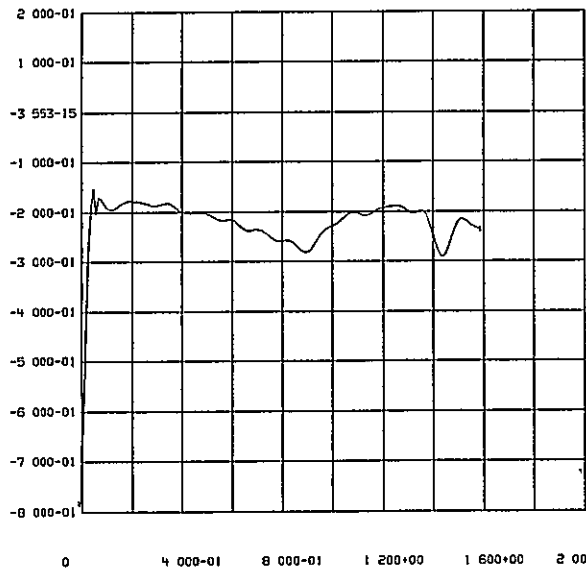


FZ(LB) VS T(SEC)  
 1 TEST06 140C77 RAW DATA TANK TRIAD

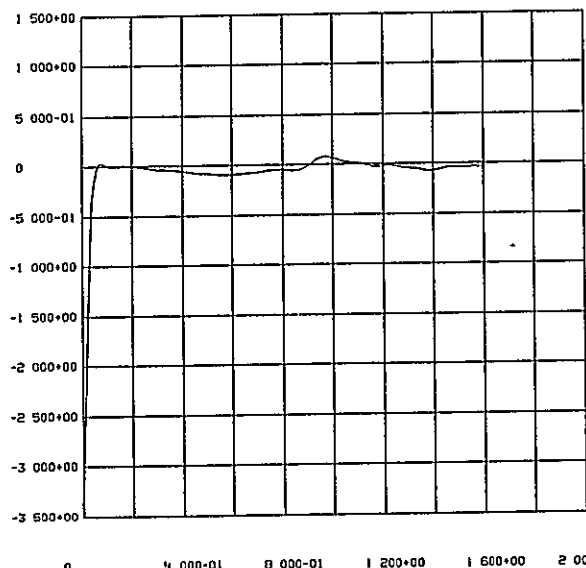


MX(IP) VS T(SEC)  
 1 TEST06 140C77 RAW DATA TANK TRIAD

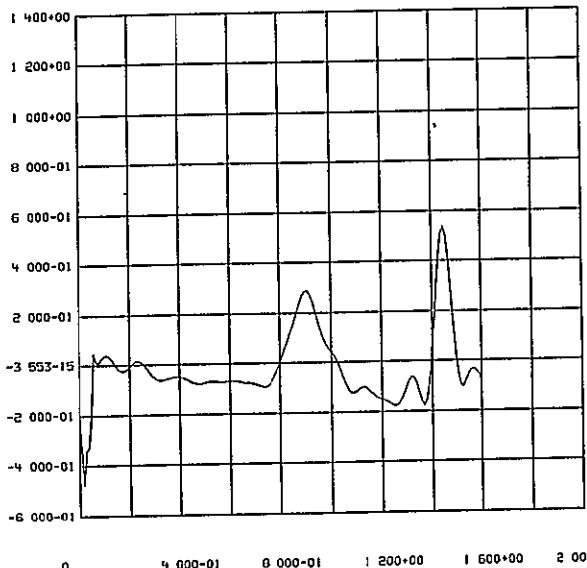
7-4



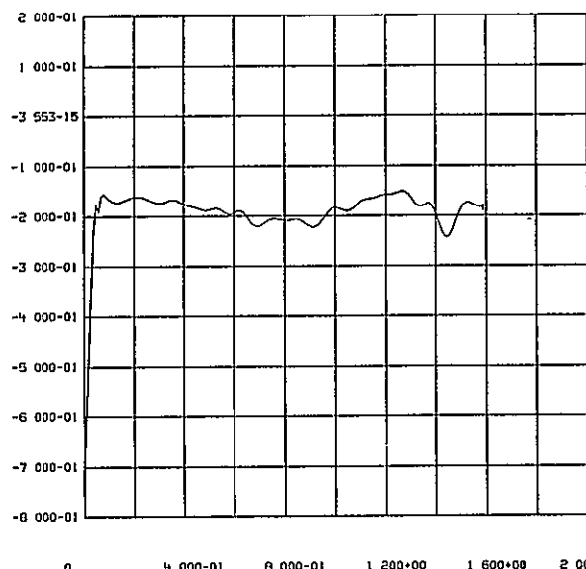
FY(LB) VS T(SEC)  
1 TEST07 03N077 RAW DATA TANK TRIAD



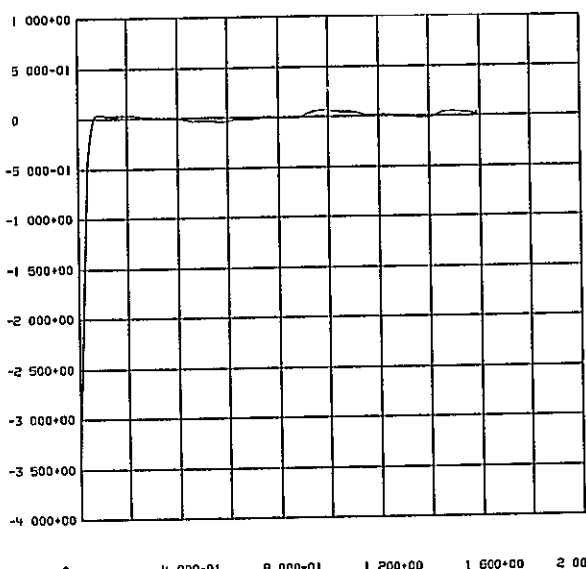
FZ(LB) VS T(SEC)  
1 TEST07 03N077 RAW DATA TANK TRIAD



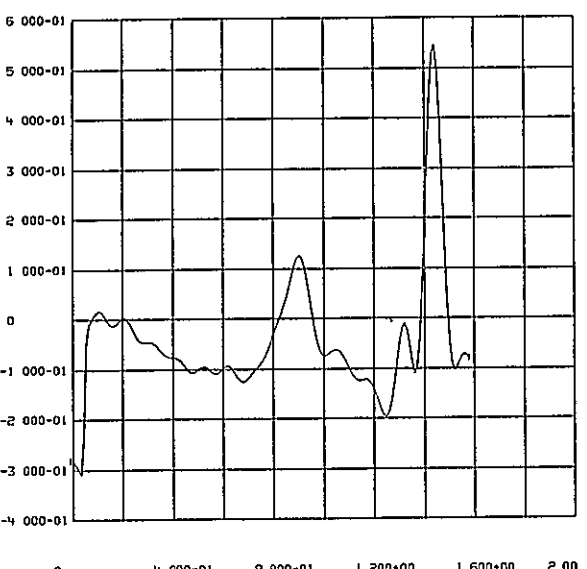
FX(IP) VS T(SEC)  
1 TEST07 03N077 RAW DATA TANK TRIAD



FY(LB) VS T(SEC)  
1 TEST08 03N077 RAW DATA TANK TRIAD

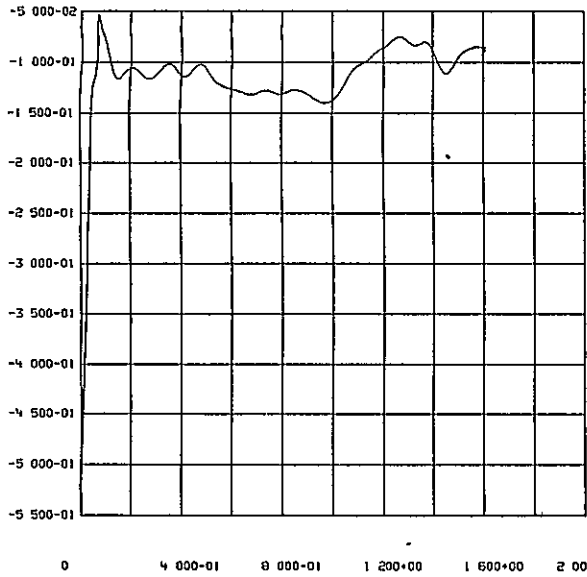


FZ(LB) VS T(SEC)  
1 TEST08 03N077 RAW DATA TANK TRIAD

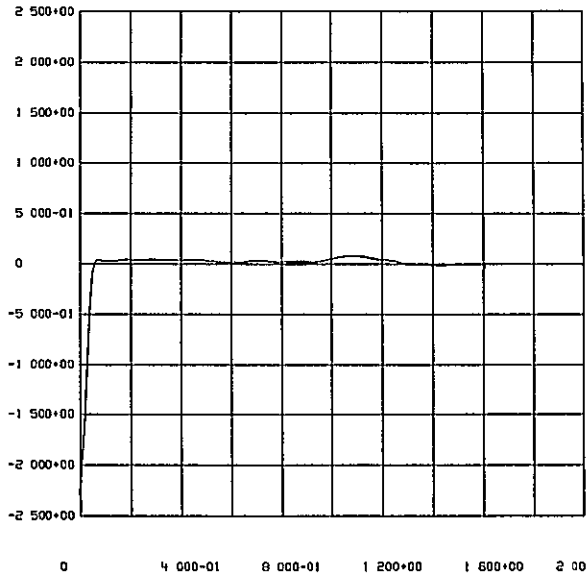


FX(IP) VS T(SEC)  
1 TEST08 03N077 RAW DATA TANK TRIAD

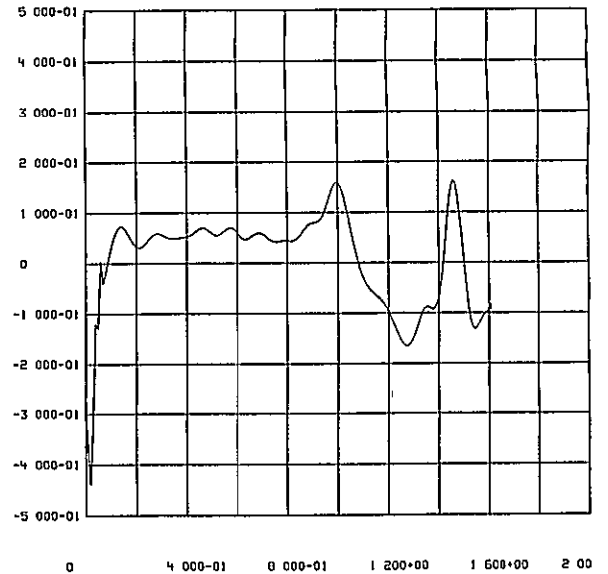
ORIGINAL PAGE IS  
OF POOR QUALITY



FY(LB) VS T(SEC)  
1 TEST09 140C77 RAW DATA TANK TRIAD

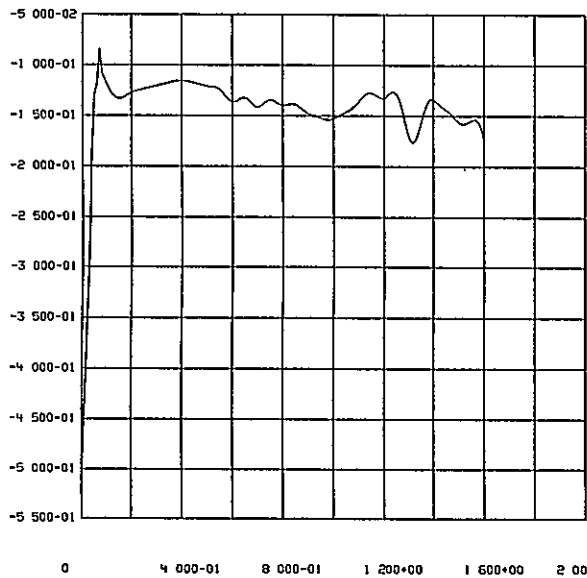


FZ(LB) VS T(SEC)  
1 TEST09 140C77 RAW DATA TANK TRIAD

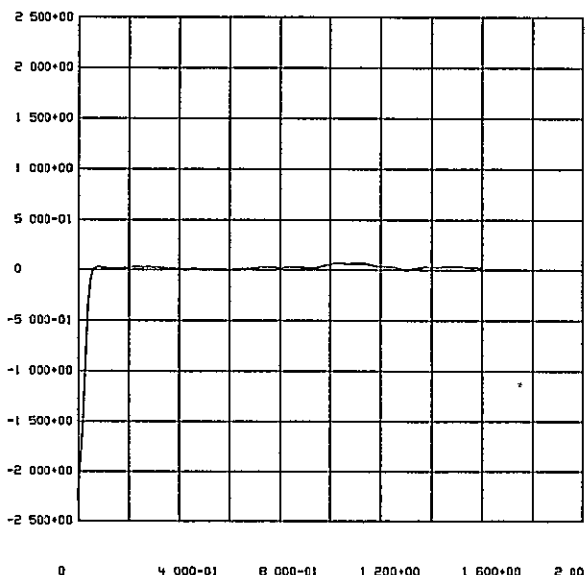


MX(IP) VS T(SEC)  
1 TEST09 140C77 RAW DATA TANK TRIAD

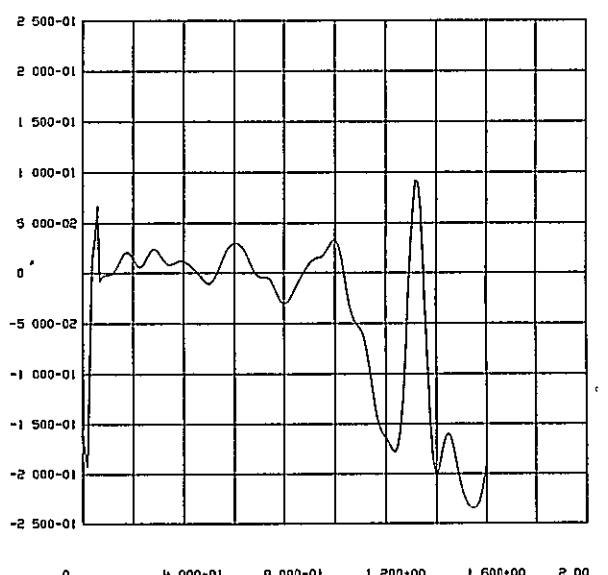
4.3



FY(LB) VS T(SEC)  
1 TEST10 140C77 RAW DATA TANK TRIAD

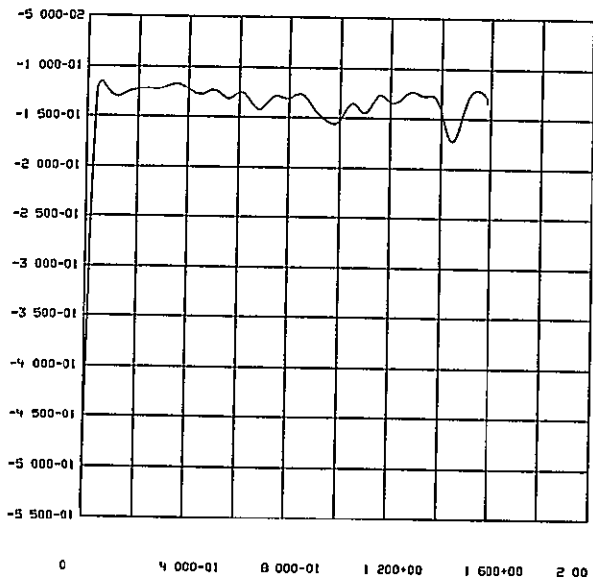


FZ(LB) VS T(SEC)  
1 TEST10 140C77 RAW DATA TANK TRIAD

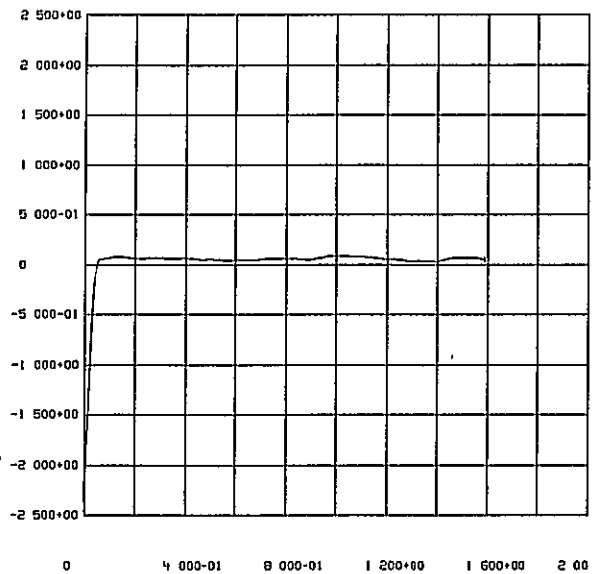


MX(IP) VS T(SEC)  
1 TEST10 140C77 RAW DATA TANK TRIAD

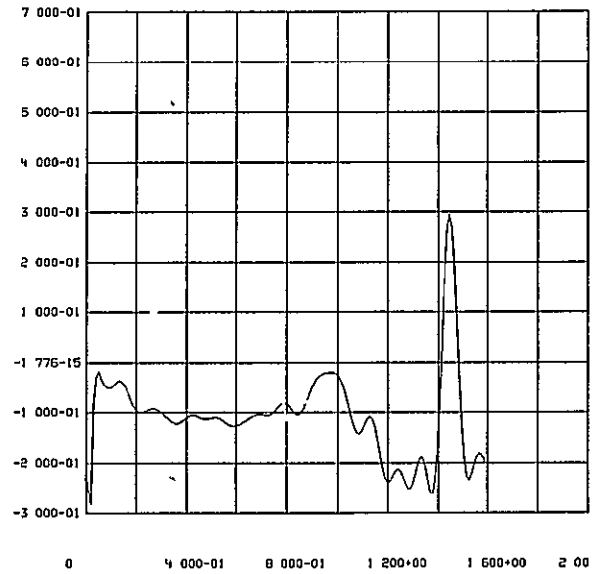
A-7



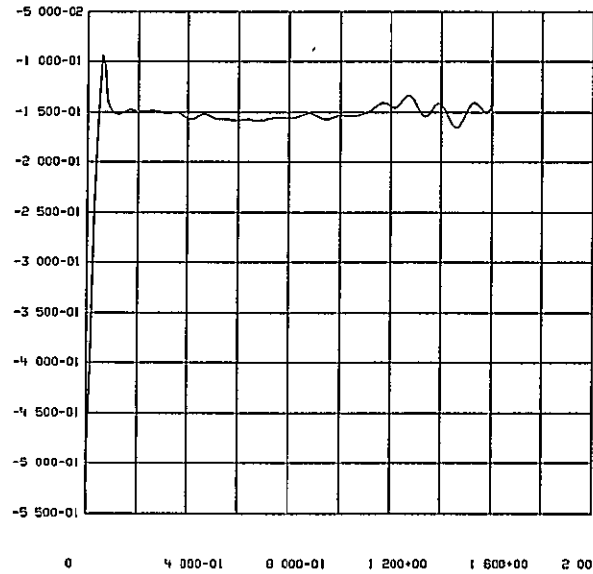
FY(LB) VS T(SEC)  
 1 TEST11 03N077 RAH DATA TANK TRIAD



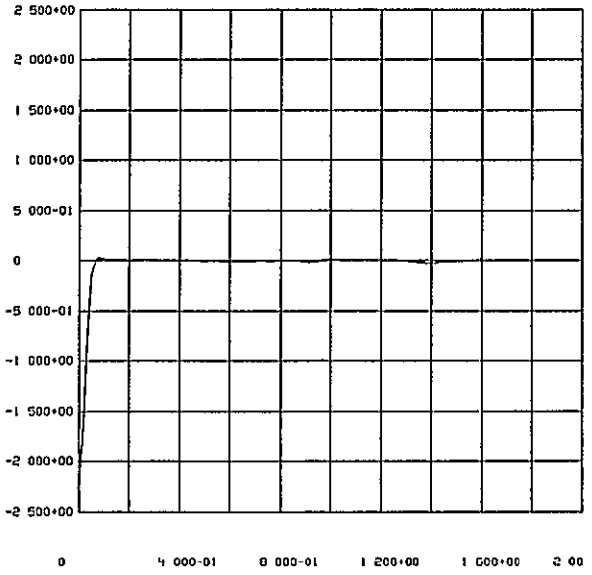
FZ(LB) VS T(SEC)  
 1 TEST11 03N077 RAH DATA TANK TRIAD



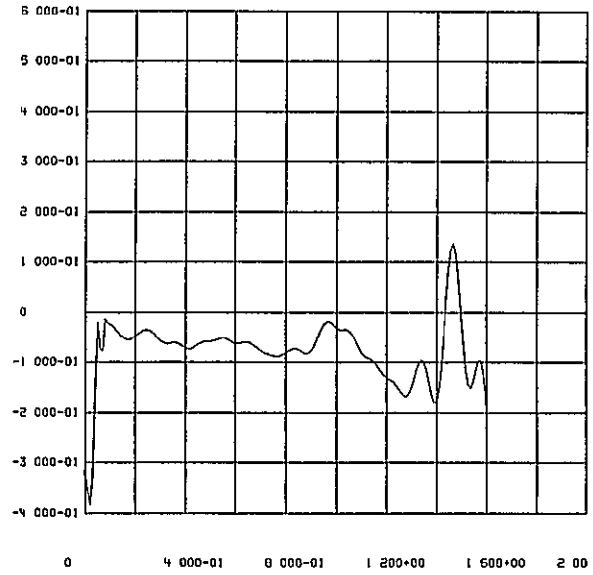
MX(1P) VS T(SEC)  
 1 TEST11 03N077 RAH DATA TANK TRIAD



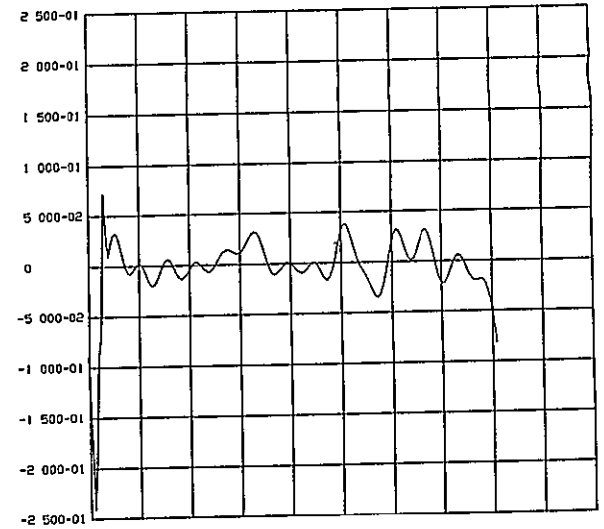
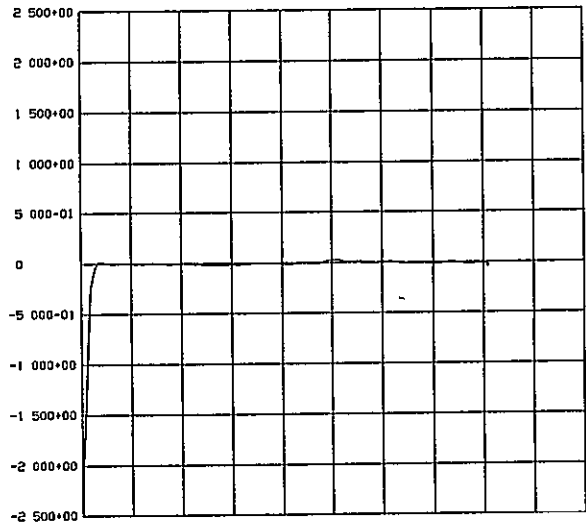
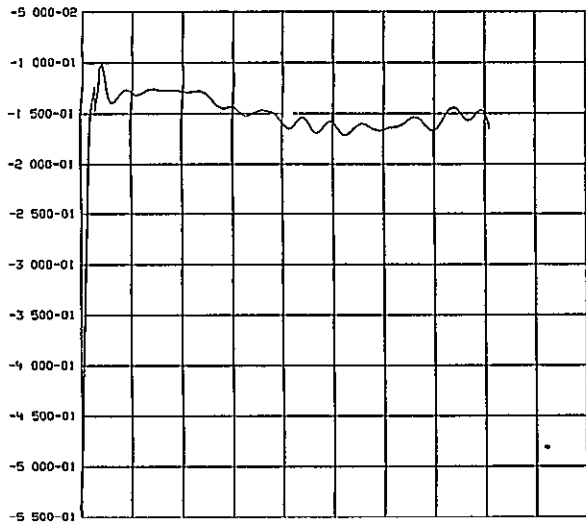
FY(LB) VS T(SEC)  
 1 TEST12 03N077 RAH DATA TANK TRIAD



FZ(LB) VS T(SEC)  
 1 TEST12 03N077 RAH DATA TANK TRIAD



MX(1P) VS T(SEC)  
 1 TEST12 03N077 RAH DATA TANK TRIAD



0 4 000-01 8 000-01 1 200+00 1 600+00 2 00

FY(LB) VS T(SEC)

1 TEST13 03N077 RAW DATA TANK TRIAD

0 4 000-01 8 000-01 1 200+00 1 600+00 2 00

FZ(LB) VS T(SEC)

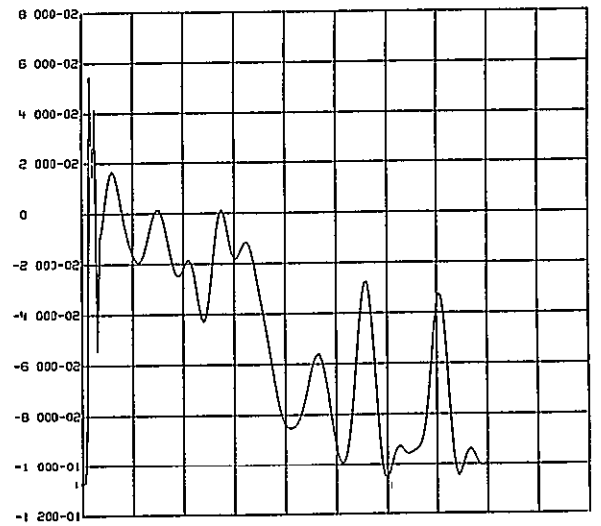
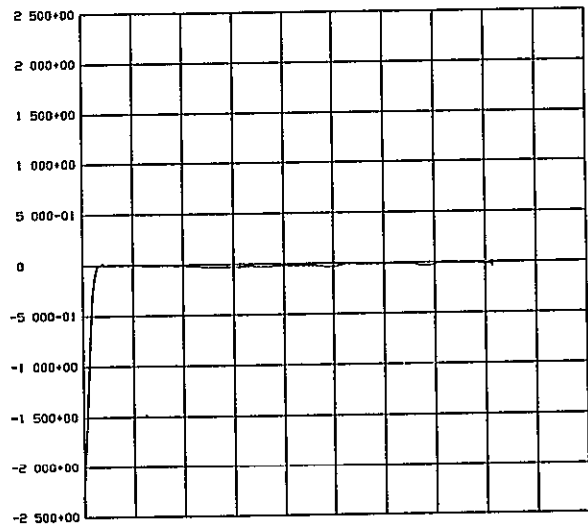
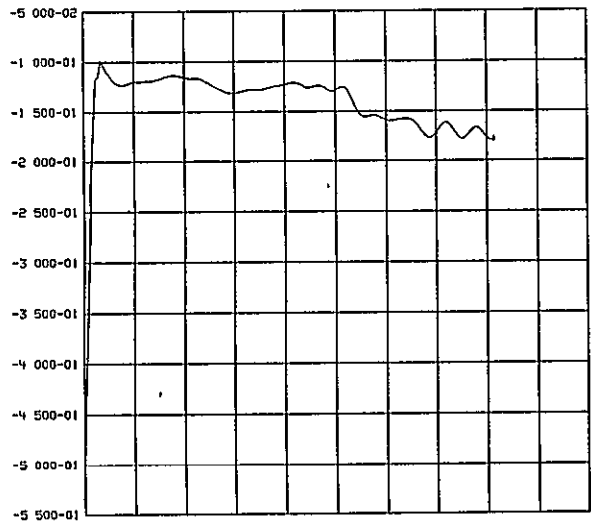
1 TEST13 03N077 RAW DATA TANK TRIAD

0 4 000-01 8 000-01 1 200+00 1 600+00 2 00

HX(IP) VS T(SEC)

1 TEST13 03N077 RAW DATA TANK TRIAD

A-8



0 4 000-01 8 000-01 1 200+00 1 600+00 2 00

FY(LB) VS T(SEC)

1 TEST14 03N077 RAW DATA TANK TRIAD

0 4 000-01 8 000-01 1 200+00 1 600+00 2 00

FZ(LB) VS T(SEC)

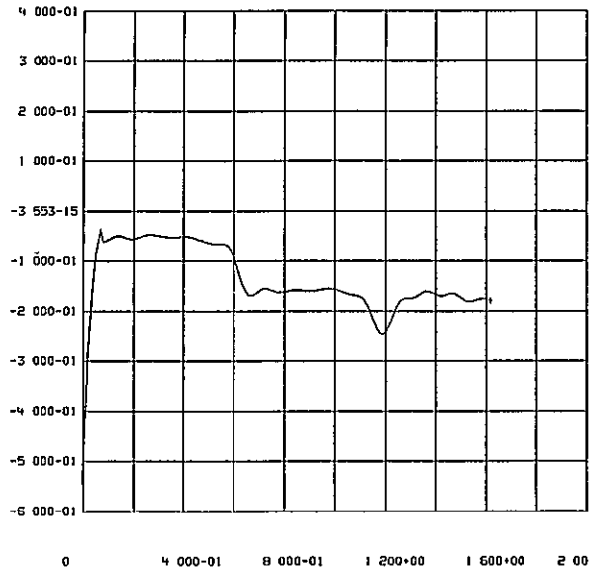
1 TEST14 03N077 RAW DATA TANK TRIAD

0 4 000-01 8 000-01 1 200+00 1 600+00 2 00

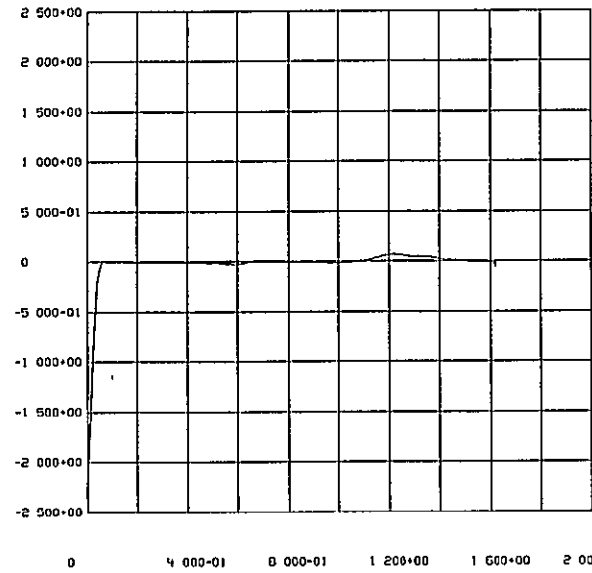
HX(IP) VS T(SEC)

1 TEST14 03N077 RAW DATA TANK TRIAD

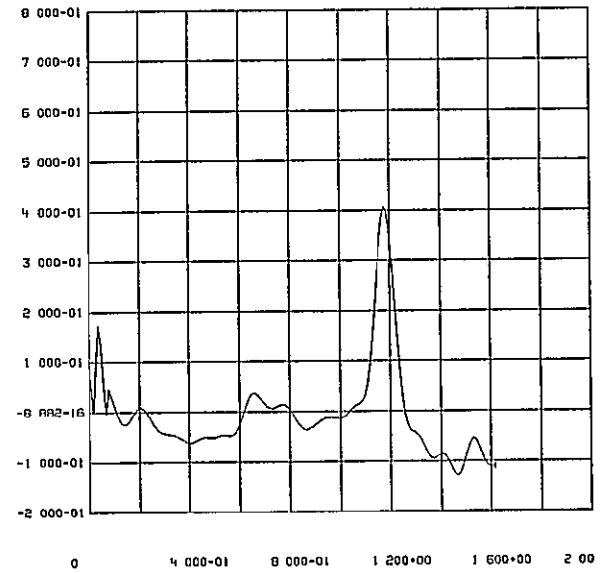
ORIGINAL PAGE IS  
OF POOR QUALITY



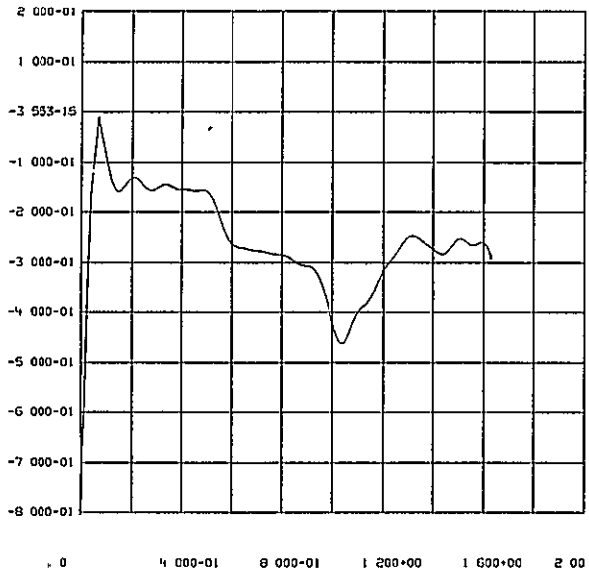
FY(LB) VS T(SEC)  
1 TEST15 140C77 RAW DATA TANK TRIAD



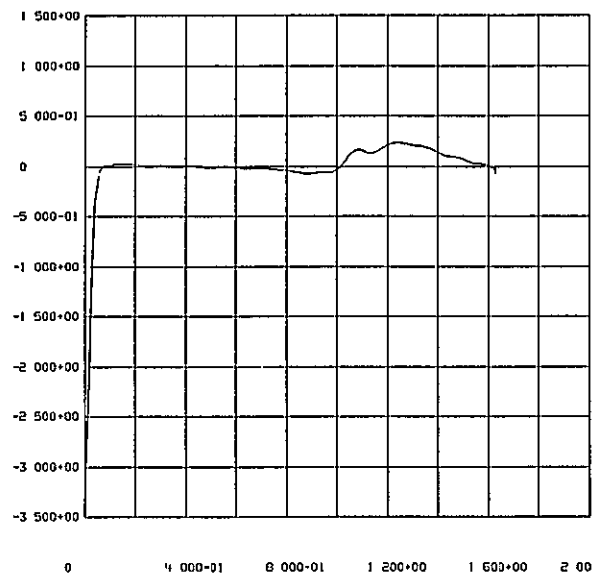
FZ(LB) VS T(SEC)  
1 TEST15 140C77 RAW DATA TANK TRIAD



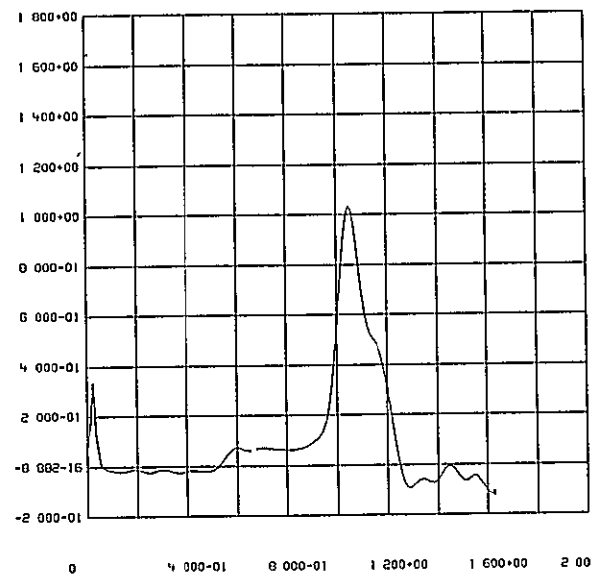
HX(IP) VS T(SEC)  
1 TEST15 140C77 RAW DATA TANK TRIAD



FY(LB) VS T(SEC)  
1 TEST16 140C77 RAW DATA TANK TRIAD

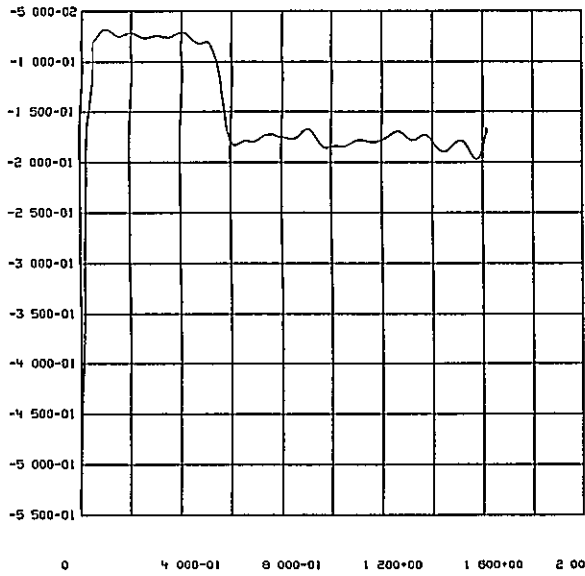


FZ(LB) VS T(SEC)  
1 TEST16 140C77 RAW DATA TANK TRIAD

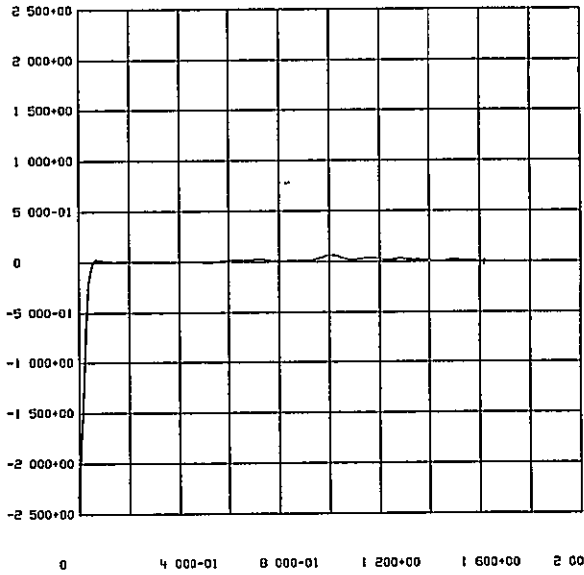


HX(IP) VS T(SEC)  
1 TEST16 140C77 RAW DATA TANK TRIAD

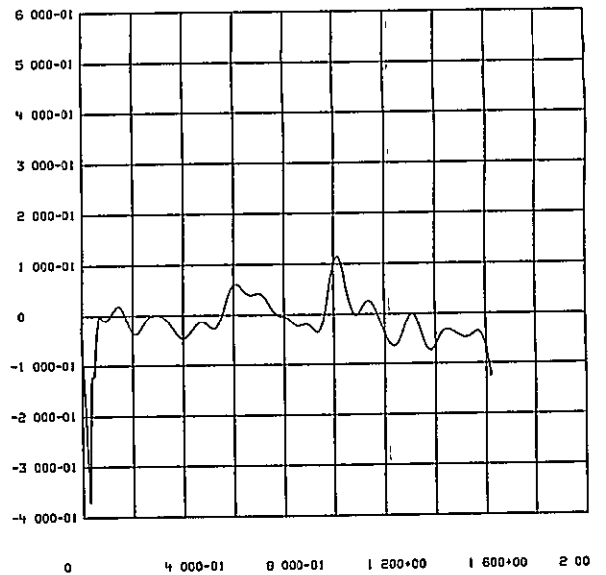
A-9



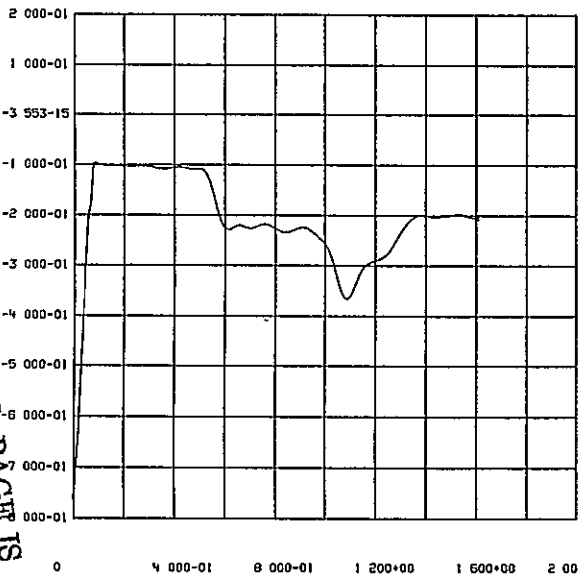
0 4 000-01 8 000-01 1 200+00 1 600+00 2 00  
 FY(LB) VS T(SEC)  
 1 TEST17 03N077 RAW DATA TANK TRIAD



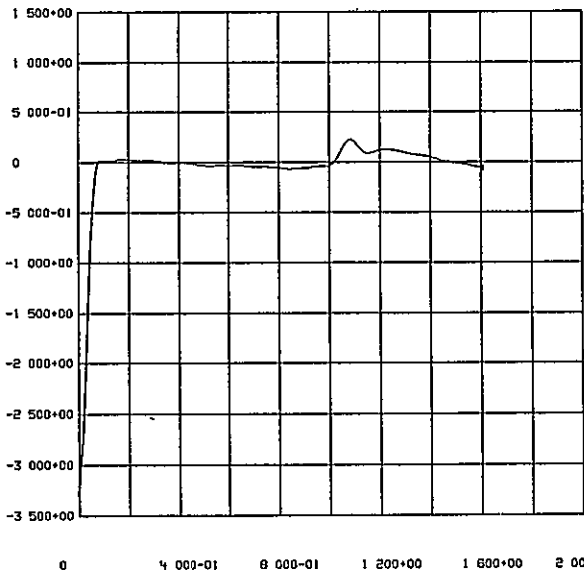
0 4 000-01 8 000-01 1 200+00 1 600+00 2 00  
 FZ(LB) VS T(SEC)  
 1 TEST17 03N077 RAW DATA TANK TRIAD



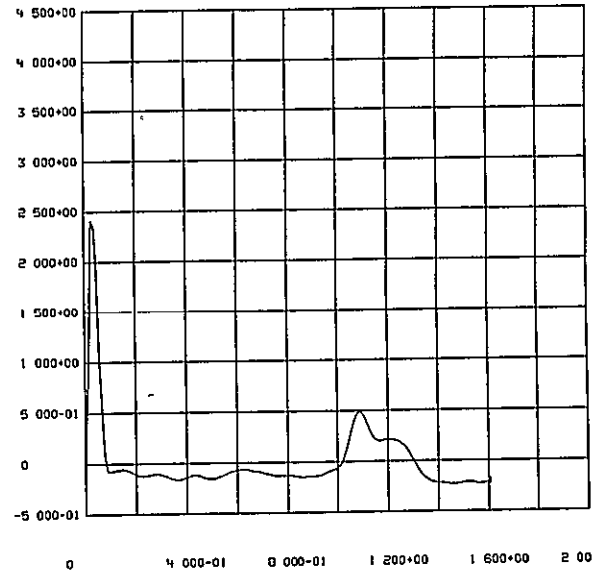
0 4 000-01 8 000-01 1 200+00 1 600+00 2 00  
 FX(IP) VS T(SEC)  
 1 TEST17 03N077 RAW DATA TANK TRIAD



0 4 000-01 8 000-01 1 200+00 1 600+00 2 00  
 FY(LB) VS T(SEC)  
 1 TEST18 03N077 RAW DATA TANK TRIAD

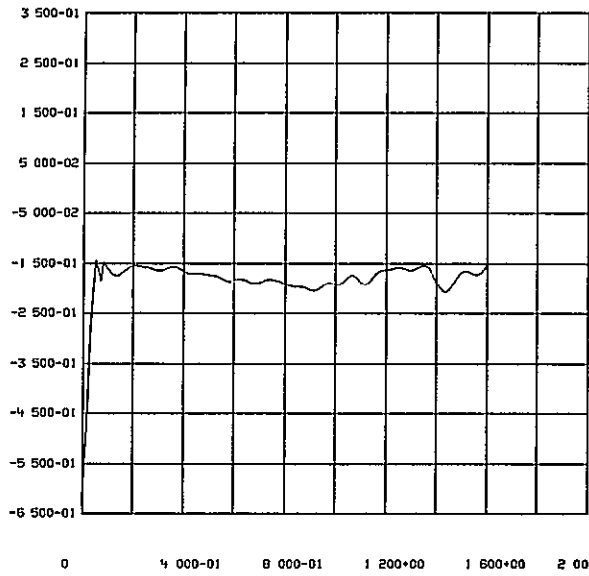


0 4 000-01 8 000-01 1 200+00 1 600+00 2 00  
 FZ(LB) VS T(SEC)  
 1 TEST18 03N077 RAW DATA TANK TRIAD

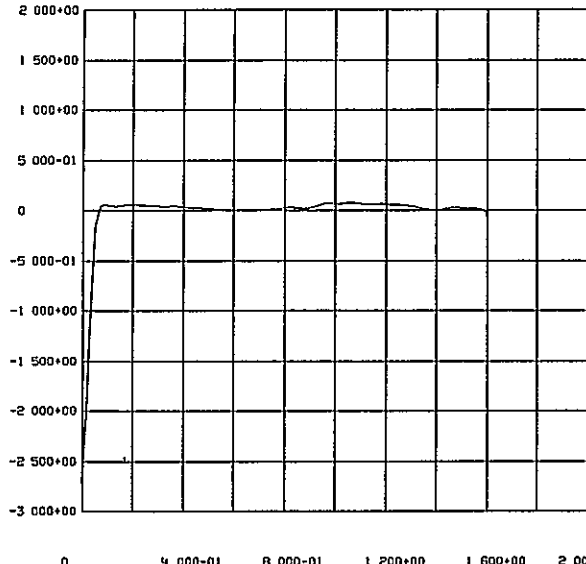


0 4 000-01 8 000-01 1 200+00 1 600+00 2 00  
 FX(IP) VS T(SEC)  
 1 TEST18 03N077 RAW DATA TANK TRIAD

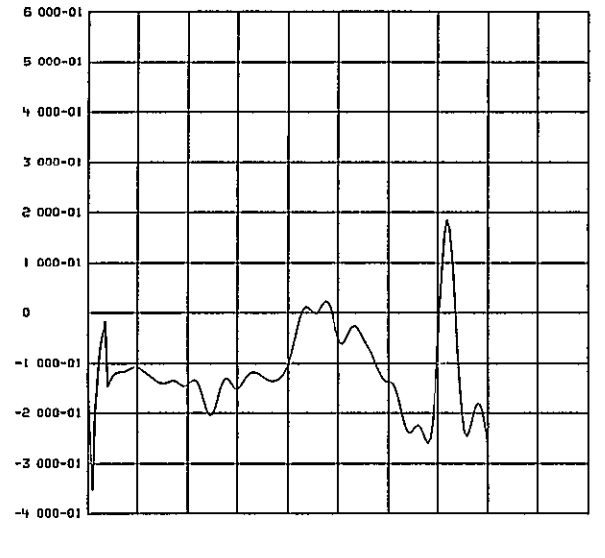
ORIGINAL PAGE IS  
 OF POOR QUALITY



FY(LB) VS T(SEC)  
1 TEST19 03N077 RAW DATA TANK TRIAD

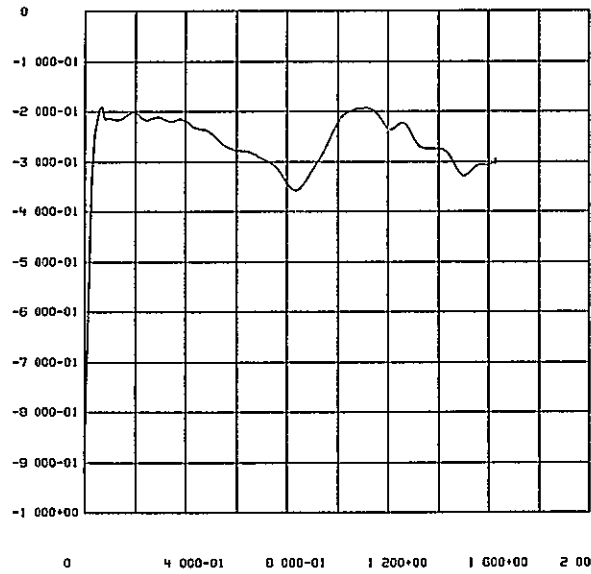


FZ(LB) VS T(SEC)  
1 TEST19 03N077 RAW DATA TANK TRIAD

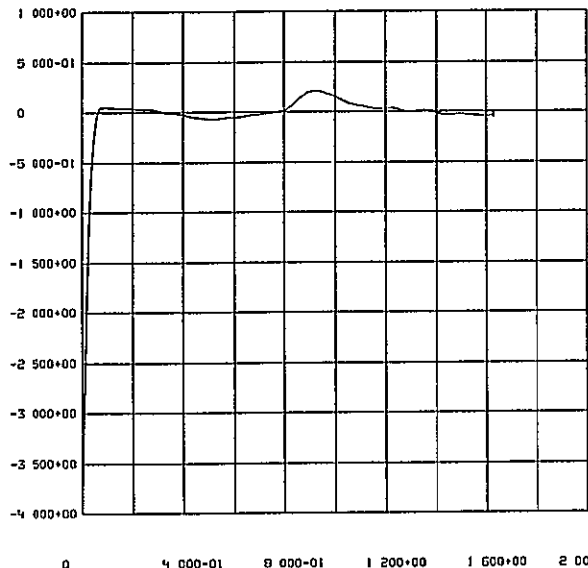


MX(IP) VS T(SEC)  
1 TEST19 03N077 RAW DATA TANK TRIAD

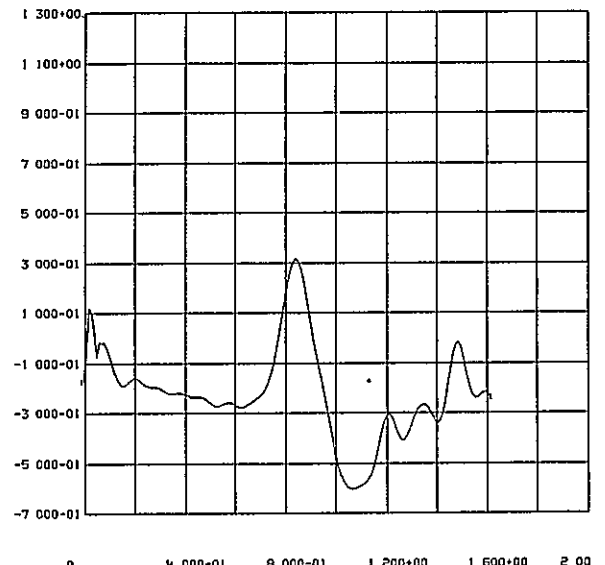
TI-Y



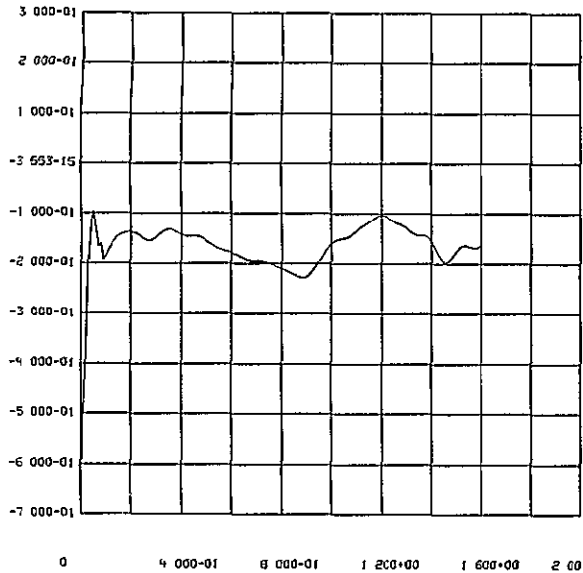
FY(LB) VS T(SEC)  
1 TEST20 03N077 RAW DATA TANK TRIAD



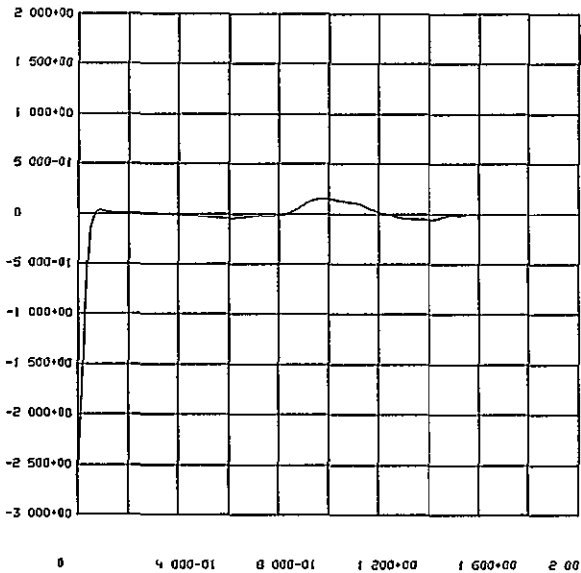
FZ(LB) VS T(SEC)  
1 TEST20 03N077 RAW DATA TANK TRIAD



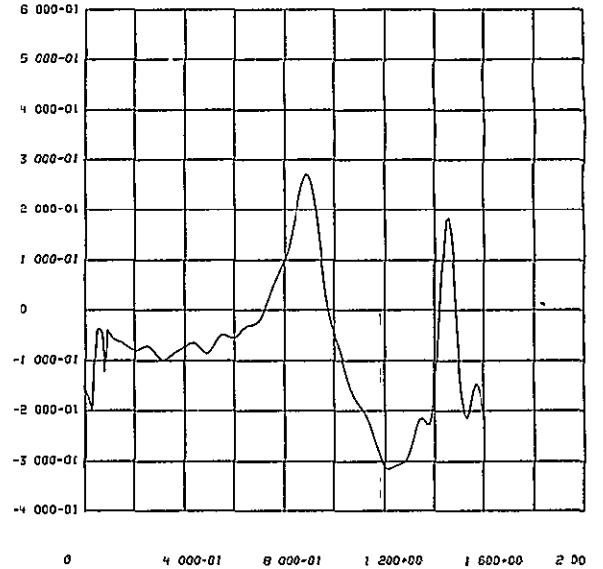
MX(IP) VS T(SEC)  
1 TEST20 03N077 RAW DATA TANK TRIAD



FY(LB) VS T(SEC)  
1 TEST21 140C77 RAH DATA TANK TRIAD

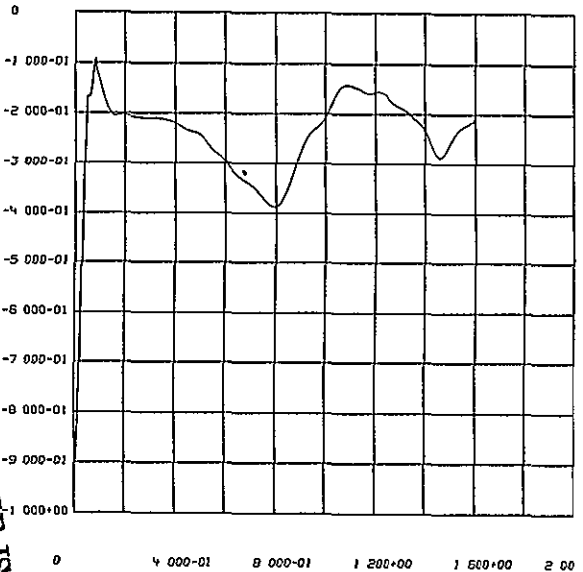


FZ(LB) VS T(SEC)  
1 TEST21 140C77 RAH DATA TANK TRIAD

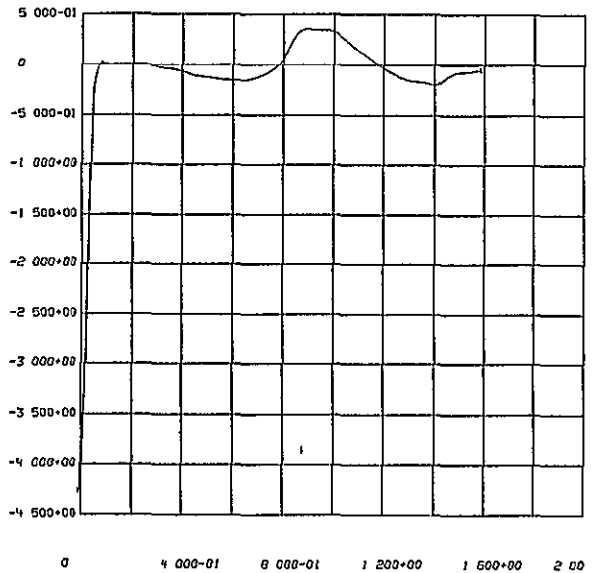


MX(IP) VS T(SEC)  
1 TEST21 140C77 RAH DATA TANK TRIAD

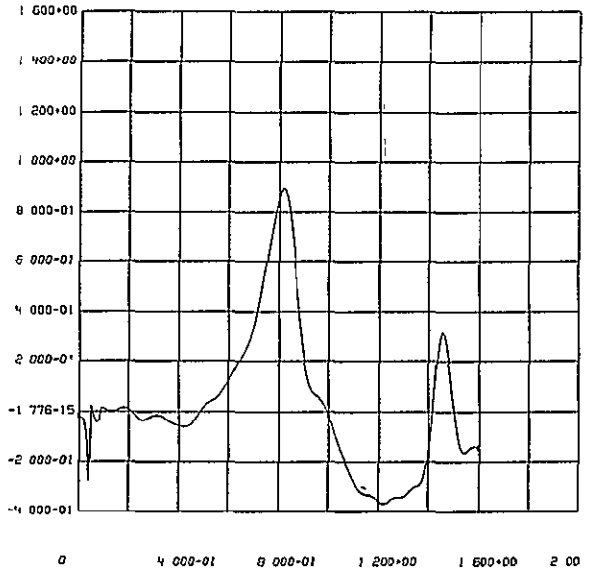
A-12



FY(LB) VS T(SEC)  
1 TEST22 140C77 RAH DATA TANK TRIAD



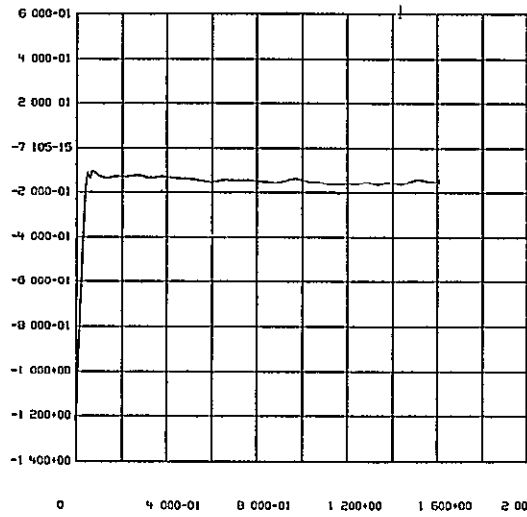
FZ(LB) VS T(SEC)  
1 TEST22 140C77 RAH DATA TANK TRIAD



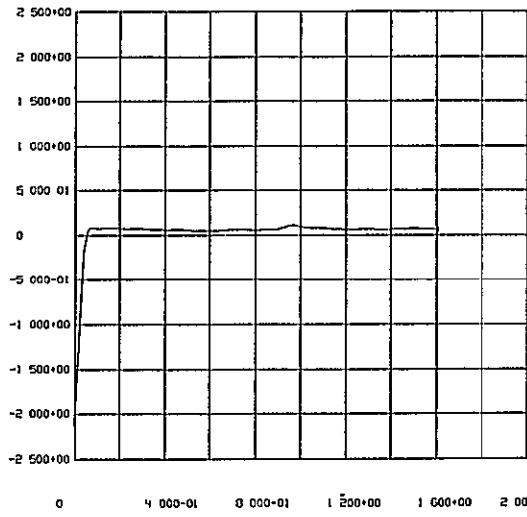
MX(IP) VS T(SEC)  
1 TEST22 140C77 RAH DATA TANK TRIAD

ORIGINAL PAGE IS  
OF POOR QUALITY

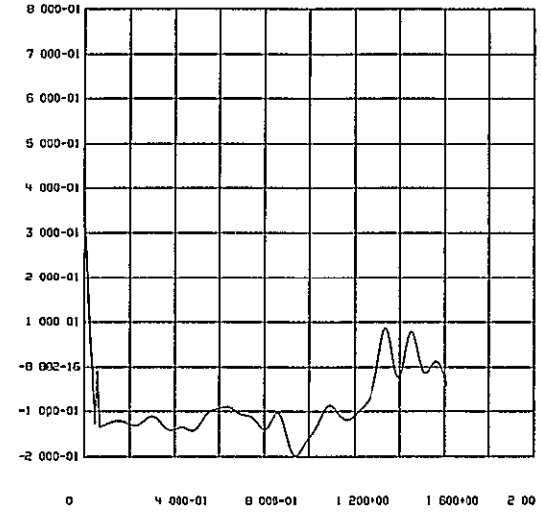
A-13



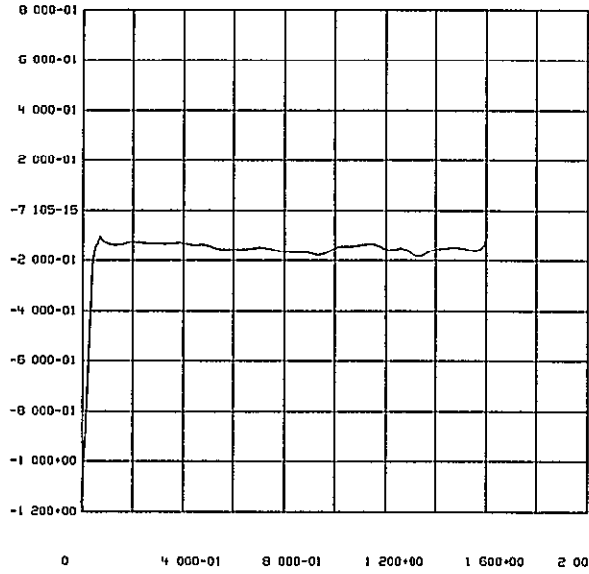
FY(LB) VS T(SEC)  
1 TEST23 07H79 RAW DATA TANK TRIAD



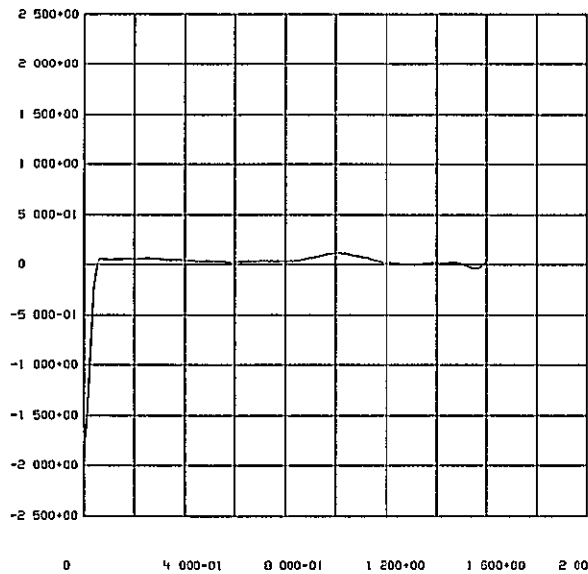
FZ(LB) VS T(SEC)  
1 TEST23 07H79 RAW DATA TANK TRIAD



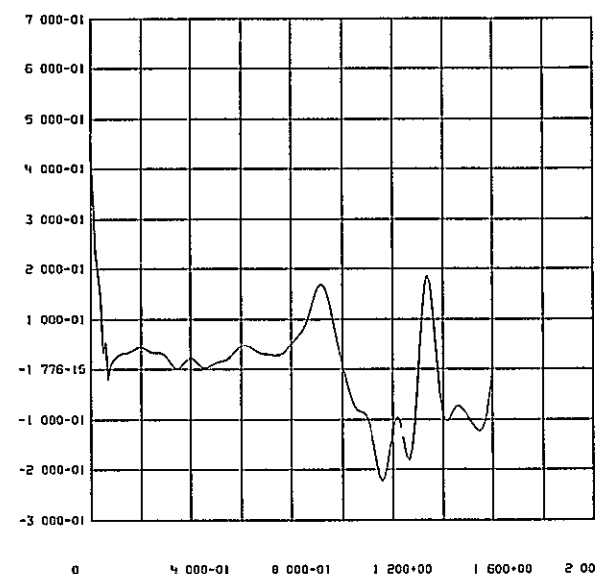
MX(1P) VS T(SEC)  
1 TEST23 07H79 RAW DATA TANK TRIAD



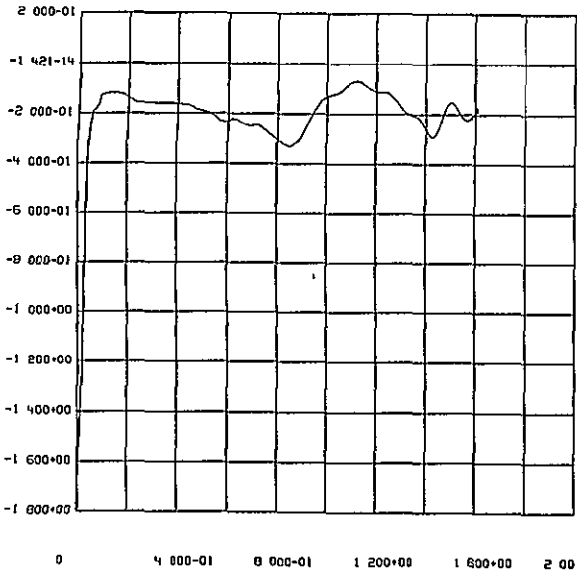
FY(LB) VS T(SEC)  
1 TEST24 14OC77 RAW DATA TANK TRIAD



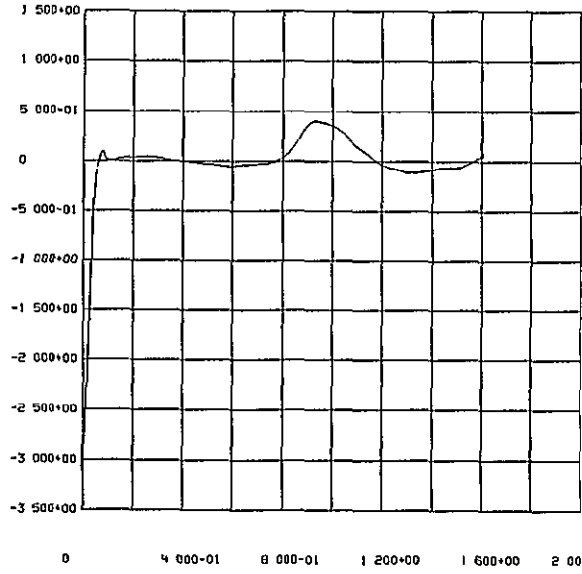
FZ(LB) VS T(SEC)  
1 TEST24 14OC77 RAW DATA TANK TRIAD



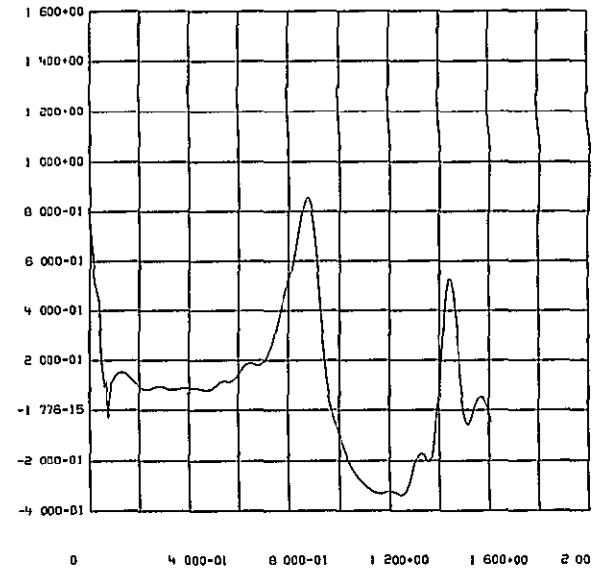
MX(1P) VS T(SEC)  
1 TEST24 14OC77 RAW DATA TANK TRIAD



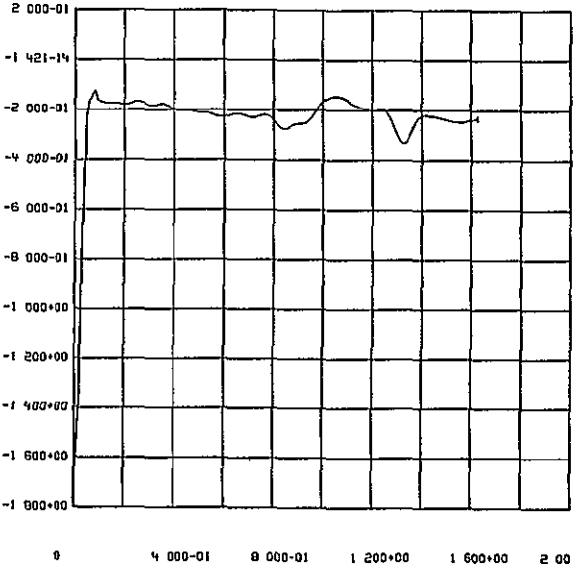
0 4 000-01 8 000-01 1 200+00 1 600+00 2 00  
 FY(LB) VS T(SEC)  
 1 TEST25 140C77 RAH DATA TANK TRIAD



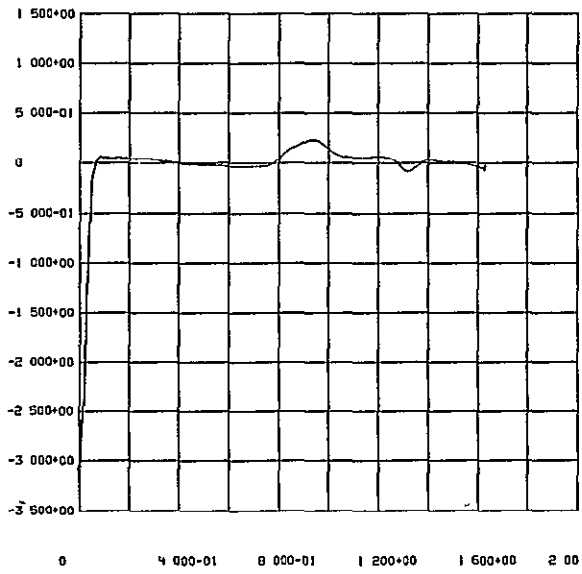
0 4 000-01 8 000-01 1 200+00 1 600+00 2 00  
 FZ(LB) VS T(SEC)  
 1 TEST25 140C77 RAH DATA TANK TRIAD



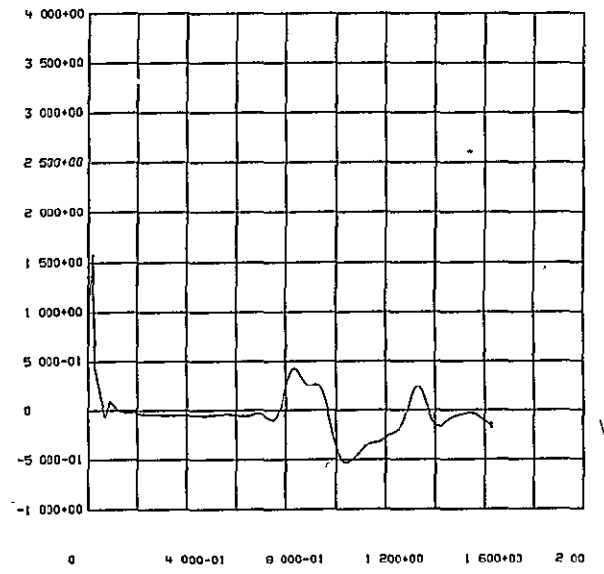
0 4 000-01 8 000-01 1 200+00 1 600+00 2 00  
 MX(IP) VS T(SEC)  
 1 TEST25 140C77 RAH DATA TANK TRIAD



0 4 000-01 8 000-01 1 200+00 1 600+00 2 00  
 FY(LB) VS T(SEC)  
 1 TEST26 03N077 RAH DATA TANK TRIAD



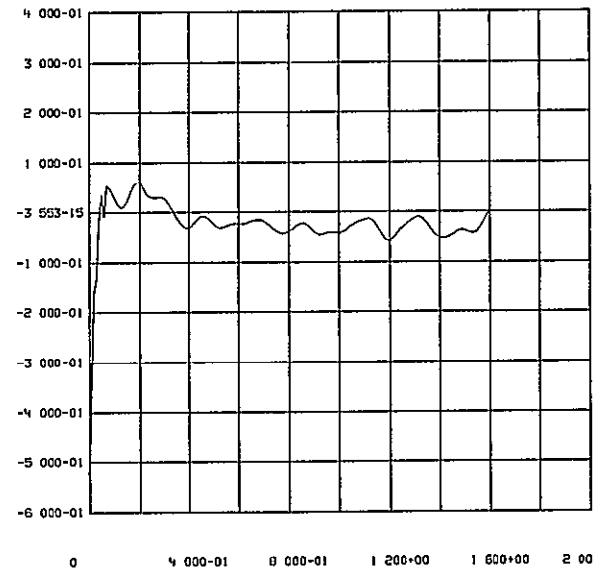
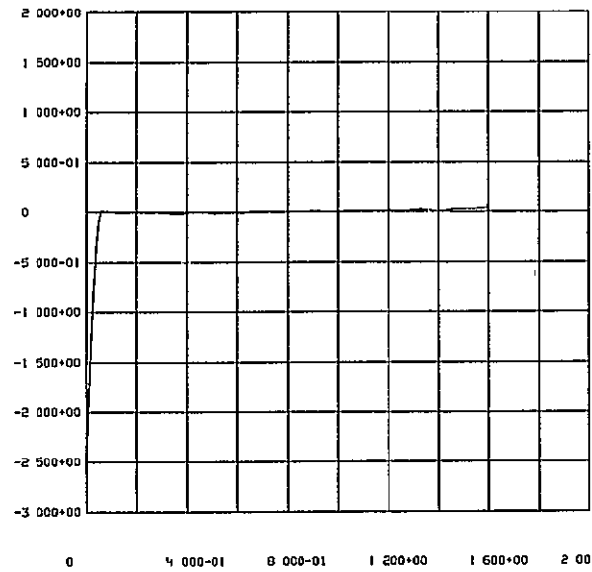
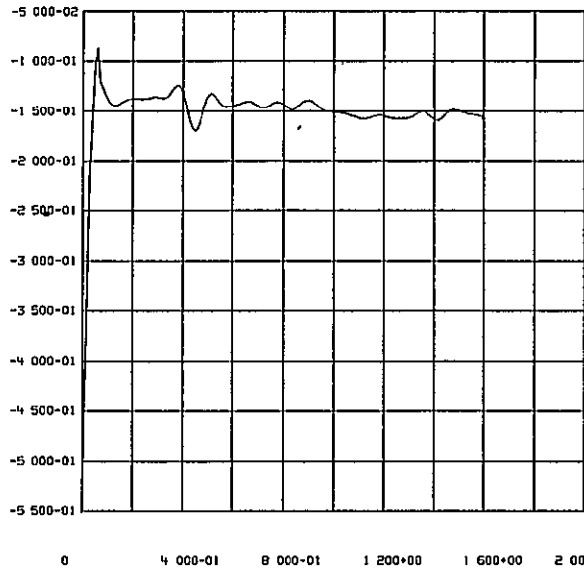
0 4 000-01 8 000-01 1 200+00 1 600+00 2 00  
 FZ(LB) VS T(SEC)  
 1 TEST26 03N077 RAH DATA TANK TRIAD



0 4 000-01 8 000-01 1 200+00 1 600+00 2 00  
 MX(IP) VS T(SEC)  
 1 TEST26 03N077 RAH DATA TANK TRIAD

A-16

ORIGINAL PAGE IS  
 OF POOR QUALITY

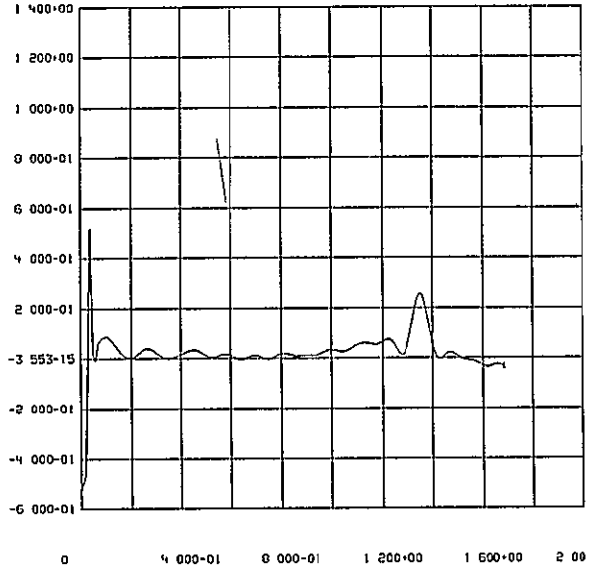
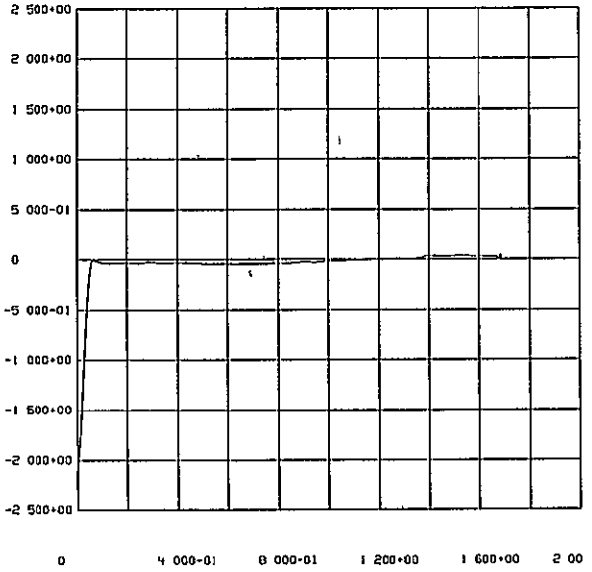
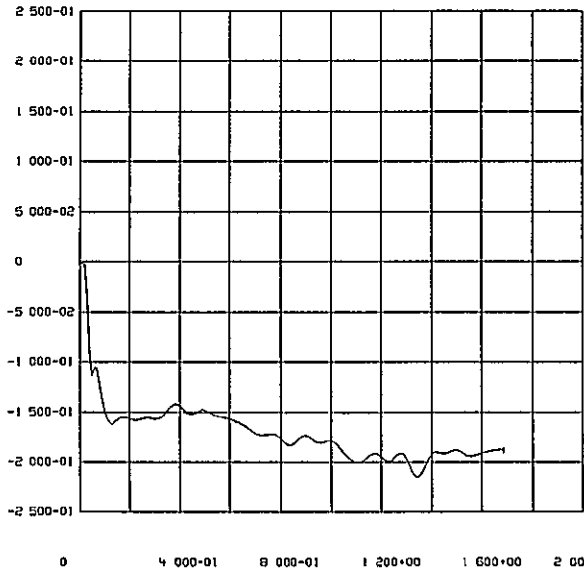


51-Y

FY(LB) VS T(SEC)  
1 TEST27 03N077 RAW DATA TANK TRIAD

FZ(LB) VS T(SEC)  
1 TEST27 03N077 RAW DATA TANK TRIAD

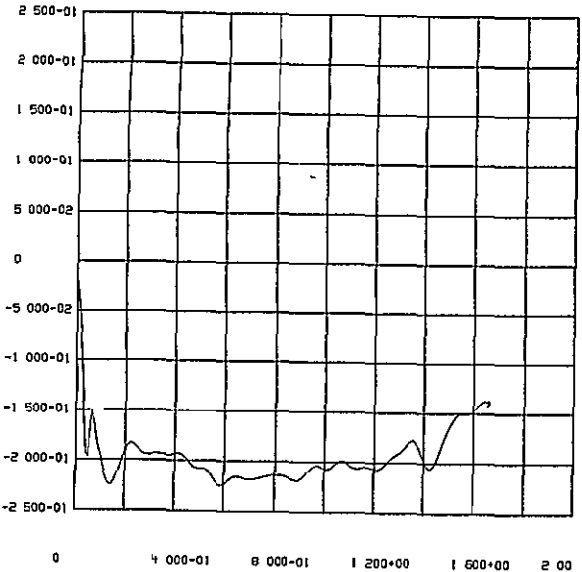
MX(IP) VS T(SEC)  
1 TEST27 03N077 RAW DATA TANK TRIAD



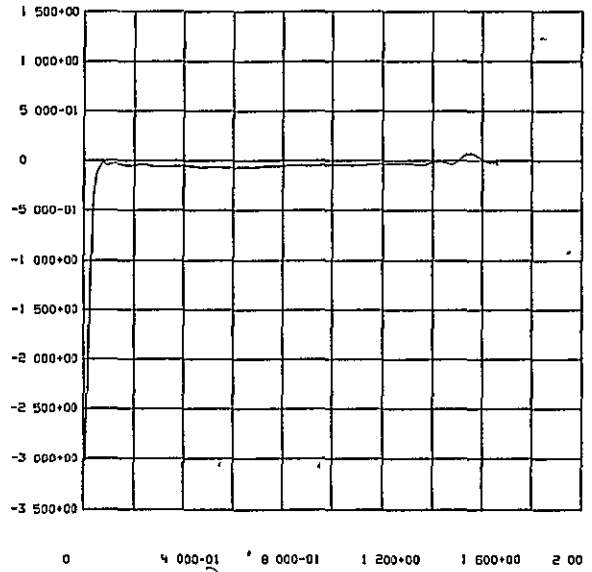
FY(LB) VS T(SEC)  
1 TEST28 140C77 RAW DATA TANK TRIAD

FZ(LB) VS T(SEC)  
1 TEST28 140C77 RAW DATA TANK TRIAD

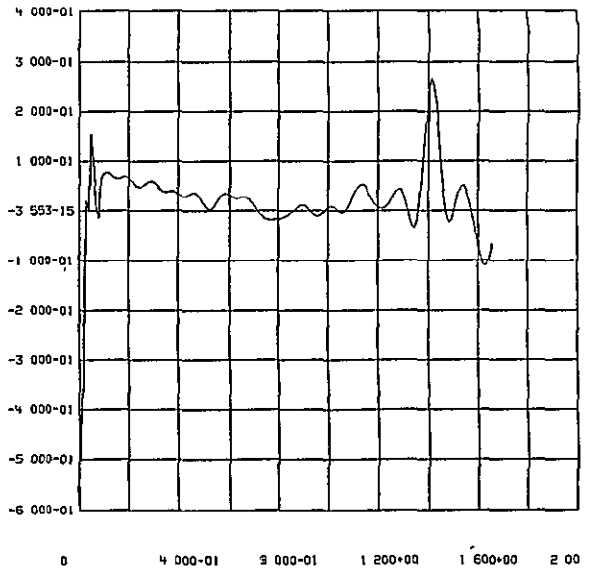
MX(IP) VS T(SEC)  
1 TEST28 140C77 RAW DATA TANK TRIAD



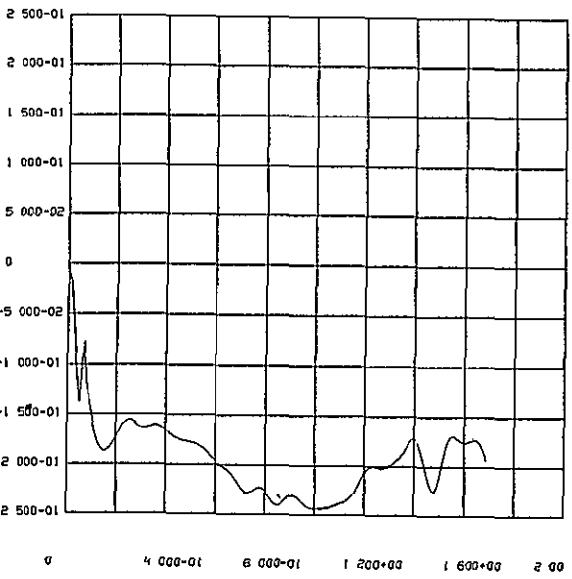
1 TEST29 03N077 RAH DATA TANK TRIAD



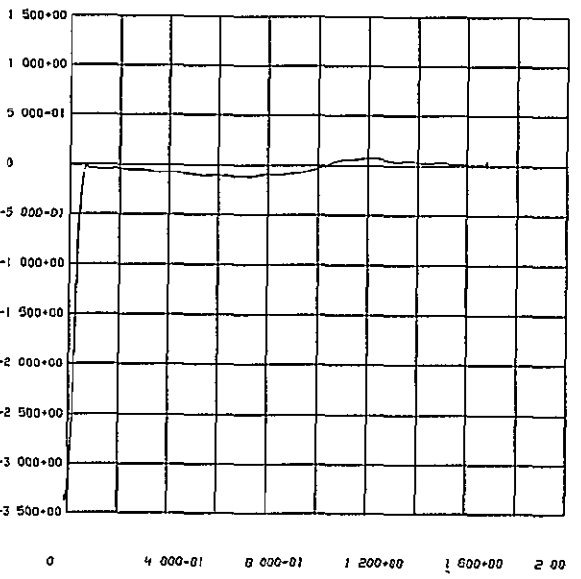
1 TEST29 03N077 RAH DATA TANK TRIAD



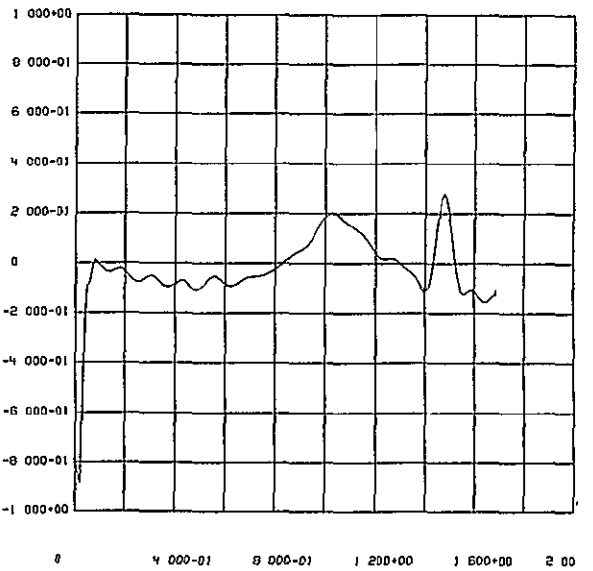
1 TEST29 03N077 RAH DATA TANK TRIAD



1 TEST30 140C77 RAH DATA TANK TRIAD



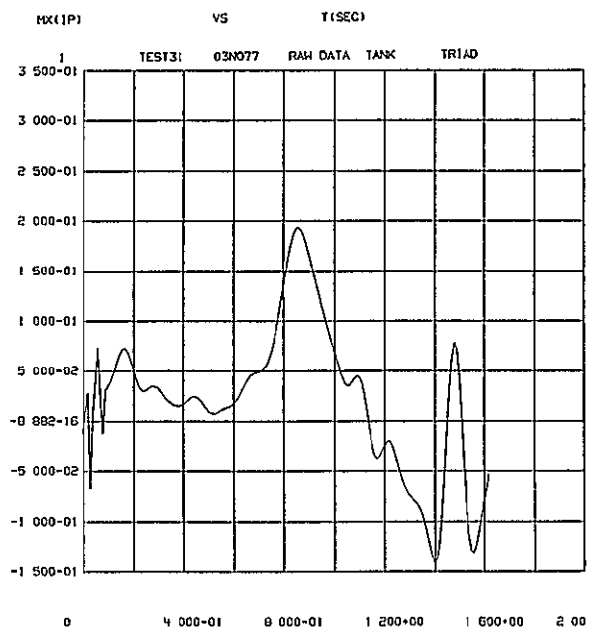
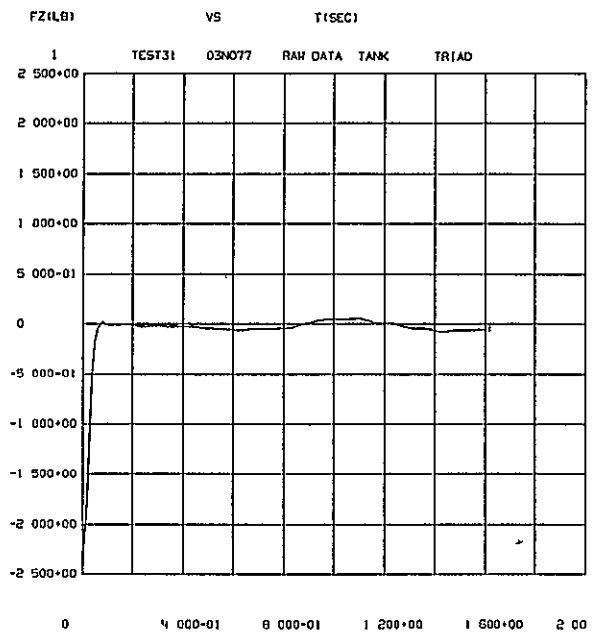
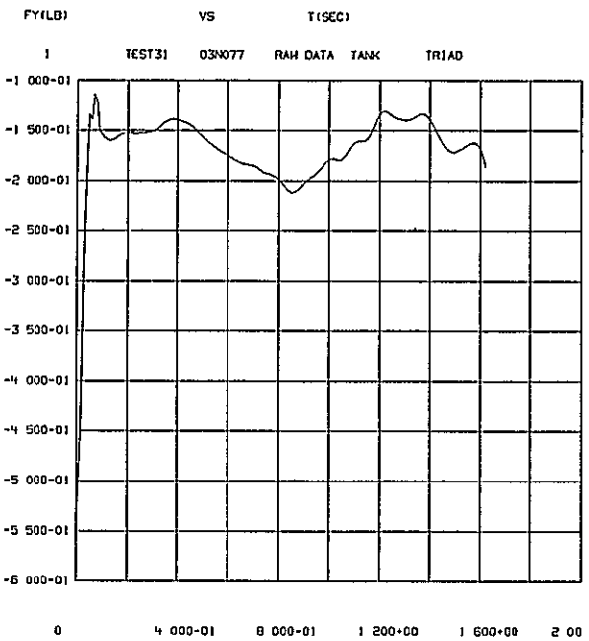
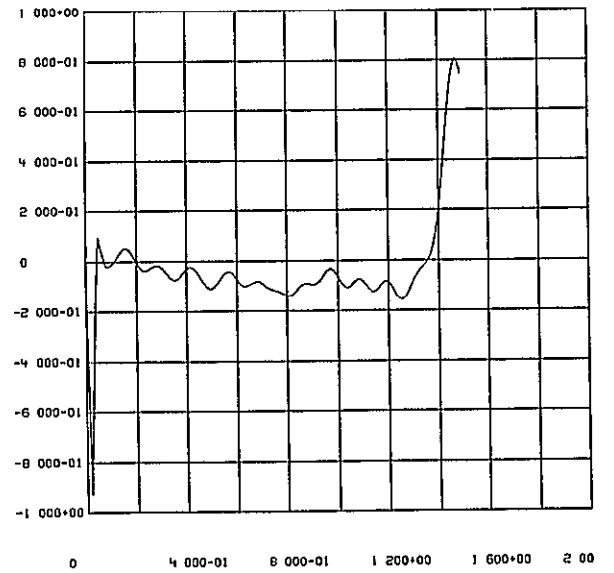
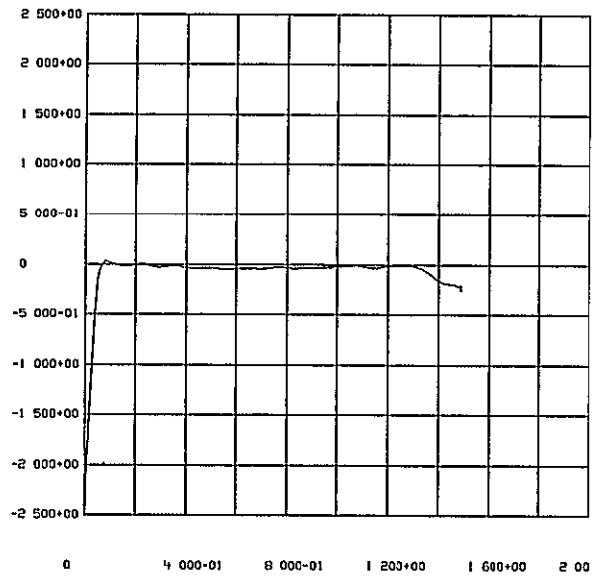
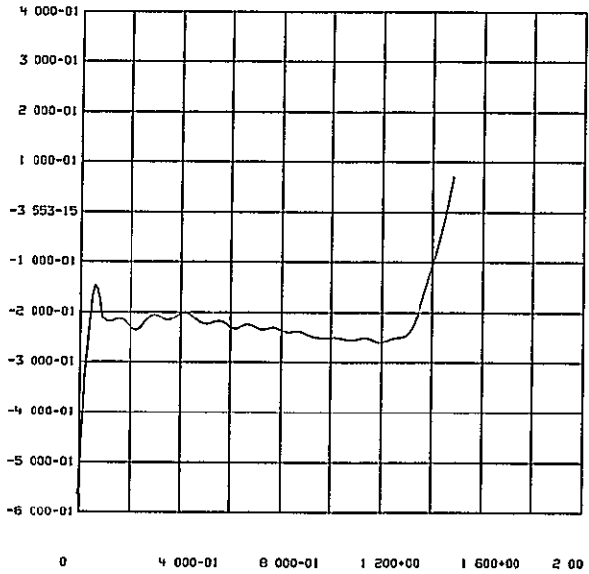
1 TEST30 140C77 RAH DATA TANK TRIAD



1 TEST30 140C77 RAH DATA TANK TRIAD

ORIGINAL PAGE IS OF POOR QUALITY

A-16



A-17

FY(LB) VS T(SEC)  
1 TEST32 140C77 RAW DATA TANK TRIAD

FZ(LB) VS T(SEC)  
1 TEST32 140C77 RAW DATA TANK TRIAD

MX(IP) VS T(SEC)  
1 TEST32 140C77 RAW DATA TANK TRIAD